Uncertainty Analysis and Control of Multiscale Process Systems

by

Shabnam Rasoulian

A thesis

presented to the University of Waterloo

in fulfillment of the

thesis requirement for the degree of

Doctor of Philosophy

in

Chemical Engineering

Waterloo, Ontario, Canada, 2015

AUTHOR'S DECLARATION

I hereby declare that I am the sole author of this thesis. This is a true copy of the thesis, including any required final revisions, as accepted by my examiners. I understand that my thesis may be made electronically available to the public.

Abstract

Microelectronic market imposes tight requirements upon thin film properties, including specific growth rate, surface roughness and thickness of the film. In the thin film deposition process, the microscopic events determine the configuration of the thin film surface while manipulating variables at the macroscopic level, such as bulk precursor mole fraction and substrate temperature, are essential to product quality. Despite the extensive body of research on control and optimization in this process, there is still a significant discrepancy between the expected performance and the actual yield that can be accomplished employing existing methodologies. This gap is mainly related to the complexities associated with the multiscale nature of the thin film deposition process, lack of practical online *in-situ* sensors at the fine-scale level, and uncertainties in the mechanisms and parameters of the system. The main goal of this research is developing robust control and optimization strategies for this process while uncertainty analysis is performed using power series expansion (PSE). The deposition process is a batch process where the measurements are available at the end of the batch; accordingly, optimization and control approaches that do not need to access online fine-scale measurements are required. In this research, offline optimization is performed to obtain the optimal temperature profile that results in specific product quality characteristics in the presence of model-plant mismatch. To provide a computationally tractable optimization, the sensitivities in PSEs are numerically evaluated using reduced-order lattices in the KMC models. A comparison between bounded and distributional parametric uncertainties has illustrated that inaccurate assumption for uncertainty description can lead to economic losses in the process. To accelerate the sensitivity analysis of the process, an algorithm has been presented to determine the upper and lower bounds on the outputs through distributions of the microscopic events. In this approach, the sensitivities in the series expansions of events are analytically evaluated. Current multiscale models are not available in closed-form and are computationally prohibitive for online applications. Thus, closed-form models have been developed in this research to predict the control objectives efficiently for online control applications in the presence of model-plant mismatch. The robust performance is quantified by estimates of the distributions of the controlled variables employing PSEs. Since these models can efficiently predict the controlled outputs, they can either be used as an estimator for feedback control purposes in the lack of sensors, or as a basis to design a nonlinear model predictive control (NMPC) framework. Although the recently introduced optical

in-situ sensors have motivated the development of feedback control in the thin film deposition process, their application is still limited in practice. Thus, a multivariable robust estimator has been developed to estimate the surface roughness and growth rate based on the substrate temperature and bulk precursor mole fraction. To ensure that the control objective is met in the presence of model-plant mismatch, the robust estimator is designed such that it predicts the upper bound on the process output. The estimator is coupled with traditional feedback controllers to provide a robust feedback control in the lack of online measurements. In addition, a robust NMPC application for the thin film deposition process was developed. The NMPC makes use of closed-from models, which has been identified offline to predict the controlled outputs at a predefined specific probability. The shrinking horizon NMPC minimizes the final roughness, while satisfying the constraints on the control actions and film thickness at the end of the deposition process. Since the identification is performed for a fixed confidence level, hard constraints are defined for thin film properties. To improve the robust performance of NMPC using soft constraints, a closed-form model has been developed to estimate the first and second-order statistical moments of the thin film properties under uncertainty in the multiscale model parameters. Employing this model, the surface roughness and film thickness can be estimated at a desired probability limit during the deposition. Thus, an NMPC framework is devised that successfully minimizes the surface roughness at the end of the batch, while the film thickness meets a minimum specification at a desired probability. Therefore, the methods developed in this research enable accurate online control of the key properties of a multiscale system in the presence of model-plant mismatch.

Acknowledgements

I would like to express my sincerest gratitude to my advisor, Prof. Luis A. Ricardez-Sandoval. With his continuous support and encouragements, he inspired me to overcome the challenges in my PhD research.

I am also grateful to the members of my supervisory committee, Prof. Panagiotis D. Christofides, Prof. Hector Budman, Prof. Thomas Duever and Prof. John Wen, for their insightful feedbacks and invaluable suggestions on my thesis.

I am also thankful to Dr. Jingde Li to be a good friend and office-mate, and all the staffs and faculty members of the Department of Chemical Engineering at the University of Waterloo.

Last but not least, I would like to thank my husband, my parents and my brother for their unconditional love and support during my PhD research.

Dedication

To Mom, Dad & Soheil

Table of contents

List of figures

List of tables

Nomenclature

List of English symbols

a	Strain rate
C_{tot}	Concentration of sites on the surface
dt	Time increment in the KMC model
E	Energy associated with a single bond
E_d	Energy associated with desorption
E_m	Energy associated with migration
F_H	Cumulative distribution function of thickness
F_r	Cumulative distribution function of surface roughness
f	Dimensionless stream function
$f_{p.d.}$	Probability distribution function
Gr	Growth rate
H	Film thickness
H_{min}	Minimum allowed thickness at the end of the batch
$H_{ref}(t)$	Thickness reference vector obtained using the nominal open-loop optimal substrate temperature trajectory
$h(i,j)$	Number of atoms at site (i,j)
$\mathbf{K}(t)$	Feedback controller gain vector
k_{d0}	Event-frequency constant
$\mathbf{L}_1(t)$	Jacobian evaluated around $\widehat{\boldsymbol{\theta}}$ at a specific time, t
$\mathbf{L}_2(t)$	Hessian evaluated around $\widehat{\boldsymbol{\theta}}$ at a specific time, t
m	Precursor molecular weight
N	Lattice size
N_a	Number of adsorbed atoms during $\Delta\mathcal{T}$
N_d	Number of desorbed atoms during $\Delta\mathcal{T}$
P	Chamber pressure

$\mathcal{P}(\kappa, t)$	probability that the system is in state κ at time, t
P_A	Rate of an adsorption event
$P_D(i)$	Rate of desorption of a surface atom with i first nearest neighbors
$P_M(i)$	Rate of migration of a surface atom with i first nearest neighbors
Pr	Prandtl number
$\mathbb{Pr}$	Probability
R	Gas constant
R_a	Rate of adsorption
R_d	Rate of desorption
$\mathcal{R}_{max}$	Maximum temperature ramp
$\mathcal{R}_{min}$	Minimum temperature ramp
r	Surface roughness
$\mathbf{S}(t)$	KMC lattice configuration at time, t
S_0	Sticking coefficient
Sc	Schmidt number of precursor
T	Substrate temperature
T_{bulk}	Bulk temperature
T_{max}	Maximum operating substrate temperature
T_{min}	Minimum operating substrate temperature
$T_{surface}$	Surface temperature
t	Time
t_f	Final batch time
t_0	Initial batch time
$\mathbf{V_\theta}$	Covariance matrix
V_y	Variance of y
$\mathbf{W}$	Vector of microscopic rates
$W(\kappa \rightarrow \kappa')$	Probability per unit time that the system will undergo the transition from

	state κ to state κ'
W_a	Total rate of adsorption
W_d	Total rate of desorption
W_m	Total rate of migration
$\mathcal{X}$	Mole fraction of precursor in the bulk
$\mathcal{X}_{max}$	Maximum applicable bulk precursor mole fraction
$\mathcal{X}_{min}$	Minimum applicable bulk precursor mole fraction
x	Mole fraction of the precursor
x_{grow}	Mole fraction of precursor on the surface
y	Output of the process using the perturbed vector, $\boldsymbol{\theta}$
$\hat{y}$	Output of the process using the nominal parameter vector, $\widehat{\boldsymbol{\theta}}$

List of Greek symbols

α	Confidence level
ΔT	Temperature interval
Δt	Time interval
Δt	Time interval at which growth rate is estimated
$\Delta \mathcal{T}$	Coupling time instance between the macroscopic and the microscopic simulations
$\Delta \mathcal{X}$	Bulk precursor mole fraction interval
δy	Deviation in the output from the nominal output
$\delta y_{w.c}$	Worst-case deviation in y
$\delta \boldsymbol{\theta}$	Perturbation about $\widehat{\boldsymbol{\theta}}$
ε_y	Expected value of y
$\mathcal{E}_\theta$	Uncertainty in parameters
ζ	A uniform random number from a (0,1) interval
$\boldsymbol{\theta}$	Vector of perturbed parameters

$\widehat{\boldsymbol{\theta}}$	Vector of nominal model parameters
$\boldsymbol{\theta}_l$	Lower limit on the vector of uncertain parameters.
$\boldsymbol{\theta}_u$	Upper limit on the vector of uncertain parameters.
μ_b	Viscosity of the bulk
υ_0	Frequency of events
ρ	Density of the mixture
ρ_b	Density of the bulk
ς	A uniform random number from a (0,1) interval
τ	Dimensionless time
$\chi^2_{n_\theta}$	Chi-squared distribution with n_θ degrees of freedom

List of abbreviations

CDF	Cumulative distribution function
KMC	Kinetic Monte Carlo
MD	Molecular dynamic
MIH	Multiscale integration hybrid
MPC	Model predictive control
NMPC	Nonlinear model predictive control
ODE	Ordinary differential equation
PCE	Polynomial chaos expansion
PDE	Partial differential equation
PDF	Probability distribution function
PI	Proportional integral
PSE	Power series expansion
SOS	Solid-on-solid
SSV	Structured singular value

Chapter 1
Introduction

Nanotechnology, biotechnology, and micro-engineering are mostly characterized by coupled chemical and physical phenomena occurring over different temporal and spatial scales. In these applications, controlling the events that evolve at the microscopic scale is essential to product quality. Efficient operations, however, require manipulated variables at the macroscopic scale for real-time feedback control (Braatz et al., 2006b). Therefore, multiscale modeling and analysis has emerged to improve the predicting capabilities in these systems by linking various length and time scales (Vlachos, 2012).

Microelectronics is a field where multiscale simulation, design and control has many applications. Due to the wide range of applications of thin film semiconductors, improving manufacturing efficiency while minimizing the costs is required (Baumann et al., 2001; Datta and Landolt, 2000). In industrial practice, these processes are currently operated empirically, without a deep knowledge of the underlying dynamics. Therefore, the development of efficient control methodologies for thin film deposition is needed to satisfy the increasingly stringent requirements in the semiconductor industry. However, three main obstacles hinder the progress in this field: *i*) development of fundamental mathematical models describing the system for optimization and control, *ii*) lack of practical *in-situ* sensors that provide real-time measurements for online control, and *iii*) uncertainties in the deposition process that are not captured by the prevalent, nominal models (Raimondeau and Vlachos, 2002).

The microelectronic devices are composed of deposited, patterned, successive layers of silicon, insulators and metals (Datta and Landolt, 2000). Thin film deposition from the gas phase is the key process in microelectronic fabrication where the atoms of the precursor deposit on the substrate to create a thin solid film (Dollet, 2004). The electrical and mechanical properties of electronic devices depend on thin film microstructure. Spatial uniformity, thickness, composition, the amount of internal defects, and also interfacial roughness and slope are referred to as critical thin film properties (Freund and Suresh, 2004). While uniformity and composition are macroscopic properties that can be modeled based on continuum hypothesis, accurate control of the thin film microstructure requires a comprehensive hierarchical model that can integrate a wide range of length and time scales (Armaou et al., 2001). To control the film properties, the thin film deposition process, and its interaction with the surroundings, need to be considered

(Braatz et al., 2004). Thin film microstructure is determined through the surface microscopic events that are strongly dependent on macroscopic phenomena; thus, multiscale modeling tools are required to provide efficient control and optimization frameworks. The evolution of the growth process on a substrate can be modeled based on a multiscale approach, coupling a deterministic continuum model representing the macroscopic scale events and a stochastic lattice-based KMC model, which describes the microscopic surface morphology (Lam and Vlachos, 2001). Although multiscale modeling is an attractive alternative tool compared to the application of molecular modeling techniques for the entire process domain, this approach often requires computationally intensive simulations. This results in profound limitations towards the development of real-time model-based control strategies for these systems.

Measuring the microscopic properties of the thin film during the fabrication process is not trivial since it is infeasible to have direct access to the surface. Although the recently introduced optical *in-situ* sensors have triggered research on feedback control of the thin film deposition process, their application is still limited in practice (Buzea and Robbie, 2005). The main limitation of these optical devices is that they are not capable of providing the measurement as frequent as it is required for online applications (Nayar et al., 1993). Hence, real-time estimators are needed to estimate the controlled outputs at a time scale comparable to the real thin film growth process while online measurements are not available. Although KMC models have been adopted for estimation and control in a few cases, the unavailability of a closed-form model constrains their applications in model-based control and optimization approaches (Lou and Christofides, 2003a).

From the modeling point of view, the evolution of the thin film encompasses microscopic processes that are subject to model parameter uncertainty (Braatz et al., 2006b). The microscopic model includes parameters that have to be either measured or inferred through fine-scale experimental data (Raimondeau et al., 2003). The estimation of these parameters is not straightforward and most of the values are not known with absolute certainty due to the limited and noisy measurements (Ulissi et al., 2011). The performance of model-based control and optimization approaches is directly affected by the accuracy of the model; not accounting for uncertainties can lead to significant losses in performance (Nagy and Braatz, 2003a). Therefore, quantifying the influence of parameter uncertainties on the process states and outputs is essential to improve productivity in industrial applications. Despite the efforts made for parameter

optimization, model-plant mismatch has mostly been overlooked in control and optimization of thin film deposition processes, mainly due to the computational costs of uncertainty analysis in multiscale process systems (Prasad and Vlachos, 2008; Raimondeau et al., 2003). The common approach for uncertainty propagation is the application of a sampling-based technique on the process model. In a thin film deposition process, however, the current multiscale models are computationally prohibitive to assess product variability using the traditional sampling-based methods. Analytical techniques such as power series expansion (PSE) and polynomial chaos expansion (PCE) provide a practical approach to this problem since the complex multiscale model can be approximated with a mathematical expansion.

1.1. Objectives and contributions

Currently, the common form of process control applied in the semiconductor industry is a run-to-run control scheme where the post process *ex-situ* measurement data are used to update the recipe for the next run. The recipe for the batch run specifies the set points for inputs and states to produce the desired device characteristics. The data obtained from each batch are employed to adjust the recipe to reduce variability in the manufactured devices. In this approach, the control actions are adjusted after the deposition process and the operating conditions cannot be modified during the process. Recent advances in computational power and *in-situ* sensors motivate the development of efficient methodologies for the design and online control of these processes. Despite the extensive body of research on multiscale system analysis and design, there are still many unresolved issues leading to a significant gap between the real world and the current methodologies. Model-plant mismatch is an important aspect in model-based control and optimization frameworks. To provide a robust online control and optimization framework, the effect of model parameter uncertainty in performance objectives has to be considered.

Based on the above, the goal of this research is to make the control of multiscale processes more realistic by addressing model parameter uncertainty in control and optimization applications. Therefore, assuming that the multiscale model captures the underlying structure appropriately, the structural uncertainty is not considered in this study. The specific objectives of the current study are outlined as follows:

- Perform an uncertainty analysis to evaluate the effect of model parameter uncertainties on thin film properties employing PSE. The PSE method is used to predict the deviation

of the performance objective from the nominal performance in thin film deposition process in the presence of model parameter uncertainty. The evolution of the epitaxial growth process on a substrate is simulated using a multiscale approach, coupling a continuum gas phase model and a KMC model that describes the evolution of the surface of the thin film.

- Develop an algorithm for open-loop optimization of thin film deposition process under uncertainty. The deposition process is considered as a batch process where open-loop optimization can be performed offline. Systematic algorithms are presented to determine probabilistic bounds on thin film properties for optimization purposes.
- Develop a robust estimator under model parameter uncertainty to evaluate the controlled outputs efficiently for online control applications in the lack of sensors. A real-time multivariable estimator is developed based on the offline identification of models using input-output data collected from the multiscale model.
- Develop a closed-form model for robust model predictive control (MPC) framework. Offline identification is performed to identify the parameters of the closed-form model that can predict the controlled outputs in the presence of model parameter uncertainty. This model can either be used as an estimator for feedback control purposes in the lack of sensor or as a basis for the design of a robust NMPC algorithm that controls the thin film deposition process.

To design a robust optimization or control framework, it is essential to take model parameter uncertainty into account. Specifically, when the performance objective of the system is highly sensitive to unpredictable or sudden changes in the system's physical parameters, this model inaccuracy or mismatch can significantly lead to loss in performance. Hence, this research provides insight regarding the qualitative and quantitative effects of parameter uncertainty in multiscale process systems. Moreover, the methods developed in this research enable accurate online control of the key properties of a multiscale system in the presence of model-plant mismatch.

1.2. Outline of the thesis

The remainder of this thesis is organized as follows:

- Chapter 2 reviews the literature pertaining to multiscale analysis and design. The importance of developing these models to bridge microscopic and macroscopic domains is indicated. The challenges associated with the multiscale modeling and control and the proposed approaches to tackle these issues are described at the end of this chapter.
- Chapter 3 provides the detailed mathematical model of the thin film deposition process which has been considered as a case study of the multiscale process system in this research. The mathematical formulation describing the macroscopic modeling of the gas phase and the microscopic modeling of the thin film surface are presented. Moreover, the dependence of the accuracy and fluctuations in the results on the lattice size in the KMC simulation is illustrated in this chapter.
- Chapter 4 presents a comparison between worst-case and distributional uncertainty analysis in a thin film deposition process in the presence of time-invariant model parameter uncertainties. The worst-case deviation in the film properties is obtained under bounded parameter uncertainties while the probabilistic bounds are estimated under distributional uncertainties. This work has been published in ADCHEM (International Symposium on Advanced Control of Chemical Processes) (Rasoulian and Ricardez-Sandoval, 2015a). Moreover, a systematic framework is explored to obtain the probabilistic bounds on the outputs in the presence of time-varying parameter uncertainties. These bounds are employed to determine the optimal temperature profile that maximizes the final thickness of the thin film under end-point product constraints and uncertainty in the model parameters. This work has been published in *Chemical Engineering Science* (Rasoulian and Ricardez-Sandoval, 2014).
- Chapter 5 presents an algorithm to develop a multivariate robust estimator that predicts the controlled outputs in a thin film deposition process for online applications. In the estimator, the issue of computationally intensive KMC simulations is circumvented by developing low-order models that are identified offline based on data collected from the thin film deposition multiscale model described in Chapter 3. The estimator predicts the surface roughness and growth rate based on the substrate temperature and the bulk precursor mole fraction during the deposition process. To provide robust estimates, the estimator is designed to evaluate upper and lower bounds on the outputs under model parameter uncertainties. To assess the uncertainty propagation into the system's outputs,

the PSE method is employed in the presence of distributional parametric uncertainties. The estimator has been coupled with traditional feedback controllers to evaluate the performance of the system in the lack of online measurements and under uncertainty in the multiscale model parameters. Although the performance of the estimator is illustrated in the presence of parameter uncertainties that are normally distributed around their nominal values, the algorithm presented in this chapter is applicable regardless of the probability distribution assigned to the uncertain parameters. The framework presented in this chapter has been published in *Journal of Process Control* (Rasoulian and Ricardez-Sandoval, 2015b).

- Chapter 6 presents nonlinear model predictive control (NMPC) applied to a thin film deposition process in the presence of model-plant mismatch while ensuring constraints on the control actions and thin film properties. A closed-form model is identified offline to predict the surface roughness and film thickness during the deposition process at a predefined specific probability. The resulting closed-form models are used as the internal models in a robust NMPC framework that aims to minimize the final surface roughness while satisfying constraints on the temperature trajectory and film thickness at the end of the deposition process. In this approach, conservative control actions are predicted by the NMPC algorithm. This work has been published in *Chemical Engineering Science* (Rasoulian and Ricardez-Sandoval, 2015c). To improve the robust performance using probabilistic constraints, closed-form models are extended to estimate the statistical moments of the thin film properties. The parameters of the closed-form model are determined offline based on the PSE method applied on the multiscale model. To evaluate the model, a shrinking horizon NMPC framework is designed to minimize the surface roughness at the end of the batch by manipulating substrate temperature in the presence of uncertainty in the multiscale model parameters. However, probabilistic constraints are assigned on film thickness obtained at the end of the batch to reduce the conservatism of the MPC framework (Rasoulian and Ricardez-Sandoval, 2015c). The model developed in this work enables the reformulation of the stochastic NMPC as a computationally tractable deterministic NMPC framework. This work has been submitted to *Chemical Engineering Science*.
- Chapter 7 provides the conclusions and recommendations derived from this research.

Chapter 2
Background and Literature Review

Modeling tools for processes occurring at specific time and length scales have been extensively explored in the literature. Recent emerging applications in material, medicine and biology, however, require the controllability of events at the molecular scale using process variables that can be adjusted at macroscopic scales (Vlachos, 2005). Efficient multiscale modeling techniques have been introduced by connecting the various models to represent phenomena occurring over different length and time scales (Crose et al., 2015; Kwon, 2015). Thin film deposition is an industrially relevant process that can be decomposed into phenomena occurring at various scales and multiscale modeling analysis are required to describe this process (Baumann et al., 2001).

Thin film manufacturing through deposition of advanced materials is widely applied in the semiconductor industry. Strong dependence of the electrical properties of the devices on the microstructure of the film has motivated research on modeling and control of the thin film deposition process (Jensen et al., 1998; Rodgers and Jensen, 1998). Despite the extensive body of research, there are still many unresolved issues leading to a significant gap between the expected and the actual performance achieved by the current control methodologies (Christofides and Armaou, 2006). This gap is mainly related to the complexities associated with the multiscale nature of the thin film deposition process, lack of practical and reliable online *in-situ* sensors at the micro-scale level, and uncertainties in the mechanisms and parameters of the system (Ricardez-Sandoval, 2011).

The aim of this chapter is to review the research efforts that have been conducted on multiscale modeling and control. The next section presents an overview of the multiscale modeling analysis. The current challenges in multiscale modeling analysis are discussed in Section 2.2. As it was described in the Introduction, the uncertainty analysis is the focus of the present research project. Despite the importance of this subject, model-plant mismatch has mostly been ignored in multiscale optimization and control approaches. Therefore, in Section 2.2, a thorough discussion on the different approaches for uncertainty analysis of continuum models is also presented. Section 2.3 reviews the challenges in optimization and control of multiscale process systems and the proposed approaches in the literature to address these issues. Due to the relevance to this work, the approaches proposed for thin film deposition process are discussed in detail. A summary of this chapter is provided in Section 2.4.

2.1. Multiscale modeling

Chemical process systems are typically modeled under the continuum hypothesis employing momentum, energy and mass conservation laws. However, there exist processes where the detailed modeling requires capturing phenomena that occurs over multiple interacting scales (Braatz et al., 2004). In microelectronic processes, macroscopic phenomena such as heat and mass transfer of the gas phase can be adequately modeled using continuum modeling, whereas the fine-scale is driven by physicochemical events that occur at time and spatial scales that cannot be modeled using the laws of classical mechanics (Braatz et al., 2006a). At fine-scale, discrete models including Molecular Dynamic (MD) or KMC are required to describe the behaviour of individual entities such as atoms and molecules. While discrete models provide more insight on the fundamental behaviour of systems, they are computationally intensive and cannot be used to simulate the entire process domain (Nieminen, 2002). To address this issue, multiscale modeling and analysis has emerged as an attractive tool to improve the predicting capabilities in these systems (Vlachos, 2012). The fundamental goal of multiscale modeling is to develop a mathematical framework that bridges various scales ranging from atomistic to macroscopic.

A typical approach in multiscale modeling is evaluating the required information at a finer scale and passing it to a coarser scale in the model. For instance, *ab initio* calculations of reaction rate constants as functions of pressure and temperature requires no further knowledge from the reactor scale. This unidirectional information passing is usually effective when the time and length scales are well separated and there is no overlap between them. Accordingly, the model does not provide any feedback from the coarse-scale to fine-scale and this approach is referred to as serial or sequential multiscale approach (Vlachos, 2005). However, when there is a strong coupling between various scales, integration and simulation is more challenging. When processes exhibit well separated length scales between phenomena, different models can be used at each scale. This type of multiscale modeling, which is based on domain decomposition, is termed as multiscale integration hybrid (MIH) approach. To bridge different domains, an interfacial region can be adopted in which both models are solved and exchange the information. This region is referred to as the *overlapping subdomain* or the *handshaking region* and is shown in Figure 2-1. The size of this region needs to be properly adjusted since both models are solved at this interface region. On the one hand, the interface has to be small enough in order to reduce

the computational costs of the microscopic scale and, on the other hand, sufficiently large for letting the macroscopic model to appropriately relax over the domain.

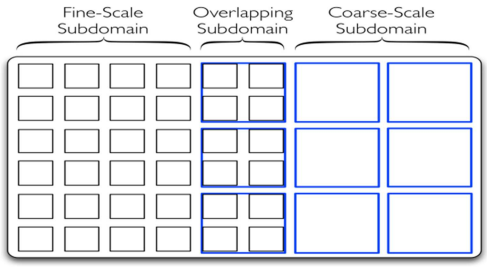

Figure 2-1. Schematic of the overlapping region in the MIH scheme.

In the MIH scheme, a solution strategy is performed involving simultaneous advancement of both fine and coarse-scale simulations. Two scales are solved independently and the quantities that are required at the *overlapping subdomain* are evaluated. In spatially homogeneous systems where there are no spatial gradients at the interface region, the information is exchanged at specific (coupling) time intervals. Following this idea, the fine-scale model has to evolve multiple time steps for every macro time step of the upper scale model. This simultaneous time evolution continues up until the final simulation time is reached. Processes that involve interfacial regions with spatial gradients are also common in engineering such as flow along a tubular reactor or growth on a large wafer with non-uniformities across the substrate (Albo et al., 2006). The gap-tooth technique has been proposed for coupling the coarse and fine-scale in the heterogeneous systems (Gear et al., 2003). As shown in Figure 2-2, this method applies a coarse mesh over large scales while at each node of the coarse mesh, fine-scale simulations using discrete models are performed on a finer mesh. Thus, multiple fine-scale models are simultaneously solved in this approach and the properties computed from these simulations are averaged and used to update the coarser mesh.

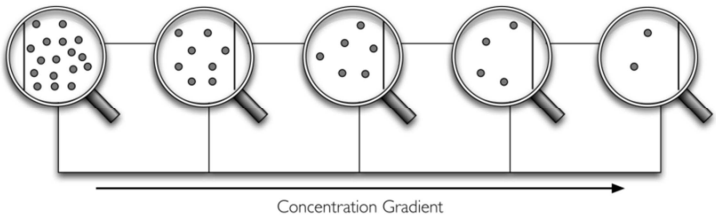

Figure 2-2. Schematic of multigrid-type simulation (adopted from (Vlachos, 2005)).

As it will be discussed in detail in Chapter 3, the evolution of the thin film studied in this work is modeled using nonlinear partial differential equations (PDEs) embedded with lattice-based

KMC simulations to capture the multiscale essence of the process (Lam and Vlachos, 2001). Traditionally, Monte Carlo simulations are used to evaluate the system properties at equilibrium; nevertheless, if the rates of the events occurring in the process can be estimated, they can also be used to study the transient evolution of the system from one state to another. While continuum modeling is a well-established area, the implementation of stochastic KMC methods to describe the evolution of phenomenological events occurring at the fine scales in non-equilibrium systems has been recently developed. Therefore, master equation and KMC technique are reviewed in detail next.

Master equation & KMC. Due to the stochastic nature of the processes taking place at the fine-scale, the probability that the system is in a particular configuration or state can be described using the so-called master equation (Kampen, 1992):

$$\frac{d\mathcal{P}(\kappa,t)}{dt} = \sum_{\kappa'} W(\kappa' \to \kappa)\mathcal{P}(\kappa',t) - \sum_{\kappa'} W(\kappa \to \kappa')\mathcal{P}(\kappa,t), \qquad (2\text{-}1)$$

where κ and κ' denote two successive states of the system, $\mathcal{P}(\kappa,t)$ is the probability that the system is in state κ at time t, and $W(\kappa \to \kappa')$ is the probability per unit time that the system will undergo the transition from state κ to state κ'. The master equation is a system of first-order ordinary differential equations (ODEs) where each equation represents the probability of an individual state in the system at a certain time. While the solution of the master equation can be obtained using traditional numerical methods for solving ODEs, the challenge of finding a solution lies on the number of states that need to be evaluated. For systems with even a relatively small size, the master equation cannot be solved since the number of possible states is prohibitively large, e.g., a surface lattice consisting of 100 sites with a maximum height of one has 2^{100} number of configurations. This imposes a limitation towards the direct application of the master equation to obtain an estimate of the system states.

A lattice-based KMC can be used as a representative of the microstructure and the KMC method provides a numerical solution to the underlying master equation (Gillespie, 2001). In this method, the states of the system are defined by occupancy of lattice sites (Dooling and Broadbelt, 2001). In contrast to MD where every vibrational change is tracked, this method assumes that the system consists of diffusive jumps from one state to another (Gilmer et al., 2000). That is, the entire system will be moved from one state to another as opposed to moving atoms to new states as it is performed in MD simulations. Hence, the KMC simulations are not

employed to determine the exact position of atoms but to evaluate the statistical properties of the microscopic system (Voter, 2007). These state-to-state transitions allow KMC to reach longer time scales, typically in order of seconds. The transition rates in the KMC simulations are independent from previous states and identify the probability per unit time that the system proceed from one state to another. Stochastic realizations that describe the evolution of a system can be obtained through KMC simulations since this method reconstructs the probability distributions of the system states and their corresponding statistics.

The theoretical foundation of KMC shows that the KMC method can provide a stochastic representation of the master equation if the following conditions are satisfied (Fichthorn and Weinberg, 1991):

- Dynamical hierarchy of transition probabilities that satisfies the detailed balance criterion is created.
- The events taking place in the system are independent.
- Time increments can be estimated precisely.

In the KMC algorithm, the microscopic rates of all possible processes are evaluated from the current state of the system. Based on the current probabilities of occurrence of those processes, a process is selected using a random number taken from a uniform distribution. Once the event has been executed in the system, the time is incremented employing a second random number taken from an exponential distribution. Updating the transition probabilities and modifying the configuration appropriately is essential for the next step execution (Reese et al., 2001). The generic flowchart of the KMC algorithm is presented in Figure 2-3 (Chatterjee and Vlachos, 2007). The implementation of the KMC method for the thin film deposition process is presented in detail in Chapter 3.

Molecular simulations based on KMC models are useful to link microscopic interactions to macroscopic descriptions; however, they are stochastic, nonlinear and typically high dimensional. In response, methodologies have been proposed to construct low-order approximations of the master equation (Gallivan and Murray, 2004, 2003). The model reduction in these approaches is performed by grouping microscopic configurations with similar overall statistics that evolve in a fixed ratio, and removing the states that are unlikely to occur. The low-order model describes the evolution of these probabilities in time which are further used to

update the surface properties. The main disadvantage of that approach is that the resulting model is constrained to a specific set of inputs and a particular range of time scales.

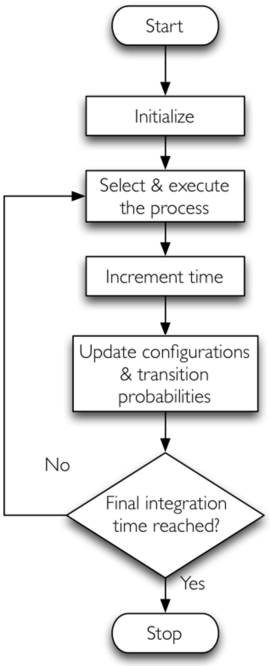

Figure 2-3. Flowchart for KMC algorithm (adopted from (Chatterjee and Vlachos, 2007)).

2.2. Challenges in multiscale modeling

The advances in computer science and optical sensors have resulted into a considerable progress in multiscale modeling research during the past decade. However, this field is still in its elementary stages and presents a variety of challenges (Braatz et al., 2006b; Ricardez-Sandoval, 2011). Specifically, coupling between the macro-scale and fine-scale models is challenging since models at different scales are of different nature and their communication is not straightforward. In spatially homogeneous systems, the temporal mismatch between the continuum and non-continuum codes can make the coupling of the models numerically instable (Rusli et al., 2004). To address this issue, filtering approaches have been proposed to reduce the fluctuations of the data passed from the stochastic micro-scale code to the continuum code (Drews et al., 2004b; Lou and Christofides, 2003a). In another approach, a robust feedback-feedforward controller is designed to maintain the fluctuations bounded between the KMC and finite difference codes (Rusli et al., 2006). In heterogeneous systems, KMC simulations provide the steady-state conditions at the interface of the coarse and fine-scale models. However, due to fluctuations in

the KMC solutions, the identification of steady-state is not trivial and filters are required to suppress the noise in the data passing to the coarse-scale (Majumder and Broadbelt, 2006). In this section, the challenges in the modeling and analysis of the multiscale systems are briefly outlined.

2.2.1. Computational intensity

Simulation of microscopic models typically requires high computational costs compared to continuum models. There are two aspects in the KMC method that makes it computationally intensive: *i*) relatively short simulation time steps (in the order of microseconds), and *ii*) execution of only one event at each step of the algorithm (Schulze, 2008). High computational costs of KMC simulations have motivated significant research efforts to accelerate this method (Chatterjee and Vlachos, 2007). To address this issue in lattice-based KMC method, reduced-order lattices can be applied in the KMC simulation with periodic boundary conditions at the edges as a representative of the process. This modeling approach enables capturing of the statistical properties of a large scale stochastic process using a limited lattice size in the KMC simulation (Makov and Payne, 1995). Spatial coarse-grained Monte Carlo is another approach that has been proposed to overcome the computational requirements of this method. This approach enables the simulation of larger length and time scales at reasonable computational costs by grouping the lattice sites into coarse cells (Katsoulakis et al., 2003). This scheme assumes that local equilibrium is acquired within a coarse cell (Drews et al., 2004a).

One of the drawbacks in the conventional KMC method is that it executes only one event at a time. This characteristic drastically limits the computational efficiency of the KMC simulation (Gillespie, 2001). To tackle this issue, temporal coarse graining has been proposed for coarse-grained lattices which is referred to as τ-leaping method (Vlachos, 2008). Acceleration in this method is achieved by executing multiple processes at once on a coarse-grained lattice and advance the time by a coarse amount τ under the τ-leap condition. In this approach, the sites with the same transition probability are grouped into the same class and τ-leaping is applied to the classes without violating the leap condition. This condition restricts τ to small values such that the change in the population for all chemical processes is small. The main assumption of this approach is that the transition probabilities are fixed and independent from each other.

2.2.2. Sensitivity analysis

Parameter sensitivity analysis is a valuable tool to identify parameters that play a significant role in system responses that have to be optimized or determined more accurately through experimental data (Saltelli et al., 2005). In optimal experimental design approaches, density functional theory calculations usually provide the prior estimates of the parameters and the parameter estimations are improved using data obtained from experiments (Braatz et al., 2006b). Application of conventional sensitivity analyses on multiscale systems, however, is not straightforward since most of the fine-scale models are not available in closed-form (Gunawan et al., 2005). That is, explicit expressions to evaluate the rate of change of the outputs of the system with respect to the model parameters are not available. This motivates the application of a black box approach such as brute force sensitivity analysis using finite differences. Although the application of finite differences method is straightforward, it is computationally demanding especially for multiscale systems. Efficient gradient estimation methods have been proposed in the literature for sensitivity analysis of these processes (McGill et al., 2012). In molecular simulations, alternative approximation methods are employed to map the key parameters to the simulation outputs (Rusli et al., 2007). That is, in the parameter optimization algorithm, the computationally intractable molecular simulations are replaced with a PSE that relates the output to the parameters (Braatz et al., 2006b).

Another issue in multiscale parameter sensitivity analysis is the inherent noise due to the discrete microscopic simulations. Hence, employing finite difference approaches requires relatively large perturbations to isolate the response from the intrinsic noise provided that the average of multiple runs is applied. A sensitivity analysis study of the model parameters involved in copper electro-deposition was conducted using finite differences (Drews et al., 2003). Condor, a high throughput computing environment, was utilized to perform this computationally intensive investigation. It has been demonstrated that the outputs of the system are sensitive to 7 out of 22 parameters studied in that work. Owing to high number of states or parameters associated with multiscale systems, clustering is an attractive method to obtain a reduced set of parameters for the system (Raimondeau et al., 2003). Moreover, experimental design studies has gained attention for parameter optimization at molecular scales (Prasad and Vlachos, 2008). In this approach, the multiscale model can be reduced using clustering or

principal component analysis to provide a computationally tractable identification algorithm (Subramanian et al., 2011).

Developing low-order models for optimization and control of multiscale systems can be performed using sensitivity analysis techniques. Moreover, many uncertainty analysis approaches take advantage of sensitivity analysis to propagate the uncertainties into the states and outputs of the system.

2.2.3. Uncertainty analysis

In model-based control and optimization frameworks, the process performance depends on the accuracy of the model used to describe the real process. In process modeling analysis, the discrepancy between the process and the model seems to be the rule rather than an exception. Uncertainties can be classified as structured and parametric uncertainties. Structured uncertainty arises due to incomplete knowledge about chemical and physical processes, inadequate numerical schemes and resolutions. Parametric uncertainty, on the other hand, is the result of inaccuracies in model parameters, initial conditions and boundary conditions. In the current work, it is assumed that the multiscale model used for the thin film deposition process captures the underlying structure appropriately; thus, structural uncertainty is not considered in the present study. Parametric uncertainty, however, can potentially occur and hence will be extensively studied here in the context of multiscale modeling analysis. To quantify the effect of parametric uncertainty on the system performance, uncertainty analysis is required. There are two fundamental steps for uncertainty quantification in process systems: *i*) characterization of parameter uncertainties, and *ii*) propagation of uncertainties through the process model. Parameter uncertainty can be characterized using data collected from the actual process; however, when access to plant data is not available, the uncertainty description is typically assumed to be bounded or takes the form of a probability distribution function (PDF) centered at a nominal value. Therefore, despite the importance of uncertainty characterization, in robustness analysis the form of the parameter uncertainty is often considered as a prior knowledge (Halemane and Grossmann, 1983; Rooney and Biegler, 1999).

To guarantee closed-loop performance under bounded parameter uncertainty, robust formulations have been proposed based on the worst-case deviation in the process performance (Braatz et al., 1994; Ma et al., 1999; Ma and Braatz, 2001). In a semiconductor manufacturing

process, this method has been applied to obtain the optimal rapid thermal annealing program that minimizes the junction depth while maintaining a satisfactory sheet resistance (Gunawan et al., 2004). This approach has been applied in this research to determine the optimal temperature profile using the worst-case deviation in the thin film properties. This method and its application on the deposition process will be explicitly discussed in Chapter 4.

For distributional uncertainties, the classical Monte Carlo method is the common approach used to produce the PDFs of the states and outputs of the system under uncertainty. Monte Carlo is a sampling-based technique that takes advantage of a large number of sample points chosen randomly from the prior distribution of parameters and a model to propagate the uncertainties into the model outputs. Despite the efficient sampling method proposed to reduce high computational costs, this method is not suitable for real-time robust applications (Birge and Louveaux, 2011; Niederreiter, 1978). In addition to high computational costs especially for complex systems, this method does not provide a mathematical representation of the process. Distributional uncertainty analysis of complex dynamic processes such as multiscale systems using Monte Carlo technique is computationally prohibitive. Alternatively, for efficiency, the original complex model can be approximated employing either PSE or PCE (Xiu, 2010). Taking advantage of a prior knowledge about the distribution of the uncertain parameters, a distributional uncertainty analysis of the states and outputs can be performed using PSE or PCE. Uncertainty analysis using these expansions has initiated significant advances in the robust optimal control of batch processes (Mandur and Budman, 2014; Nagy and Braatz, 2004). It has been shown that, while first-order expansions provide acceptable accuracy, higher order expansions can improve the accuracy in the predictions (Bahakim et al., 2014; Nagy and Braatz, 2007). The key advantage of the PSE approach is that it is not necessary to have the analytical expression for the function since it only requires the function sensitivities with respect to the uncertain parameters. Following this approach; the issue of absence of closed-form models can then be addressed by deriving a low-order model.

An alternative tool for distributional uncertainty analysis is the PCE (Ghanem and Spanos, 2003; Wiener, 1938). Uncertainty analysis using this method has initiated significant advances in the robust optimal control of batch processes (Mandur and Budman, 2014; Nagy and Braatz, 2004). The PCE technique is appropriate for highly nonlinear processes or when a large variability in the uncertain parameters is expected (Najm, 2009).

2.3. Challenges in control of multiscale processes

The majority of cutting-edge semiconductors are manufactured through batch processes in the microelectronics industry (Gorman and Shapiro, 2011). The objective of a generic process unit operation is improving manufacturing efficiency while minimizing plant costs. In batch processes, systematic methodologies are needed to optimize product quality specifications under tight operational constraints (Christofides et al., 2007). The film microstructure, however, is determined by the surface microscopic events that strongly depend on the macroscopic behaviour of this process. As such, highly efficient control and optimization frameworks are needed to achieve specific thin film's characteristics by manipulating the macroscopic variables of the process (Ulissi et al., 2013). As an illustrative example, an integrated circuit entails several layers of thin films and the device performance depends on the sharpness of these patterned thin films, the interface between layers and the microstructure configuration of the films (Datta and Landolt, 2000). Moreover, thin film deposition is sensitive to unmeasured disturbances, contaminants and deposition on the reactor walls which affect product reproducibility. Thus, advanced control strategies are required to improve product quality specifications (Braatz et al., 2006a). In essence, the basis of an advanced control framework is a closed-form model that represents the complex dynamics of the process under study. Particularly, in a MPC framework, which is the most prominent advanced control strategy, a system model is required to predict the control actions which optimize the performance index in the presence of constraints (Allgöwer et al., 2004; García et al., 1989; Qin and Badgwell, 2003). There are, in essence, three major obstacles that limits the performance of a control scheme in the thin film deposition process: *i*) the lack of practical *in-situ* sensors that provide real-time, micro-scale measurements for online applications, *ii*) the lack of a closed-form expression for mode-based control and optimization purposes, and *iii*) model-plant mismatch.

2.3.1. Lack of sensor

Thin film deposition has a wide range of applications in the microelectronic industry, optics and photovoltaics. Real-time measurements at the surface of the thin film, however, are not practical and usually offline measurements techniques are employed only at the end of the batch process (Renaud et al., 2003). Implementation of feedback control approaches to design high-quality nanostructures in a high-throughput manufacturing setting is impractical without real-

time measurements (Su et al., 2008). In a methodology, the combination of online gas phase composition measurements with offline roughness measurements has been applied for feedback control of surface roughness (Ni et al., 2004). Recently, the development of modern measurement techniques has enabled to obtain the required data in real-time. The available *in-situ* thickness and deposition rate monitoring sensors has been extensively reviewed (Buzea and Robbie, 2005). Spectroscopic ellipsometry, and grazing incidence small range X-ray scattering are introduced to assess the microstructure of the thin films (Pickering, 2001). Particularly, spectroscopic ellipsometry is a non-intrusive, sensitive tool that can provide the measurements in real-time (Liu et al., 1999). The major limitation of this sensor is that it provides an indirect measurement technique where model-based estimators are needed to infer the film properties from the data provided (Grover and Xiong, 2009; Xiong et al., 2006). While these sensors present novel techniques for monitoring and control purposes, they are not able to provide measurement at a frequency that is required for online control applications. Hence, real-time estimators are needed to estimate the controlled outputs at a time scale comparable to the real thin film deposition process while online measurements are not available. Efficient estimation strategies are explored based on the reduction of the KMC model to control the thin film properties that cannot be measured directly (Gallivan, 2005). A methodology for real-time estimation of thin film properties during the growth process has been proposed based on lattice-based KMC simulations, an adaptive filter and a measurement error compensator (Lou and Christofides, 2003a, 2003b). In that methodology, although state-of-the-art sensors are required to improve the estimations, frequent measurements are not available for an efficient online control (Lou and Christofides, 2004). To provide a computationally tractable approach, reduced-order lattices are employed in the KMC simulations.

2.3.2. Lack of closed-form model

Multiscale models are not available in closed-form and are computationally prohibitive for online applications. In KMC simulations, the lattice size determines the accuracy of the results and the simulation time. Although employing reduced-order lattices in the KMC simulations are computationally efficient, the results obtained from these simulations are noisy compared to high-order lattices. Computationally efficient estimators have been developed using the average of responses from multiple reduced-order lattices in the KMC simulations. The proposed

estimator has been coupled with a proportional integral (PI) controller to control the surface roughness manipulating the substrate temperature (Lou and Christofides, 2003a). That control methodology has also been extended to multivariable feedback control of surface roughness and growth rate (Lou and Christofides, 2003b). To illustrate the effectiveness of the estimator/controller structure proposed in (Lou and Christofides, 2003a), that technique has been employed for closed-loop control in *GaAs* thin film deposition (Lou and Christofides, 2004). A KMC-based MPC scheme for film deposition has also been proposed in the literature (Christofides et al., 2008).

While it is possible to employ KMC models for estimation and control in a few cases, these models are typically unavailable in closed-form and evolve by successively advancing the state of the system by small incremental time steps (Ni and Christofides, 2005a). There are deposition processes for which closed-form process models describing the surface morphology of thin films can be identified in the form of stochastic PDEs. For instance, the surface height evolution in one-dimensional thin film growth process can be described by Edward-Wilkinson equation (Hu et al., 2008; Lou and Christofides, 2006; Zhang et al., 2010). In these approaches, the construction and validation of the stochastic PDE models are conducted through a set of snapshots obtained from the KMC simulations that cover the complete operating region (Ni and Christofides, 2005a). Taking advantage of these stochastic PDEs, methodologies have been developed for multivariable predictive control of the deposition process (Hu et al., 2009; Ni and Christofides, 2005b).

Although multiscale models embedded with KMC simulations are computationally intensive, these detailed models can be employed to derive low-order models that are practical for model-based control techniques (Varshney and Armaou, 2008a). The input-output behaviour of a coupled KMC and finite difference code is employed to develop a low-order model for copper electrodeposition process (Rusli et al., 2006). For control purposes, reduction of multiscale systems is performed through proper orthogonal decomposition (Raimondeau and Vlachos, 2000; Varshney and Armaou, 2008b). In (Varshney and Armaou, 2006a), the feedback control of thin film microstructure has been achieved via offline identification of a low-order model for a finite set of coarse observable variables. Moreover, a computationally efficient methodology has been proposed to maximize film uniformity and minimize the roughness in a thin film deposition process (Varshney and Armaou, 2005). To efficiently solve a dynamic optimization problem in

GaN film epitaxy process, model reduction techniques have been linked with the vector parameterization scheme (Varshney and Armaou, 2006b). It has been shown that an optimal change in the precursor concentration reduces considerably the thickness non-uniformity in a *GaN* thin film. The low-order model developed through reduction of the master equation has been used to estimate the optimal time-varying temperature profile offline (Gallivan, 2003; Oguz and Gallivan, 2008). In another approach, computationally efficient solution methodologies are developed for optimal operation of spatially distributed multiscale processes (Behrens and Armaou, 2010).

To address the issue of absence of closed-form dynamics, coarse time-steppers have been proposed which enables the integration of macroscopic system level tasks to multiscale systems without driving the required equations in the closed-form expression. The key assumption in this method is that the macroscopic models are available in closed-form for low moments of microscopically evolving distribution. While mapping from microscopic to macroscopic scale (restriction) is unique, mapping from macroscopic to microscopic scale (lifting) is not. This equation-free methodology provides a mean to employ well-established controller design techniques, such as linear feedback control to multiscale process systems (Armaou et al., 2004; Siettos et al., 2003).

2.3.3. Model-plant mismatch

The performance of model-based control and optimization techniques can be deteriorated due to inappropriate or unrealistic assumptions applied in the model development and model uncertainty. Specifically, when the performance objective is highly sensitive to changes in the physical parameters of the system, model-plant mismatch can lead to significant loss in the performance. Although multiscale processes mostly encompass fine-scale features that cannot be known with absolute certainty, model-plant mismatch has mostly been overlooked in the proposed multiscale modeling approaches in the literature. To design a robust control or optimization framework, it is therefore essential to take model parameter uncertainty into account. As a result, multiscale system tools are required to account for uncertain mechanisms and uncertainty in the model parameters.

In thin film deposition, Lou and Christofides have shown that the coupled estimator/controller proposed to control surface roughness is robust in the presence of uncertainty in one of the KMC

parameters (Lou and Christofides, 2003a). This result was only validated using simulations, i.e. a formal uncertainty quantification analysis was not performed in that study. Nagy and Allgöwer have designed a robust shrinking horizon NMPC scheme that aims to minimize the end-point surface roughness and its variance using a second-order PSE technique (Nagy and Allgöwer, 2007). The deposition model considered in that work is a low-order state-space model developed through reduction of the chemical master equation, which describes the temporal evolution of the surface (Gallivan and Murray, 2004). Therefore, the effect of macro-scale was not accounted for in that model. Moreover, that study assumed that state-of-the-art sensors are available to provide accurate measurements for the NMPC algorithm. Therefore, even though model-plant mismatch is an important aspect of process control and optimization, it is still an open problem in multiscale system design.

2.4. Summary

This chapter presented an overview of the recent developments in multiscale process systems analysis. The multiscale modeling approaches proposed in the literature to capture coupled phenomena over different length and time scales have been discussed. Since the focus of the current work is on thin film deposition process, the related works published on control and optimization of this process are reviewed in this chapter. Model parameter uncertainty, lack of closed-form model between manipulated variables and controlled outputs, computationally intensive KMC simulations and sporadic sensor data are among the main challenges in this area. Despite the extensive studies on multiscale systems, the effect of model-plant mismatch in control and optimization applications has mostly been ignored. The current study aims to fill this gap by incorporating model parameter uncertainty into multiscale modeling analysis. The next chapter presents the detailed modeling of the thin film deposition process which is considered as a representative multiscale process in this study.

Chapter 3
Thin Film Deposition Process

Thin film deposition is an industrially relevant process which comprises phenomena that evolve at different time and length scales (Gilmer et al., 1998). The evolution of the film morphology entails microscopic processes such as adsorption of the precursor atoms on the surface or migration of adsorbed atoms on the film surface. While the microstructure of the surface evolves at the fine-scale level, the film deposition process takes place inside a chamber of macroscopic dimensions at specific operating conditions. The simulation of the entire process requires the coupling of micro-scale events, i.e., the surface evolution, with macroscopic phenomena, i.e., the operating conditions in the chamber. Thin film deposition is considered as a simple yet effective representative of a multiscale process system and is used as the case study to evaluate the methods proposed in the current research.

In this chapter, a multiscale model of the thin film deposition is presented and described in detail in Section 3.1. As it is shown below, conventional momentum, energy and mass balances are used to describe the changes in the operating conditions inside the chamber whereas a lattice-based KMC model is used to simulate the evolution of the thin film on the surface. Section 3.2 provides the required formulations to determine the thin film properties. The coupling between the continuum model and the KMC simulation, as well as the solution strategy followed to simulate the thin film multiscale model, are explicitly described in Section 3.3.

3.1. Thin film deposition modeling

For many technological applications, high quality films are produced by the process of vapor deposition (Armaou and Christofides, 1999; Baumann et al., 2001; Granneman, 1993) (Armaou and Christofides, 1999). In a typical vapor deposition chamber, the gas flow in the chamber develops a uniform boundary layer of gas adjacent to the surface of the deposition. This uniform boundary layer of width δ is shown in Figure 3-1. The precursor atoms diffuse from the bulk through this boundary layer to create a thin solid film. In the present study, an epitaxial thin film growth process in the stagnation point flow chamber is considered (Gadgil, 1993). A schematic of this chamber is depicted in Figure 3-2, which employs a gas distributer to provide a uniform distribution in the chamber (Dollet, 2004). To handle the disparate length and time scales, continuum momentum, energy and mass conservation balances are employed to describe the

boundary layer of gas whereas the evolution of the surface microstructure is captured through KMC simulations (Lam and Vlachos, 2001).

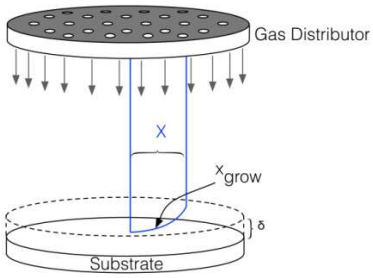

Figure 3-1. Schematic of the boundary layer on the substrate.

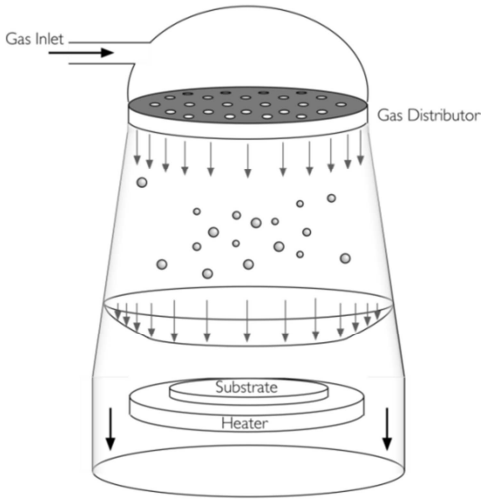

Figure 3-2. Schematic of stagnation point flow vapor deposition chamber.

Creating an axially uniform high velocity flow in the inlet of the chamber is a prerequisite to set up a stagnation point flow system. This condition also avoids the development of velocity, temperature and concentration gradients along the radial direction inside the chamber. Hence, only the gradients in the axial direction are considered in the analysis. This characteristic reduced the spatial dimensions of the PDEs used to describe the momentum, energy and mass balances.

Chamber scale model: modeling the macro-scale. At the macroscopic level, continuum descriptions of fluid flow, heat transfer and mass transfer can be employed as follows (Sharma and Sirignano, 1969; Song et al., 1991):

$$\frac{\partial}{\partial\tau}\left(\frac{\partial f}{\partial\eta}\right)=\frac{\partial^3 f}{\partial\eta^3}+f\frac{\partial^2 f}{\partial\eta^2}+\frac{1}{2}\left[\frac{\rho_b}{\rho}-\left(\frac{\partial f}{\partial\eta}\right)^2\right], \tag{3-1}$$

$$\frac{\partial T}{\partial\tau}=\frac{1}{\mathrm{Pr}}\frac{\partial^2 T}{\partial\eta^2}+f\frac{\partial T}{\partial\eta}, \tag{3-2}$$

$$\frac{\partial x}{\partial\tau}=\frac{1}{\mathrm{Sc}}\frac{\partial^2 x}{\partial\eta^2}+f\frac{\partial x}{\partial\eta}. \tag{3-3}$$

The boundary conditions for the bulk ($\eta\to\infty$) are as follows:

$$T=T_{bulk},$$

$$\frac{\partial f}{\partial\eta}=1, \tag{3-4}$$

$$x=\mathcal{X}.$$

Likewise, the boundary conditions on the surface ($\eta\to 0$) are as follows:

$$T=T_{surface},$$

$$f=0, \tag{3-5}$$

$$\frac{\partial f}{\partial\eta}=0,$$

$$\frac{\partial x}{\partial\eta}=\frac{\mathrm{Sc}(R_a-R_d)}{\sqrt{2a\mu_b\rho_b}}. \tag{3-6}$$

In Eqs.(3-1)-(3-6), f denotes the dimensionless stream function, η is the dimensionless distance to the surface, ρ is the density of the mixture. T is the temperature and Pr is the Prandtl number. x and Sc are respectively the mole fraction and Schmidt number of the precursor. The parameters μ_b and ρ_b are the viscosity and the density of the bulk, respectively; $\mathcal{X}$ represents the bulk precursor mole fraction; a is the hydrodynamic strain rate and $\tau=2at$ is the dimensionless time. R_a and R_d are the rates of adsorption and desorption, respectively. As it will be described later in this chapter, the coupling between the microscopic processes occurring at the surface and the gas phase scale processes is accounted for in the boundary condition indicated in Eq.(3-6).

Surface structure model: modeling the micro-scale. In the KMC algorithm, the microscopic rates of all possible processes or events are calculated from the current state of the system. Based on the current probabilities of occurrence of those processes, a process is selected using a random number taken from a uniform distribution. Once the event has been executed in the system, the time is incremented through another random number. Updating the transition probabilities and modifying the configuration appropriately is essential for next step execution.

The temporal and spatial changes occurring at the surface are dominated by the microscopic processes. In this work, three microscopic processes contribute towards the development of the thin film: *i*) adsorption of atoms from the gas phase to the surface, *ii*) desorption of atoms from the surface to the gas phase, and *iii*) migration of atoms to an adjacent site on the surface. The surface of a simple cubic lattice is used to describe the thin film deposition process. In the present multiscale model, the KMC lattice at any time t is represented as a matrix, **S**, where each element in this matrix represents the number of atom located on each site within the surface lattice, i.e.,

$$\mathbf{S}(t) \triangleq \{h(i,j): i,j = 1 \dots N\}, \tag{3-7}$$

where N denotes the lattice size and $h(i,j)$ is the number of atoms at site (i,j). In the present analysis, the surface of a simple cubic lattice is used to describe the thin film growth. To reduce the computational costs, the method has been implemented for a limited-size lattice assuming periodic boundary conditions at the edges. Another assumption is solid-on-solid (SOS) approximation, based on which, overhangs and vacancies are not allowed and atoms are located directly on top of other atoms on the surface. The interactions among the surface atoms have been considered between only first nearest neighbors. Moreover, the present model assumes that all the surface sites are available for adsorption. As shown in Figure 3-3, the adsorbed atoms can be either desorbed to the gas phase or migrate to an adjacent lattice site depending on the energy barriers and the number of neighbors surrounding that atom.

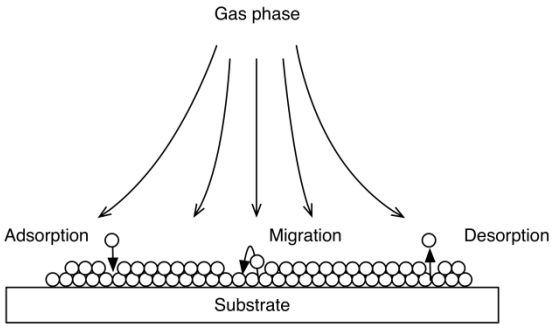

Figure 3-3. Schematic of a thin film growth process on a substrate.

In the adsorption process, an incident atom from the gas phase comes into contact with the film and is eventually incorporated in the surface. The rate of an adsorption event can be determined from the kinetic theory of ideal gases :

$$P_A = \frac{S_0 P x_{grow}}{\sqrt{2\pi m R T} C_{tot}}, \quad (3\text{-}8)$$

where S_0 is the sticking coefficient, P is the total pressure of gas phase, x_{grow} is the mole fraction of precursor on the surface, C_{tot} is the concentration of sites on the surface, m is the precursor molecular weight, R is the gas constant and T is the substrate temperature. Macroscopic scale affects the film growth on the surface through P_A since estimates for x_{grow} are obtained from the solution of the gas phase mass transfer equation. To execute an adsorption event, a site needs to be randomly picked among the sites of the entire lattice and eventually an atom will be added to that site as shown in Figure 3-4.

Figure 3-4. Execution of an adsorption event on the lattice by picking a site and adding an atom on top of that lattice site.

The first nearest neighbors assumption results in five classes of surface atoms, which can have from one (only a vertical bond) neighbor, up to five (all surface bonds and a vertical bond) neighbors. In the present analysis, desorption and migration events are considered to be site-dependent. Therefore, atoms in each class have the same probability of desorption and migration since they have the same number of nearest neighbors.

In the desorption process, an atom overcomes the energy barrier of the surface and returns to the gas phase as shown in Figure 3-5. The rate of desorption depends on the local configuration on the surface and the activation energy. The rate of desorption of a surface atom with *n* first nearest neighbors is as follows:

$$P_D(n) = \upsilon_0 e^{-\frac{nE}{RT}}, \qquad n = 1, \ldots 5, \quad (3\text{-}9)$$

where E denotes the energy associated with a single bond on the surface and υ_0 is the frequency of events, which is determined as follows:

$$v_0 = k_{d0} e^{-\frac{E_d}{RT}}, \tag{3-10}$$

where E_d is the energy associated with desorption and k_{d0} is an event-frequency constant. To implement this event, a desorption class has to be picked among the five classes available. Then, a site from that specific class is selected randomly. Once the site for desorption event is selected, the atom at the top of that site is removed from the surface.

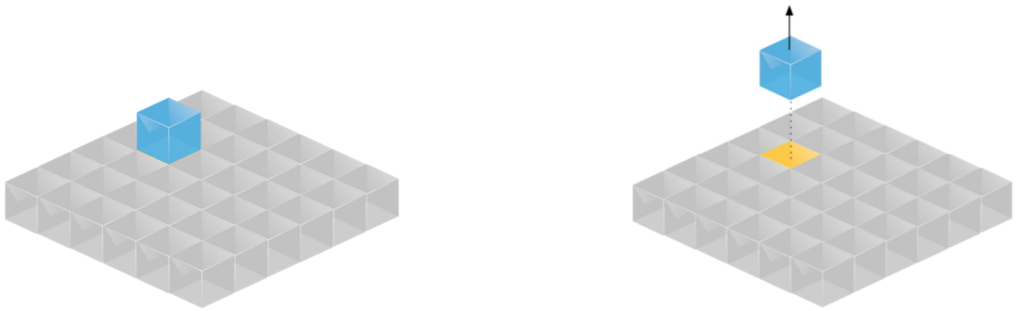

Figure 3-5. Execution of a desorption event on the lattice by picking an atom and removing it from top of the site.

In the migration process, an atom overcomes the energy barrier of the site and jumps to one of the neighboring sites randomly as shown in Figure 3-6. The surface migration process is modeled as desorption followed by re-adsorption. The rate of a migration event on the surface is estimated from the following expression:

$$P_M(n) = v_0 A e^{-\frac{nE}{RT}}, \quad n = 1, \ldots 5 . \tag{3-11}$$

The pre-factor A is associated with the energy difference that an atom on the surface has to overcome in jumping from a lattice site to an adjacent one and is given by:

$$A = e^{\frac{E_d - E_m}{RT}}, \tag{3-12}$$

where E_m is the energy associated with migration. To implement a migration event, one of the five classes needs to be selected. Then, a lattice site will be picked randomly for the execution of this event. The atom located at the top of that site is moved (migrates) to one of its four nearest neighbors. The selection of nearest neighbor site is also performed randomly (Gilmer and Bennema, 1972).

Figure 3-6. Execution of a migration event on the lattice via diffusing an atom to the neighbor site.

The execution of a KMC event, i.e., adsorption, desorption or migration, is accomplished based on the total probabilities of the events. Since the adsorption event is assumed to be site independent, the total rate of adsorption is calculated as follows:

$$W_a = P_A N^2 \,, \tag{3-13}$$

where P_A is calculated from Eq.(3-8). Likewise, the total rates of desorption and migration are estimated as follows:

$$W_d = \sum_{i=1}^{5} M_i P_D(i) \,, \tag{3-14}$$

$$W_m = \sum_{i=1}^{5} M_i P_M(i) \,, \tag{3-15}$$

where M_i is the number of surface atoms with i nearest neighbors. $P_D(i)$ and $P_M(i)$ are defined in Eq.(3-9) and Eq.(3-11), respectively.

These rates are used to select an event through Monte Carlo sampling method. That is, a random number generated from a uniform distribution, ζ, is used to select the next event to be executed on the surface according to the following rules:

$$0 < \zeta < W_a/(W_a + W_d + W_m) \;\rightarrow adsorption$$

$$W_a/(W_a + W_d + W_m) < \zeta < (W_a + W_d)/(W_a + W_d + W_m) \;\rightarrow desorption$$

$$(W_a + W_d)/(W_a + W_d + W_m) < \zeta < 1 \;\rightarrow migration$$

Then, a second random number is needed to pick the site within the lattice where the event will be executed. Upon successful event execution, the time, which was needed to execute the Monte Carlo event on the surface, is incremented using the following expression:

$$dt = \frac{-\ln \varsigma}{W_a + W_d + W_m} \,, \tag{3-16}$$

where ς is a uniform random number from a (0,1) interval and dt is the time increment in the KMC model. The evolution of the thin film growth process including the gas phase model and KMC simulation is performed using MIH algorithm shown in Figure 3-7.

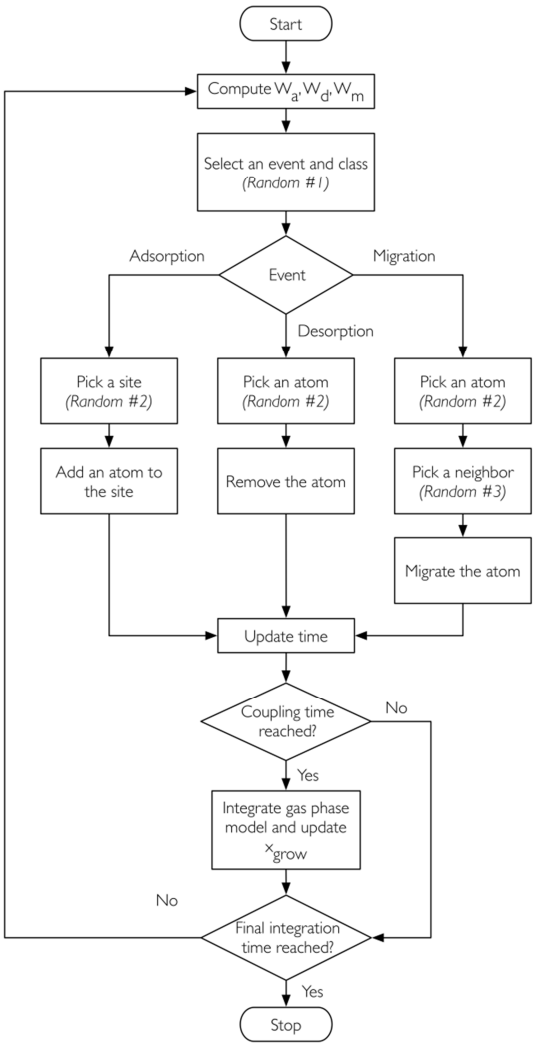

Figure 3-7. Flowchart of the MIH algorithm.

3.2. Surface roughness, film thickness and growth rate

In this study, the quantitative evaluation of the thin film microstructure is assessed using surface roughness. In thin film fabrication, surface roughness is a key factor that determines the electrical and mechanical properties of microelectronic devices. Surface roughness can be determined based on the number of broken bonds on the surface (Raimondeau and Vlachos, 2000):

$$r = 1 + \frac{\sum_{i,j}(|h_{i+1,j}-h_{i,j}|+|h_{i-1,j}-h_{i,j}|+|h_{i,j+1}-h_{i,j}|+|h_{i,j-1}-h_{i,j}|)}{2N^2}, \quad (3\text{-}17)$$

where $h_{i,j}$ is the number of atoms deposited at the lattice site (i,j). Thin film deposition process is a batch operation where a desired film thickness specification is required to avoid an under-

grown thin film at the end of the deposition process. Thickness of the thin film at any time during the deposition can be calculated from average of the surface height using the following expression:

$$H = \frac{1}{N^2}\sum_{i,j} h_{i,j} \ . \quad (3\text{-}18)$$

Another critical characteristic of the thin film process that needs to be controlled is the growth rate. A specific growth rate is needed during the deposition to meet manufacturing productivity targets. Growth rate can be determined as follows:

$$Gr = \frac{\sum_{i,j} \Delta h_{i,j}}{N^2 \Delta t}, \quad (3\text{-}19)$$

where $\Delta h_{i,j} = h_{i,j}(t + \Delta t) - h_{i,j}(t)$ is the change in the surface height at site (i,j) during Δt. Δt is a specific time interval at which growth rate is estimated.

3.3. Implementation strategy and coupling

In this simulation, the KMC lattice is represented as a matrix where each element represents the number of atoms located on each site within the surface lattice (e.g., in Figure 3-8, there are 3 atoms at site (2,2)). As shown in Figure 3-8, besides this matrix, two additional shadow data structures are required to maintain important information about the number of neighbors of sites. The first data structure is a matrix of the same size that stores the number of neighbors of each surface atom. For example, if site (i,j) has one neighbor, this shadow matrix stores 1 at site (i,j). The second shadow data structure is an array of 5 elements; the k^{th} element in that array stores the number of surface atoms that have *k* neighbors (e.g., the first element represents the number of coordinates with one neighbor). Local algorithms have been implemented to accelerate the process of updating these three data structures in every step of KMC. Local algorithms optimize the search process using available information about the executed event and the site on which the event is executed. This approach is more efficient in comparison with the global algorithm where it is necessary to screen the entire lattice at every KMC step.

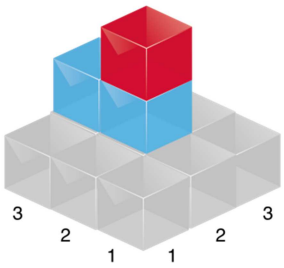

$$\begin{bmatrix} 1 & 1 & 1 \\ 1 & 3 & 1 \\ 1 & 2 & 1 \end{bmatrix} \qquad \begin{bmatrix} 5 & 5 & 5 \\ 5 & 1 & 5 \\ 5 & 2 & 5 \end{bmatrix} \qquad \begin{bmatrix} 1 & 1 & 0 & 0 & 7 \end{bmatrix}$$

(a) (b) (c) (d)

Figure 3-8. (a) Surface configuration, (b) Each element of this matrix indicates the number of atoms on the corresponding site, (c) Each element represents the number of neighbors of the corresponding surface atom, (d) The k^{th} element of this array stores the number of surface atoms that have k neighbors.

To simplify the analysis, the accumulation terms in the heat and flow transfer equations in the gas phase model shown in Eqs.(3-1)-(3-2) are neglected. This reduces those two PDEs into ODEs that can be solved along the η direction using a finite difference scheme. The concentration of the precursor in the gas phase, however, fluctuates in time due to changes in the microstructure of the surface. Therefore, the mass transfer equation is a PDE that is solved using the method of lines. The spatial domain η is discretized resulting in a set of time-dependent ODEs that are solved at every coupling time instance.

The transport phenomena in the gas phase influence the deposition on the surface via the local supply of mass to the surface whereas the microscopic phenomena on the surface affect the overall mass transfer taking place above the surface. That is, the amount of precursor available to deposit on the surface depends on the macroscopic properties of the system. Conversely, the consumption of the precursor on the surface affects the mass flux above the surface. Hence, the macroscopic model and the KMC model depend on each other and are connected through the boundary condition indicated in Eq.(3-6). The parameter of the adsorption rate at the microscopic scale, i.e., the precursor mole fraction on the surface x_{grow}, is provided from the mass transfer balance shown in Eq.(3-3). In addition, the mass transfer boundary condition at the surface depends on the microscopic processes. As shown in Eq.(3-6), R_a and R_d correspond to adsorption and desorption events; the difference between these values can be obtained as follows:

$$R_a - R_d = \frac{N_a - N_d}{2aN^2\Delta\mathcal{T}}, \quad (3\text{-}20)$$

where $\Delta\mathcal{T}$ is the coupling time instance between the macroscopic and the microscopic simulations. N_a is the number of adsorbed atoms during $\Delta\mathcal{T}$ and N_d is the number of desorbed atoms in the same time interval. The values of the parameters used in this study are depicted in Table 3-1.

Table 3-1. Model parameters and their corresponding values and units.

Parameter	Value
a	$5\ 1/\mathrm{s}$
C_{tot}	$1.6611 \times 10^{-5}\ \mathrm{sites.mol/m^2}$
E	$17000\ \mathrm{cal/mol}$
E_d	$17000\ \mathrm{cal/mol}$
E_m	$10200\ \mathrm{cal/mol}$
k_{d0}	$1 \times 10^9\ 1/\mathrm{s}$
m	$0.028\ \mathrm{kg/mol}$
P	$1 \times 10^5\ \mathrm{Pa}$
S_0	0.1
Sc	0.75
$\mathcal{X}$	2×10^{-6}
$\mu_b\rho_b$	$9 \times 10^{11}\ \mathrm{kg^2/(m^4.s)}$
ρ_b/ρ	1

In the KMC simulations, the size of the lattice significantly affects the accuracy of the results and the simulation time. Extensive studies have been conducted to investigate the effects of lattice size on the surface roughness adopting the lattice-based KMC models (Huang et al., 2011, 2010). The accuracy of the results relies on the lattice size used to simulate the evolution of the thin film. Since KMC is a stochastic realization of the so-called master equation shown in Eq.(2-1), large lattice sizes produce results that converge to the solution of the master equation. Nevertheless, the simulation of large lattice sizes is computationally expensive and there is a trade-off between accuracy in the system predictions and computational cost. In Figure 3-9, the evolution of the surface roughness at $T = 800\ \mathrm{K}$ is demonstrated from KMC simulations using 150×150 and 100×100 lattices. The accuracy of the results is not significantly improved

employing a 150×150 surface lattice. The computational time required to simulate the growth process are also indicated in Table 3-2 for different lattice sizes in the KMC simulation. The KMC simulation using a 100×100 lattice provides a good approximation of the process with relatively low computational costs. Accordingly, in the current study, a 100×100 surface lattice is used to represent the actual thin film deposition process. It is important to note that, to average the results obtained from multiple simulations, the KMC simulations are executed in parallel.

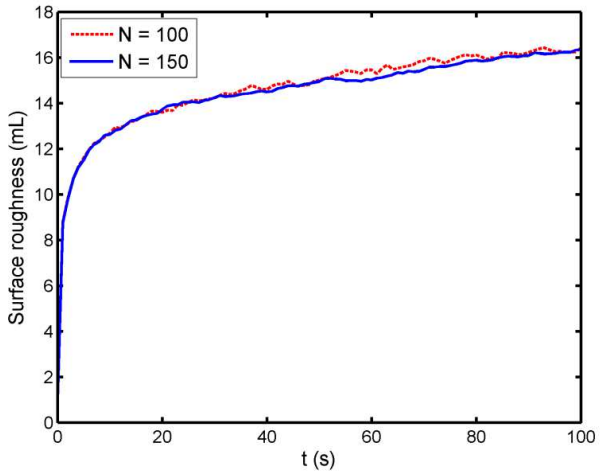

Figure 3-9. Surface roughness trajectories obtained from different simulations using 150×150 and 100×100 lattices.

Table 3-2. Computational cost of various lattice sizes employed in the KMC simulation.

Lattice size	**Computational Time (s)**
$N = 150$	2,448
$N = 100$	747
$N = 30$	47
Average of six $N = 30$	135

Figure 3-10 shows the evolution of the surface roughness at $T = 800$ K from three independent simulations employing a 100×100 lattice for the KMC simulation. Due to the stochastic nature of the method used to describe the evolution of the surface, i.e., KMC, the results obtained from the simulations are slightly different. The roughness evolution from three independent 30×30

lattices is depicted in Figure 3-11. When compared to Figure 3-10, the variability or noise in the surface roughness in a 30 × 30 lattice-based simulation is significantly larger. As the lattice size decreases, the fluctuation in the surface roughness among different runs increases.

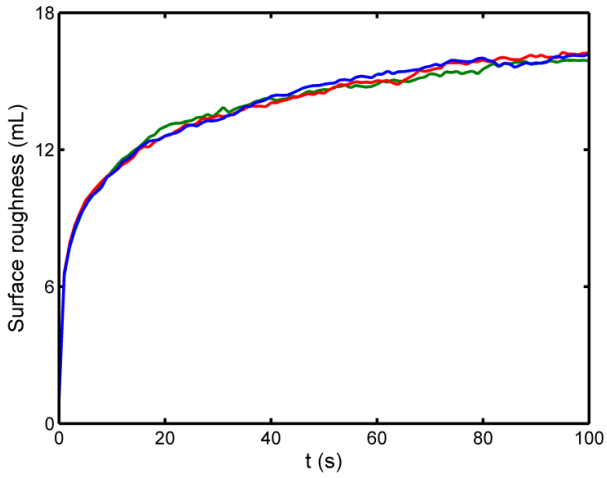

Figure 3-10. Surface roughness trajectories from three independent simulations using a 100 × 100 lattice in the KMC simulations.

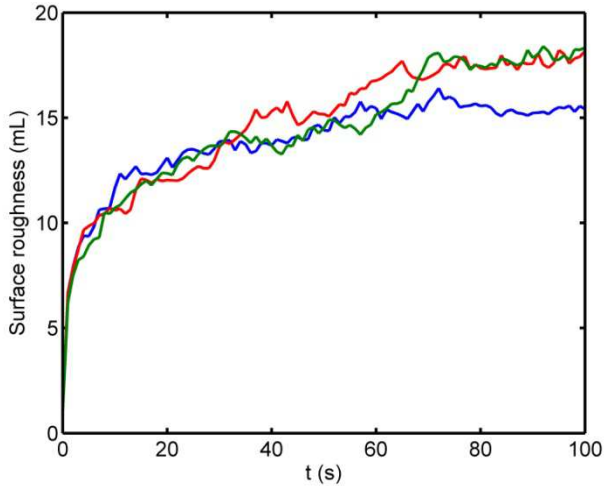

Figure 3-11. Surface roughness trajectories from three independent simulations using a 30 × 30 lattice in the KMC simulations.

Figure 3-12 shows the growth rate obtained from the corresponding simulations which illustrates the small variability in the responses. The film thicknesses estimated from different simulations is shown in Figure 3-13. The variability in the film thickness is so small that is not

visible in this figure and the final 500 ms of the figure is magnified to provide a better observation of its variability.

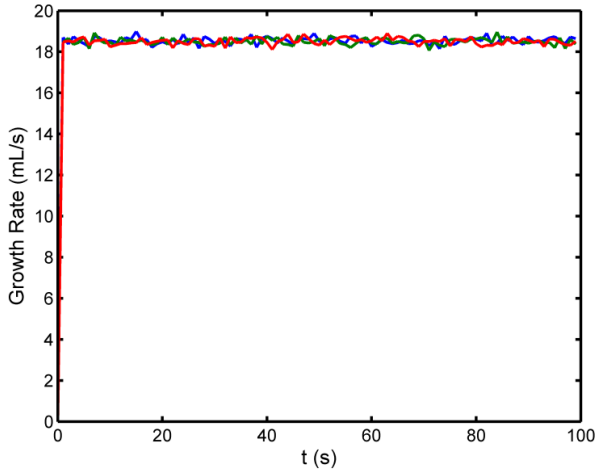

Figure 3-12. Growth rate trajectories from three independent simulations using a 100×100 lattice in the KMC simulations.

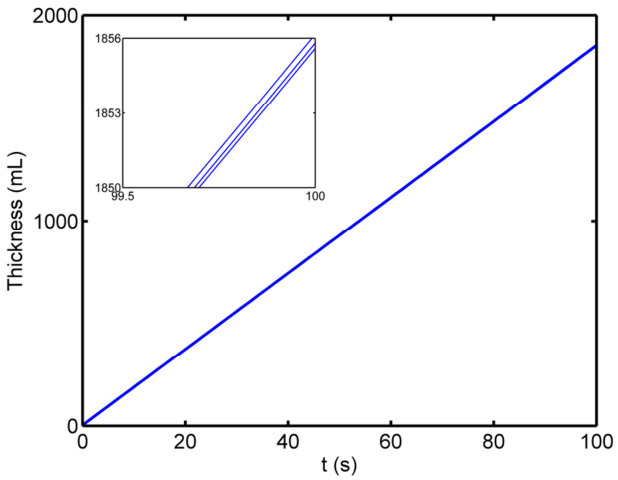

Figure 3-13. Film thickness trajectories from three independent simulations using a 100×100 lattice in the KMC simulations.

To implement an online scheme for the surface roughness, the size of the lattice has to be selected in such a way that the computational time needed to obtain an estimate of the surface properties be comparable to the real-time process. In these simulations, when the lattice size is reduced to $N = 30$, it captures the evolution of the responses with reasonable computational efficiency. As depicted in Figure 3-14, the result obtained from reduced-order lattice simulation

contains significant fluctuations in comparison to the simulation which uses a 100×100 lattice; however, the overall transient evolution of the surface is captured by the 30×30 surface lattice. To circumvent the issue of fluctuations, similar to the approach presented in (Lou and Christofides, 2003a), the responses obtained from multiple independent KMC simulations using reduced-order lattices can be averaged. Figure 3-14 shows that the roughness estimated from averaging six 30×30 lattices provides a suitable representation of the actual process, i.e., a 100×100 KMC-lattice model. According to Figure 3-14 and Table 3-2, averaging six 30×30 lattices provides accurate results at low computational costs.

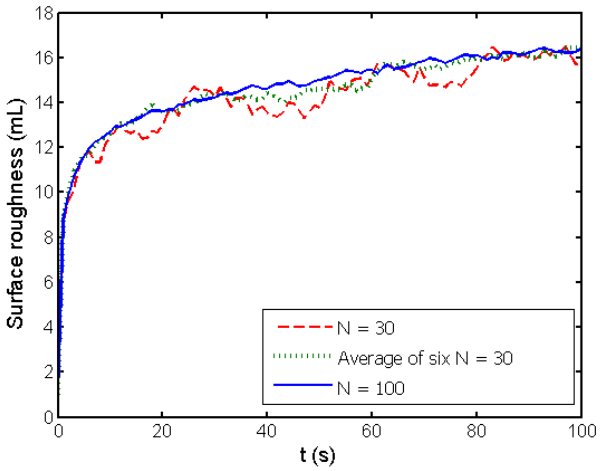

Figure 3-14. Surface roughness trajectories obtained from different simulations using 100×100, 30×30 lattices and average of six 30×30 lattices.

3.4. Summary

As a common practice, a multiscale model is adopted to simulate the thin film deposition process that augments PDEs, describing the macro-scale phenomena, with a high-order lattice-based KMC model, which aims to capture the evolution of the thin film microstructure. It is important to note that, the multiscale model and the KMC parameters used in this work, have been originally employed by Vlachos (Vlachos, 1999). That paper provides an extensive sensitivity analysis to investigate the effect of microscopic and macroscopic parameters on the growth process. Moreover, Lou and Christofides have applied this model to propose an estimator for feedback control of the process (Lou and Christofides, 2003a, 2003b). The dependence of the open-loop simulation results and the computational time on the lattice size has been illustrated in

this chapter. Although increasing the lattice size leads to convergence of the results to the so-called chemical master equation, the computational load will be prohibitive for online applications. Reduced-order lattices, on the other hand, capture the evolution of the process yet contain considerable stochastic fluctuations.

Chapter 4
Open-loop Robust Optimization in a Thin Film Deposition Process*

Model-based optimization and control approaches rely on the accuracy and efficiency of the process model used in the analysis to predict the outputs. While the model presented in Chapter 3 provides a fair representation of the deposition process, the evolution of the thin film encompasses phenomena that are subject to model parameter uncertainty that can significantly affect the performance objectives for this process. The film microstructure is directly shaped by the stochastic microscopic events taking place on the surface. At this level, the surface can be affected by changes in the rates of these microscopic events as a consequence of parameter uncertainty. The effect of model parameter uncertainty can result in suboptimal operational conditions that can lead to loss in performance. Although recently introduced optical *in-situ* sensors motivate the feedback control of this process, their application is still limited in practice. In the industry, most of the measurements are available at the end of the thin film deposition process; accordingly, optimization and control approaches that do not have an access to online fine-scale measurements need to be developed. The thin film deposition is a batch process where open-loop optimization can be performed offline, based on certain product quality specifications. Thus, the focus of this work is to determine a robust optimal control trajectory in the absence of sensor. The aim of this chapter is to explore and propose a systematic framework to analyze model parameter uncertainty for robust optimization in multiscale process models. Such an analysis is challenging due to *i*) the lack of a closed formulation between the process optimization objective and the model parameters and *ii*) the computational costs incurred in the KMC simulation. To overcome these challenges, PSE is employed for uncertainty propagation.

In this chapter, worst-case and distributional uncertainty analyses are compared in the thin film deposition process (Rasoulian and Ricardez-Sandoval, 2015a). The parameters are assumed to be constant unknown values during the deposition that can change randomly from batch to batch. Model parameters with this description are considered as time-invariant parameters while the true value is not known. Due to embedded KMC simulations, the sensitivity analysis required for PSEs is computationally intensive and this method is appropriate for open-loop optimization. In the second part of this chapter, to circumvent sensitivity analysis of the KMC simulations, the

* This chapter has been written based on the following published papers: (Rasoulian and Ricardez-Sandoval, 2015a, 2014)

uncertainty is propagated into rates of microscopic events, then probabilistic bounds on the outputs are computed through KMC simulations. An algorithm is presented to determine the probabilistic bounds on the thin film properties while the model parameter uncertainties are time-varying. This type of uncertainty description is often assigned to those model parameters that have high frequency contents so that their value changes during the operation of the process. The potential application of these methods is illustrated through an optimization problem that aims to specify the robust optimal substrate temperature profile that maximizes the endpoint thin film thickness in the presence of uncertainty.

The remainder of the chapter is organized as follows: Section 4.1 presents the PSE method in detail. Worst-case and distributional uncertainty analysis of the thin film deposition process is presented in Section 4.2. In Section 4.3, an algorithm is presented to determine the probabilistic bounds on thin film properties using the distribution of rate of microscopic events.

4.1. Uncertainty analysis using PSE

PSE takes advantage of an expansion to describe the performance of the process around the nominal control trajectory. In this method, the uncertainty is quantified using a series expansion that approximates the nonlinear complex behaviour of the system. The key advantage of this approach is that it is not necessary to have the analytical expression for the process since it only requires the sensitivities with respect to the uncertain parameters. Following this approach, the issue of absence of closed-form models can be addressed by deriving a low-order model. Although the order of the series expansion depends on the process nonlinearity and variability in the uncertain parameters, first or second-order expansions are usually sufficient for engineering applications since the expansion needs to be accurate in a narrow neighbourhood around the nominal values (Nagy and Braatz, 2004).

In uncertainty analysis, the perturbed model parameter vector, $\boldsymbol{\theta} \in \mathbb{R}^{n_\theta}$ can be defined as follows:

$$\boldsymbol{\theta} = \widehat{\boldsymbol{\theta}} + \delta\boldsymbol{\theta}, \tag{4-1}$$

where $\widehat{\boldsymbol{\theta}}$ is the nominal model parameter vector and $\delta\boldsymbol{\theta}$ is the perturbation about $\widehat{\boldsymbol{\theta}}$. The objective is to analyse the deviation in the output from the nominal output, i.e.,

$$\delta y = y - \hat{y}, \tag{4-2}$$

where $\hat{y}$ is the output when the system is operated with the nominal model parameter $\widehat{\boldsymbol{\theta}}$ and y is the output when parameter vector $\boldsymbol{\theta}$ is used. Employing PSE, the deviation from the nominal output, δy, is computed as follows:

$$\delta y = \mathbf{L}_1(t)\delta\boldsymbol{\theta} + \frac{1}{2}\delta\boldsymbol{\theta}^T\mathbf{L}_2(t)\delta\boldsymbol{\theta} + \cdots, \tag{4-3}$$

where $\mathbf{L}_1(t) = (dy(t)/d\boldsymbol{\theta})_{\widehat{\boldsymbol{\theta}}} \in \mathbb{R}^{n_\theta}$ and $\mathbf{L}_2(t) = (d^2y(t)/d\boldsymbol{\theta}^2)_{\widehat{\boldsymbol{\theta}}} \in \mathbb{R}^{n_\theta \times n_\theta}$ are respectively the Jacobian and Hessian evaluated around $\widehat{\boldsymbol{\theta}}$ at a specific time, t.

4.1.1. Worst-case deviation under bounded uncertainties

Analytical techniques have been proposed to characterize the worst-case deviation of the control performance under bounded model parameter uncertainty in continuum models (Ma et al., 1999; Ma and Braatz, 2003, 2001). In the worst-case robustness analysis, the worst-case deviation in the output is evaluated under bounded uncertainties in the model parameters, i.e.,

$$\boldsymbol{\theta} = \{\boldsymbol{\theta} | \boldsymbol{\theta}_l \leq \boldsymbol{\theta} \leq \boldsymbol{\theta}_u\}, \tag{4-4}$$

where $\boldsymbol{\theta}_l$ and $\boldsymbol{\theta}_u$ represent the lower and upper limits on the vector of uncertain parameters. The effect of parameter uncertainty on the output of the system can be estimated from the following optimization problem:

$$\max_{\boldsymbol{\theta}_l \leq \boldsymbol{\theta} \leq \boldsymbol{\theta}_u} |\delta y|. \tag{4-5}$$

Using first-order PSE, the worst-case variability in the process output, δy, is calculated as follows:

$$\delta y_{w.c} = \max_{\boldsymbol{\theta}_l \leq \boldsymbol{\theta} \leq \boldsymbol{\theta}_u} |\mathbf{L}_1\delta\boldsymbol{\theta}|. \tag{4-6}$$

More accurate estimates of the worst-case variability can be obtained by adding more terms into the expansion and can be formulated in terms of the skewed structured singular value (SSV) or μ analysis (Braatz et al., 1994). For the second-order PSE, $\delta y_{w.c}$ can be obtained as follows:

$$\delta y_{w.c} = \max_{\boldsymbol{\theta}_l \leq \boldsymbol{\theta} \leq \boldsymbol{\theta}_u} |\mathbf{L}_1\delta\boldsymbol{\theta} + \delta\boldsymbol{\theta}^T\mathbf{L}_2\delta\boldsymbol{\theta}| \underline{=} \max_{\mu_\Delta(\mathbf{M}) \geq \gamma} \gamma, \tag{4-7}$$

where,

$$\mathbf{M} = \begin{bmatrix} \mathbf{0} & \mathbf{0} & \gamma\boldsymbol{\omega} \\ \gamma\mathbf{L}_2 & \mathbf{0} & \gamma\mathbf{L}_2\mathbf{z} \\ \mathbf{z^T L}_2 + \mathbf{L}_1 & \mathbf{W}_{\boldsymbol{\theta}}^T & \mathbf{z^T L}_2\mathbf{z} + \mathbf{L}_1\mathbf{z} \end{bmatrix}. \quad (4\text{-}8)$$

The $\mathbf{0}$ in $\mathbf{M}$ denotes a zero matrix of consistent dimensions; $\boldsymbol{\omega} = 0.5(\boldsymbol{\theta}_u - \boldsymbol{\theta}_l)$ and $\mathbf{z} = 0.5(\boldsymbol{\theta}_u + \boldsymbol{\theta}_l)$. $\Delta = diag(\Delta_r, \Delta_r, \delta_c)$ is the perturbation block in the μ analysis. δ_c is a complex scalar while Δ_r consists of real scalars. Upper and lower bounds on y can be calculated using the worst-case deviation from the nominal output in the positive and negative directions, respectively, i.e., $y^{up} = \hat{y} + \delta y_{w.c},\ y^{low} = \hat{y} - \delta y_{w.c}$.

4.1.2. Probabilistic bounds under distributional uncertainty

The probabilistic parameter description relaxes the restriction imposed by the bounded uncertainty description and assumes that the uncertainty in the parameter can be described by a PDF. These types of uncertainties are usually described as a distribution around the point estimate with a specific variability. The parameter uncertainty can be characterized using the data collected from the actual process; however, when access to plant data is not available, the uncertainty is typically assumed to be normally distributed around the parameter's nominal values. Moreover, the available algorithms for parameter estimation from the experimental data mostly result in a normal distribution (Nagy and Braatz, 2007). Therefore, the uncertainties in the parameters can be described by a multivariate normal distribution around the nominal parameter estimates as follows:

$$\mathcal{E}_{\boldsymbol{\theta}} = \left\{\boldsymbol{\theta} | \delta\boldsymbol{\theta}^T \mathbf{V}_{\boldsymbol{\theta}}^{-1} \delta\boldsymbol{\theta} \leq \chi^2_{n_\theta}(\alpha)\right\}, \quad (4\text{-}9)$$

where $\mathbf{V}_{\boldsymbol{\theta}} \in \mathbb{R}^{n_\theta \times n_\theta}$ denotes the positive definite covariance matrix, $\chi^2_{n_\theta}$ is a chi-squared distribution with n_θ degrees of freedom and α is the confidence level. PSE presents an analytical approach to approximate the PDFs of the controlled objectives when it is impractical to evaluate them using the primary model. The distributional uncertainty in the controlled outputs can be quantified at low computational costs based on the expansions that describe the outputs as a function of the uncertain parameters. Assuming that the process can be accurately described using a first-order PSE, the normal distribution of the output can be obtained from (Beck and Arnold, 1977):

$$f_{p.d.}(y) = \frac{1}{\sqrt{2\pi \mathbf{L_1 V_\theta L_1^T}}} \exp\left(\frac{-(y-\hat{y})^2}{2\mathbf{L_1 V_\theta L_1^T}}\right). \quad (4\text{-}10)$$

For second and higher order PSEs, however, the distribution cannot be estimated analytically and random Monte Carlo realizations from the PDFs of the parameters are needed to propagate the uncertainty (Nagy and Braatz, 2007). Once the output distribution is obtained either analytically or through the Monte Carlo sampling method, the probabilistic upper and lower bounds can be estimated at a specific probability as follows:

$$y^b = F^{-1}(\mathbb{Pr}|y) = \{y: F(y)\}, \quad (4\text{-}11)$$

where $b \in \{low, up\}$ and $F^{-1}(\mathbb{Pr}|y)$ represents the inverse of cumulative distribution function (CDF) evaluated at a predefined probability, $\mathbb{Pr}$.

4.2. Worst-case and distributional robustness analysis in a thin film deposition process

The microelectronic market imposes stringent requirements upon thin film properties including specific thickness and surface roughness. Surface roughness is referred to as an important film quality variable that controls the electrical and mechanical properties of micro-electronic devices. The thin film deposition process is a batch operation where a desired minimum film thickness is required to avoid an under-grown thin film at the end of the deposition process. Moreover, growth rate is an important factor which determines the manufacturing productivity. To show the effect of parameter uncertainties on these properties of the thin film, the PSE is used next to obtain the PDF of the outputs.

4.2.1. Uncertainty propagation using PSE

The uncertainties in the process are assumed in the energy associated with a single bond, and the bulk precursor mole fraction, i.e. $\boldsymbol{\theta}^T = [E, \mathcal{X}]$. In the case of parametric uncertainty, the parameters E and $\mathcal{X}$ are described as follows:

$$E = \hat{E}(1 + \omega_E),\ \mathcal{X} = \hat{\mathcal{X}}(1 + \omega_{\mathcal{X}}), \quad (4\text{-}12)$$

where the nominal values ($\hat{E}$ and $\hat{\mathcal{X}}$) are given in Table 3-1 and the uncertainties are:

$$-0.2 \leq \omega_E \leq 0.2,\ -0.2 \leq \omega_{\mathcal{X}} \leq 0.2. \tag{4-13}$$

For a fair comparison between the worst-case scenario and probabilistic bounds, the covariance matrix in the multivariate normal distribution is constructed such that 99.7% of the uncertain parameters are within the bounded uncertainties (three standard deviations rule); therefore,

$$\mathbf{V_\theta} = \begin{pmatrix} (0.2\hat{E}/3)^2 & 0 \\ 0 & (0.2\hat{\mathcal{X}}/3)^2 \end{pmatrix} \tag{4-14}$$

To determine the order of the PSE, an iterative approach is implemented. The commonly used algorithm starts with the first-order PSE and evaluates the approximation error using the brute-force Monte Carlo method. The algorithm iteratively increases the order of the PSE up until the error reaches an acceptable value. This approach has also been previously suggested to determine the order of the PCE (Nagy and Braatz, 2010, 2007). Once the algorithm converged, the resulting PSE order will be used for approximating the PDF of the event rates. The order of the PSE depends on the nonlinearity of the function and the variability of the uncertain parameter. For first-order PSEs, the PDF can be evaluated analytically while, for higher order PSEs, the Monte Carlo sampling method is applied to the PSE model obtained from Eq.(4-3).

To investigate the effect of probabilistic uncertainty and determine the order of the PSE for each output, 1000 sample points have been generated randomly from a normal PDF with the covariance matrix shown in Eq.(4-14). Then, applying Monte Carlo method on the multiscale model presented in Chapter 3 at $T = 800$ K, the PDF of each output has been obtained at $t = 20$ s. The PDFs are also estimated using PSEs while the sensitivities in the expansions have been calculated using finite differences from the average of the outputs obtained through multiple multiscale models employing reduced-order lattices in the KMC simulations. Figure 4-1 shows the PDF obtained using the Monte Carlo method applied to the full multiscale model along with the PDFs estimated using PSEs. As shown in this figure, a first-order PSE is not sufficient to describe the variability in the surface roughness. However, a second-order PSE has successfully captured the nonlinearity observed in this PDF.

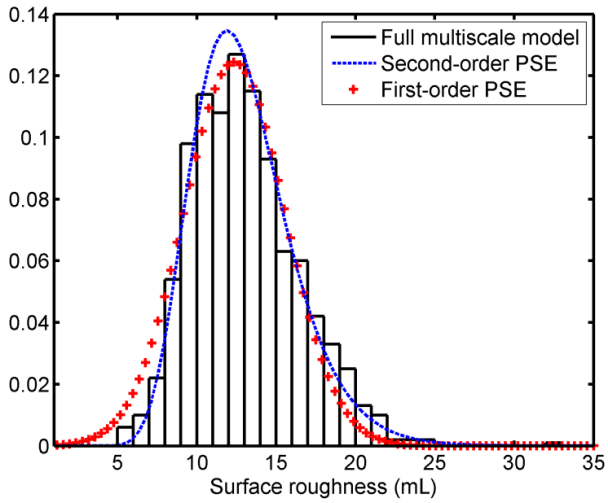

Figure 4-1. Roughness PDFs at $T = 800$ K obtained using the multiscale model, first and second-order PSEs at $t = 20$ s.

To determine the order of the PSE for growth rate and thickness, first-order PSEs have been applied. As shown in Figure 4-2 and Figure 4-3, first-order PSEs has successfully captured the variability in these outputs of the system.

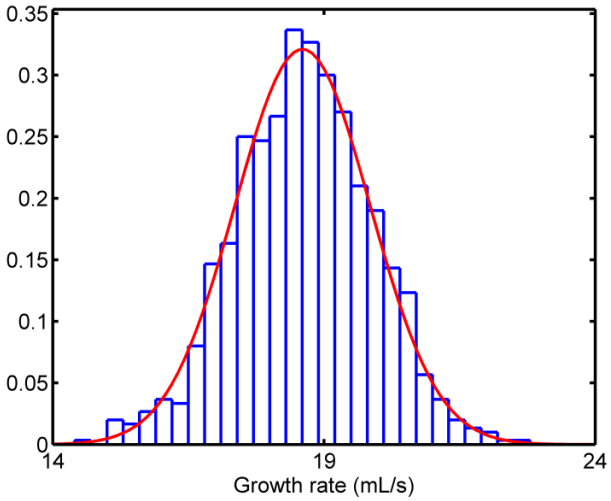

Figure 4-2. Growth rate PDFs at $T = 800$ K obtained using the multiscale model, first-order PSE at $t = 20$ s.

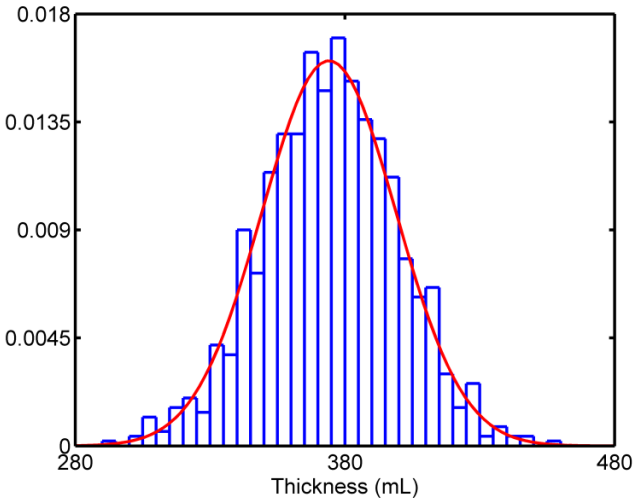

Figure 4-3. Thickness PDFs at $T = 800$ K obtained using the multiscale model, first-order PSE at $t = 20$ s.

4.2.2. Robust optimization based on worst-case and probabilistic analysis

The key manipulated variable for this process is the substrate temperature since it affects the outputs of the system significantly. In this optimization problem, while the thickness of the thin film needs to be maximized for a finite batch time, the surface roughness has to be minimized to assemble high-performance electronic devices. These are two conflicting objectives since thick films can be obtained at low temperatures whereas smooth film surfaces can only be realized at relatively high temperatures. Moreover, uncertainties lead to product quality variability resulting in a potential loss in profits. Thus, the optimization problem aims to determine the substrate temperature time-dependent profile that optimizes the process performance under uncertainty:

$$\max_{T(t)} \; H^{low}(t_f)$$

Subject to:

Multiscale model presented in Chapter 3

$$h_1 = T_{min} - T(t) \leq 0$$

$$h_2 = T(t) - T_{max} \leq 0$$

$$h_3 = r^{up}(t_f) - r_{max} \leq 0 \qquad (4\text{-}15)$$

$$h_4 = Gr_{min} - Gr^{low}(t_f) \leq 0$$

$$h_5 = \frac{dr^{up}(t_f)}{dt} - \Re \leq 0$$

$$h_6 = \frac{dGr^{low}(t_f)}{dt} - \Re \leq 0$$

$$t = [0, t_f]; \; \forall k = 1,2, \dots, K$$

where the constraints h_1 and h_2 ensure that the temperature profile remains within the feasible operating region for the deposition process. Constraints h_3 and h_4 specify the maximum allowed surface roughness at the end of the batch, r_{max} to satisfy market demands and the minimum growth rate, Gr_{min} to ensure process productivity, respectively. h_5 and h_6 ensure minimum variability of these properties at the end of the batch. The superscripts *low* and *up* correspond to the end-point properties evaluated via the lower and upper bounds, respectively. At every evaluation of the optimization, $H^{low}(t_f)$, $r^{up}(t_f)$ and $Gr^{low}(t_f)$ are determined using either probabilistic or worst-case scenario approaches. To overcome the infinite-dimensional nonlinear optimization problem, the batch time t_f is discretized into *K* equally spaced time intervals while the temperature at each time interval, $T(k)$ is kept piecewise constant between successive intervals and is considered as one of the decision variables in the optimization problem.

Problem (4-15) has been solved under the assumption of bounded parametric uncertainty and distributional uncertainty in E and $\mathcal{X}$, respectively. As shown in 4.2.1, a second-order PSE has been employed to describe the effect of uncertainties on the surface roughness whereas first-order PSEs were sufficient to propagate uncertainties in thickness and growth rate. To estimate upper and lower bounds, three different approaches were considered while solving optimization problem defined in Eq.(4-15): *i)* worst-case deviation in the outputs using description (4-12), *ii)*

probabilistic bounds on outputs at 99.7% confidence interval ($\mathbb{Pr} = 3\sigma$ in (4-11)) and *iii)* probabilistic bounds at 68% confidence interval ($\mathbb{Pr} = \sigma$ in (4-11)) using description (4-14). In the case of the worst-case scenario, the roughness at the end of the batch is estimated using SSV analysis as shown in Section 4.1.1 while the worst-case deviations in thickness and growth rate can be calculated analytically since they are described using first-order PSEs. On the other hand, to propagate the uncertainty in surface roughness in the probabilistic-based approaches, Monte Carlo sampling is applied to the second-order PSE as explained in Section 4.1.2 whereas the bounds on thickness and growth rate are obtained analytically using first-order PSEs.

The batch time was divided into ten equally spaced time intervals. For better comparison of the results, the initial temperature was fixed at 800 K. Figure 4-4 shows the optimal temperature profiles obtained from problem (4-15) using the three approaches. These profiles correspond to specifications in r_{max} and Gr_{min} of 7 mL and 13 mL/s, respectively. T_{min} and T_{max} were set to 600 and 1200 K, respectively. As shown in this figure, the optimal temperature profile demands low temperatures at earlier stages of the deposition process to maximize the thickness by high adsorption rates. However, close to end of the batch process, high substrate temperatures are needed to promote migration on the surface and meet the constraints on surface roughness. The profile obtained using 99.7% confidence interval in probabilistic approach is slightly different from the profile obtained using the worst-case scenario approach. However, the temperature profile based on 68% confidence interval is the most optimistic, since this approach estimates less conservative bounds on surface roughness. Note that other reasonable product specification constraints result in similar conclusions to that presented here.

Figure 4-5 shows the bounds evaluated for surface roughness using the optimal temperature profiles shown in Figure 4-4. As depicted in this figure, the bounds obtained by the worst-case scenario approach using the SSV analysis are more conservative compared to the bounds obtained using the probabilistic-based approach. The worst-case bounds are computed using the worst-case deviation from the nominal outputs. Moreover, this figure also shows 100 random open-loop variations of the surface roughness under bounded uncertainty (4-12) using the temperature profile obtained from the worst-case scenario. As shown in this figure, the roughness during the batch is bounded within upper and lower bounds estimated based on the worst-case deviation. The final film thicknesses employing these temperature profiles are given

in Table 4-1. As expected, the worst-case scenario approach returned the most conservative film thickness at the end of the batch.

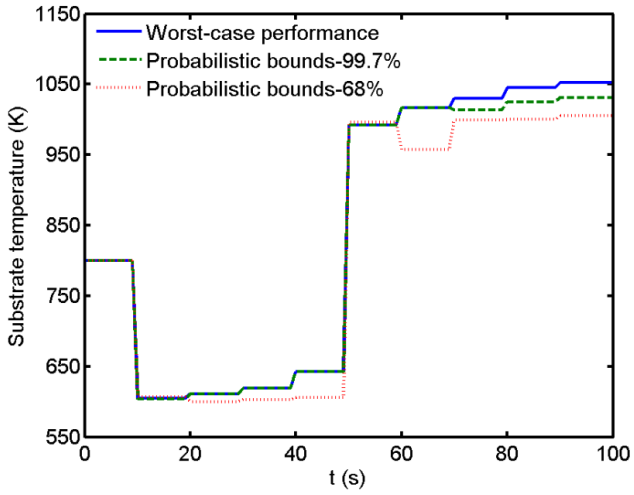

Figure 4-4. Robust optimal temperature profiles using different approaches.

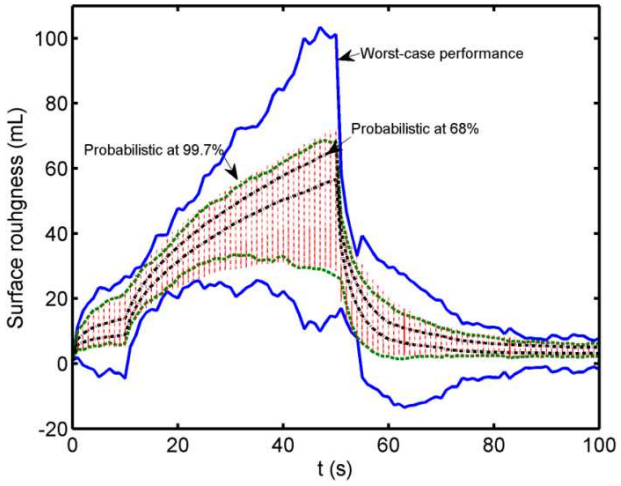

Figure 4-5. Upper and lower bounds on surface roughness using different approaches and open-loop simulations using the temperature profile obtained for worst-case performance.

Figure 4-6 shows the final properties obtained under bounded parametric uncertainty using the temperature profiles obtained from these three approaches. As shown in this figure, regardless of a few violations using the temperature profile estimated by the probabilistic approach with 68% confidence interval, the three estimated optimal temperature profiles satisfy the constraints imposed on the optimization problem (4-15). That is, the final roughness of the thin film is mostly less than 7 mL in reality, even if the most optimistic temperature profile estimated by the

probabilistic approach with 68% confidence interval is being used. In essence, the measurable benefits in using the worst-case scenario will be limited since it results in an overly conservative temperature profile that may eventually lead to economic losses. In practice, the probabilistic approach with 68% confidence interval not only achieves an acceptable roughness, but also results in larger thickness and larger growth rate. This is a direct consequence of the optimistic temperature profile identified from the present approach.

Table 4-1. Optimal end-point thickness from different approaches.

Approach	Thickness (1000 mL)
Worst-case scenario	1.4595
Probabilistic at 99.7%	1.4759
Probabilistic at 68.0%	1.7293

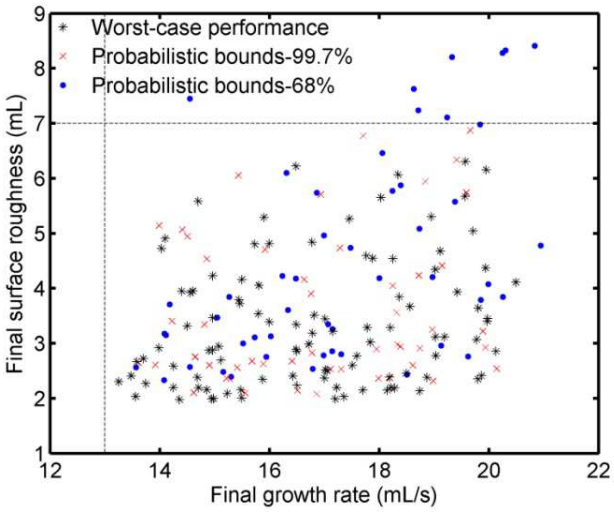

Figure 4-6. Variation of final properties due to bounded parameter uncertainties, obtained from open-loop simulations applying various temperature profiles.

4.3. Probabilistic bounds in thin film deposition process through uncertainty propagation in the rate of microscopic events

Due to issues associated with the sensitivity analysis of outputs with respect to the uncertain parameters, the uncertainty propagation is performed for the rate of the microscopic events. The main reason for uncertainty quantification of the states is the availability of a closed-form

formulation between these rates and the uncertain parameters. Therefore, PSEs are employed to avoid the high computational load corresponding with simulation of the primary model for multiple realizations of the uncertain parameters. Estimation of the distribution of these rates using the PSE-based approach is not sufficient for execution of KMC events. Accordingly, once the distributions are obtained, specific values can be selected based on a predefined confidence level. The detailed description of the proposed framework to address the uncertainty analysis for multiscale systems is described next.

4.3.1. Uncertainty propagation into event rates using PSE

Define the vector of uncertain parameters $\boldsymbol{\theta} = \{\theta_1, \dots, \theta_q, \dots, \theta_Q\} \in \mathbb{R}^Q$, $\widehat{\boldsymbol{\theta}}$ as the vector of nominal model parameters and the microscopic rates vector $\mathbf{W} = \{W_1, \dots, W_i, \dots W_I\} \in \mathbb{R}^I$, the algorithm to obtain the distributional uncertainty of rates of microscopic events at any time during the process can be outlined as follows:

1. Specify the prior PDF of each uncertain parameters, $f_{p.d}(\theta_q)$.

$$\theta_q = \{\theta_q | \theta_q \in f_{p.d.}(\theta_q)\}. \tag{4-16}$$

2. Evaluate the sensitivities of rate of each of the microscopic events with respect to the uncertain parameters using the multiscale model at a specific time t. The order of the required sensitivities relies on the order of PSE. For instance, the first and second-order sensitivities are as follows:

$$\mathbf{L}_1(t) = \left(\frac{\partial \mathbf{W}}{\partial \boldsymbol{\theta}}\right)_{\boldsymbol{\theta}=\widehat{\boldsymbol{\theta}}}, \mathbf{L}_2(t) = \left(\frac{\partial^2 \mathbf{W}}{\partial \boldsymbol{\theta}^2}\right)_{\boldsymbol{\theta}=\widehat{\boldsymbol{\theta}}}. \tag{4-17}$$

3. Estimate the PDF of W_i using the following truncated PSE:

$$W_i = \widehat{W}_i + \mathbf{L}_1\left(\boldsymbol{\theta} - \widehat{\boldsymbol{\theta}}\right) + \frac{1}{2}\left(\boldsymbol{\theta} - \widehat{\boldsymbol{\theta}}\right)^T \mathbf{L}_2\left(\boldsymbol{\theta} - \widehat{\boldsymbol{\theta}}\right) + \cdots, \tag{4-18}$$

where $\widehat{W}_i$ is the nominal microscopic event rate. The PDF of W_i can be obtained by solving (4-18) for different Monte Carlo realizations in $\boldsymbol{\theta}$ that comply with the prior distribution assigned to each of the uncertain parameters. For first-order PSEs, the PDF of the rate can be evaluated analytically while, for higher order PSEs, the distribution is estimated by applying the Monte Carlo sampling method to the PSE model obtained from Eq.(4-18).

4. Estimate the upper and lower bounds on W_i at a predefined confidence level, α.

$$W_i^{\,b} = F^{-1}(\mathbb{Pr}|W_i) = \{W_i : F(W_i)\}, \quad (4\text{-}19)$$

where $b \in \{low, up\}$ and the function $F^{-1}(\mathbb{Pr}|W_i)$ represents the inverse of CDF evaluated at a predefined probability, $\mathbb{Pr}$. Setting $\mathbb{Pr}$ in Eq.(4-19) to $\alpha/2$ and $1-\alpha/2$ yields respectively the lower bound, W_i^{low}, and the upper bound, W_i^{up}, for the i^{th} event rate, W_i.

In order to investigate the performance of PSE, the PDF of rate of adsorption obtained using the primary model and the PSE are compared. The uncertainty analysis was performed with respect to the bulk mole fraction, $\mathcal{X}$ which according to the multiscale model presented in Chapter 3 is the boundary condition of the mass transfer equation shown in Eq.(3-4). This parameter has a significant effect on the total rate of adsorption (W_a) and therefore on the overall multiscale model. To that end, after a finite time interval in the open-loop simulation, the PDF of the total adsorption rate were obtained from Monte Carlo simulations using the primary model and the PSE. As it was previously mentioned, the Monte Carlo method requires a large number of samples from the uncertain parameter distribution. Particularly for this system, more than 500 data points have to be generated to obtain a representative distribution for the total rate of adsorption while using the primary multiscale model. To study the effect of uncertainty in the bulk mole fraction, random numbers are generated from a normal distribution, $\mathcal{N}(2 \times 10^{-6}, 2 \times 10^{-7})$. Employing these data points, the uncertainty is propagated into the total adsorption rate using the multiscale model presented in Chapter 3 at $T = 800$ K. The PDF obtained at $t = 10$ s is presented in Figure 4-7. The variability is also assessed using a first-order PSE and the fitted normal distribution is shown in Figure 4-7. As shown in this figure, the distribution obtained from the PSE accurately describes the variability in the total rate of adsorption due to the uncertainty in $\mathcal{X}$. The required computational times are indicated in Table 4-2. As shown in that table, the Monte Carlo method is at least two orders of magnitude more intensive than the PSE, which indicates the key benefit of the present approach. Using the distribution obtained for total rate of adsorption, then upper and lower bounds for the adsorption rate at the current time t, i.e., $W_a^{low}(t), W_a^{up}(t)$, can be estimated at a given confidence level. The corresponding values at $\alpha = 1\%$ are shown in Table 4-2.

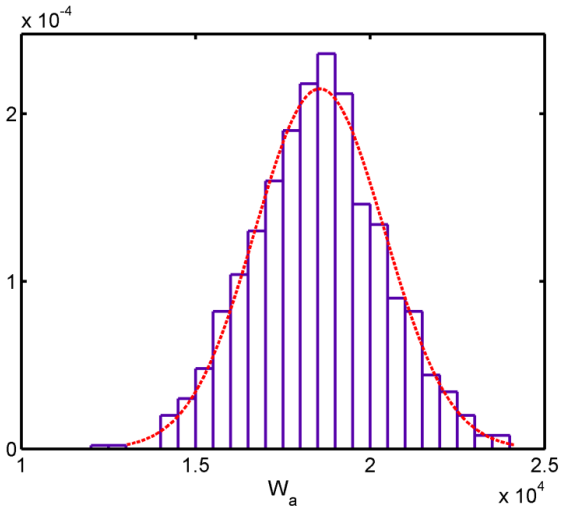

Figure 4-7. PDF of the total adsorption rate from Monte Carlo applied to multiscale model using 500 points and the PDF obtained using first-order PSE.

Table 4-2. The probabilistic bounds of the total rate of adsorption from different approaches at $t = 10$ s and the corresponding computational costs.

Approach	$\boldsymbol{W_a^{low}(1/s)}$	$\boldsymbol{W_a^{up}(1/s)}$	**Computational Time (s)**
Monte Carlo using the primary model	1.41×10^4	2.33×10^4	34,980
First-order PSE	1.38×10^4	2.34×10^4	390

The first-order PSE is not sufficient for uncertainty analysis in other parameters of the system, e.g., E and E_m. As shown in Eqs.(3-9) and (3-11), the energy associated with a single bond and migration affect the microstructure through nonlinear Arrhenius-type expressions of desorption and migration rates. In this case, higher order PSEs are needed due to the existence of nonlinearity between the uncertain parameters and the microscopic events. Therefore, second-order PSE is applied to study the uncertainty propagation in total rate of desorption and migration due to variability in these parameters. To study the effect of variability, the uncertainty considered for $\mathcal{X}$ was similar to that described above, i.e., $\mathcal{N}(2 \times 10^{-6}, 2 \times 10^{-7})$ whereas E and E_m were assumed to follow normal distributions around their nominal values, $[\hat{E}, \hat{E}_m] = [17000, 10200]$, with the standard deviation of 500 cal/mol. The PDFs obtained using PSE for the rate of microscopic events at different times are shown in Figure 4-8.

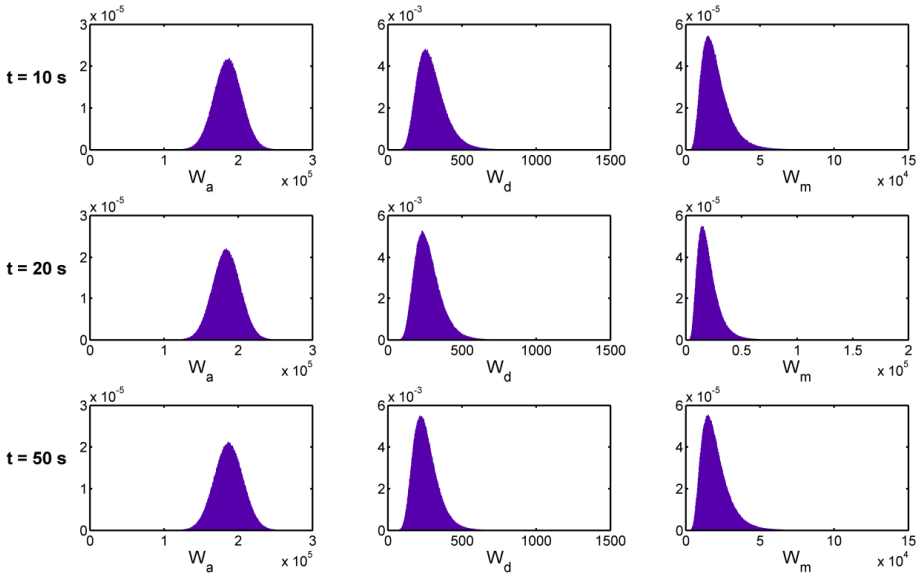

Figure 4-8. PDFs obtained from PSE during deposition.

4.3.2. Computation of the probabilistic-based bounds

The algorithm described above to obtain the bounds for each of the microscopic events at a specific confidence level, α, produces a time-dependent hyper-rectangle box **m** formed by the extreme values of each microscopic event, W_i^b, considered in the KMC simulation, i.e.,

$$\mathbf{m}(t) = \{[\mathbf{m}_1(t), \dots \mathbf{m}_j(t), \dots, \mathbf{m}_J(t)] : \mathbf{m}_j(t) = [W_1^b(t), \dots, W_i^b(t), \dots, W_I^b(t)]\}, \quad (4\text{-}20)$$

where the block vector $\mathbf{m}(t)$ of length 2^I includes all the possible combinations between the upper and lower bounds of the I total rate of microscopic events at time t. Each element of **m**, e.g. $\mathbf{m}_j$, is a vector of length I that includes a particular combination between the upper and lower limits of the I microscopic events. Similarly, the surface describing the microstructure of the system at any time t is defined as follows:

$$\mathbf{S}(t, \mathbf{m}) = \{\mathbf{S}_1(t, \mathbf{m}_1), \dots, \mathbf{S}_j(t, \mathbf{m}_j), \dots, \mathbf{S}_J(t, \mathbf{m}_J), \mathbf{S}_{nom}(t, \mathbf{m}_{nom})\}, \quad (4\text{-}21)$$

where $\mathbf{S}_j(t, \mathbf{m}_j)$ is a KMC lattice that represents the morphology of the surface as shown in Eq.(3-7) at time t due to the combination in the upper and lower limits specified on the microscopic events by the vector $\mathbf{m}_j$. Similarly, $\mathbf{S}_{nom}(t, \mathbf{m}_{nom})$ represents a surface describing the evolution at time t of the film using the nominal values in the I microscopic events and is defined as follows:

$$\mathbf{m}_{nom}(t) = [W_1^{nom}(t), \dots, W_i^{nom}(t), \dots, W_I^{nom}(t)],$$

where $W_i^{nom}(t)$ represents the nominal (expected) value of the i^{th} event rate at time t.

Based on the above, *J+1* parallel lattice-based KMC models need to be simulated simultaneously to compute the lower and the upper bounds on the fine-scale properties of the system. Each simulation describes the microstructure of the surface due to a particular combination in the event rates. Accordingly, lower and upper bounds on the outputs of the thin film deposition process at a given time *t* can be obtained as follows:

$$\hat{y}^{up}(t) = \max_{\hat{\mathbf{y}}} \hat{\mathbf{y}}(t),$$

$$\hat{y}^{low}(t) = \min_{\hat{\mathbf{y}}} \hat{\mathbf{y}}(t), \qquad (4\text{-}22)$$

$$\hat{\mathbf{y}}(t) = [\hat{y}_1(t), \dots, \hat{y}_j(t), \dots, \hat{y}_J(t), \hat{y}_{nom}(t)],$$

where $\hat{y}_j(t)$ represents an output predicted from the KMC model that is calculated using properties of the microstructure of the surface $\mathbf{S}_j(t, \mathbf{m}_j)$. The output $\hat{\mathbf{y}}(t)$ can represent the roughness, growth rate or thickness of the film at a given time t, i.e., $r(t), Gr(t)$ and $H(t)$**,** respectively.

In general, the number of parallel KMC simulations depends on the number of microscopic events. Specifically for the thin film deposition process described in Chapter 3, $J = 2^3$ since there are three different microscopic processes occurring on the surface, i.e., adsorption, desorption and migration. Nevertheless, the sensitivities are time-varying and correspondingly the lower and upper bounds on microscopic events will change during the deposition process. When the parameter uncertainties are time-varying, propagating the uncertainty using fixed upper and lower bounds on microscopic events results in overly conservative bounds for the outputs. To alleviate this problem, $\mathbf{S}_{nom}(t, \mathbf{m}_{nom})$ is used as the reference (nominal) surface using the nominal values of events rates. This lattice is used to update other KMC simulations, every sampling time instance, Δt. That is, assuming that the uncertain parameter is changing every Δt according to its PDF, $f_{p.d.}(\theta_q)$, all the KMC lattices to be used for the next sampling interval, i.e., $\mathbf{S}(t + \Delta t, \mathbf{m}_j)$ are initialized with $\mathbf{S}_{nom}(t, \mathbf{m}_{nom})$ to compute the lower and upper bounds of outputs for the next sampling time interval. This procedure continues up until the final integration time is reached. Figure 4-9 summarizes the algorithm proposed in this work to determine the probabilistic-based bounds for the thin film deposition process.

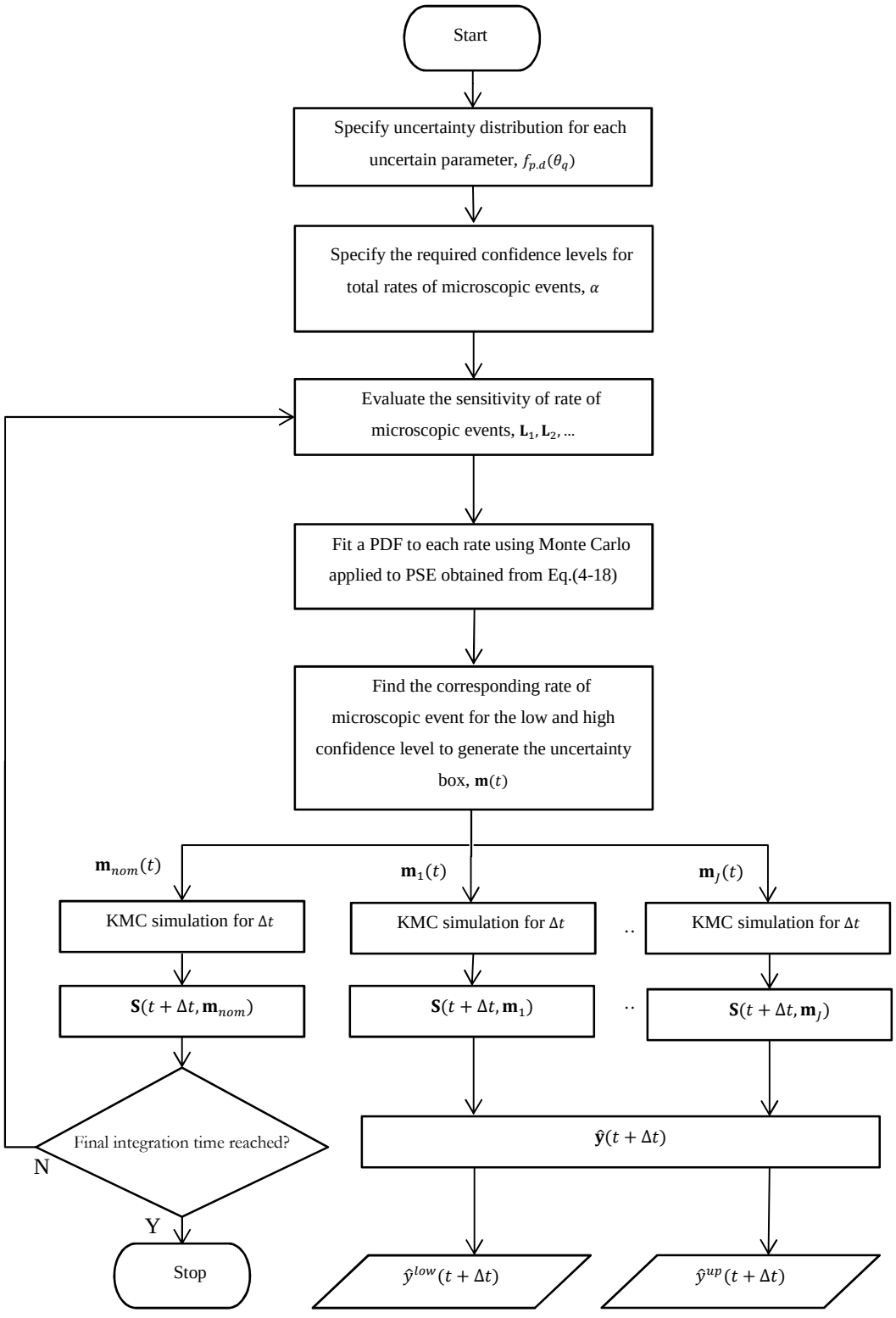

Figure 4-9. Flowchart of the algorithm used to approximate the upper and lower bounds of the outputs.

The major limitation of the proposed algorithm is its computational cost for control and optimization applications. To accelerate the simulations, reduced-order lattices are employed in the KMC simulations which give rise to other challenges. The new issues arise due to higher fluctuations encountered with smaller lattice sizes as shown in Figure 3-14. To eliminate the fluctuations presented due to reduced-order lattices, the probabilistic bounds are estimated based on averaging the estimates obtained from multiple independent simulations.

4.3.3. Robust optimization based on the probabilistic bounds

In this section, problem (4-15) is solved assuming $\boldsymbol{\theta}^T = [\mathcal{X}, E, E_m]$ is the set of uncertain parameters that are normally distributed around their nominal values listed in Table 3-1 with specific standard deviations. $\mathcal{X}$ is assumed as a time-invariant uncertain parameter with a standard deviation of 2×10^{-7} whereas E and E_m are assumed to change during operation every $\Delta t = 1$ s with standard deviations of 500 cal/mol. The bounds on the rates of microscopic event are calculated at 99% confidence level. The batch time is discretized into 10 stages of $\Delta t = 10$ s; the substrate temperature at the initial time of the batch is kept constant at $T = 800$ K. In this optimization, r_{max} and Gr_{min} are set to 5.25 mL and 10.5 mL/s whereas T_{min} and T_{max} are 600 and 1100 K, respectively.

The optimal substrate temperature profiles for the endpoint optimization problem using only nominal values in the parameters, as well as the robust approach under parametric uncertainty are shown in Figure 4-10. Figure 4-11 shows the bounds obtained using the optimal robust temperature trajectory profile. The corresponding open-loop variations of the surface roughness while using the robust temperature profile are also shown in that figure, i.e., random realizations in the uncertain parameters $\boldsymbol{\theta}$ that follow their description given above were simulated using the robust temperature profile. As shown in this figure, open-loop simulations are bounded with the upper and lower bounds obtained for roughness; the remaining constraints were also validated in the same fashion and are not shown here for brevity.

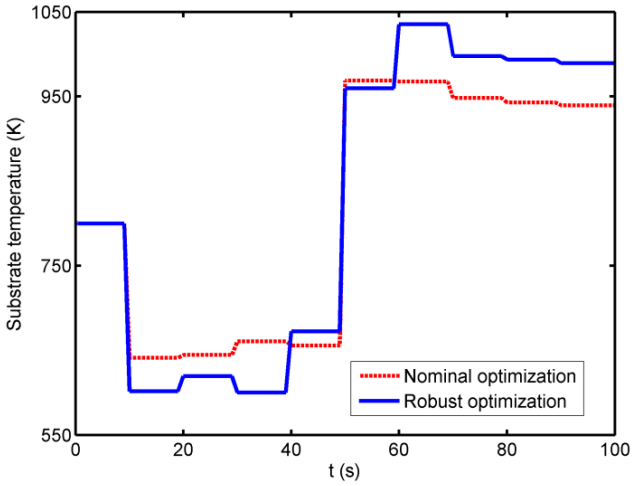

Figure 4-10. Optimal temperature profile obtained using the nominal parameters and robust approach.

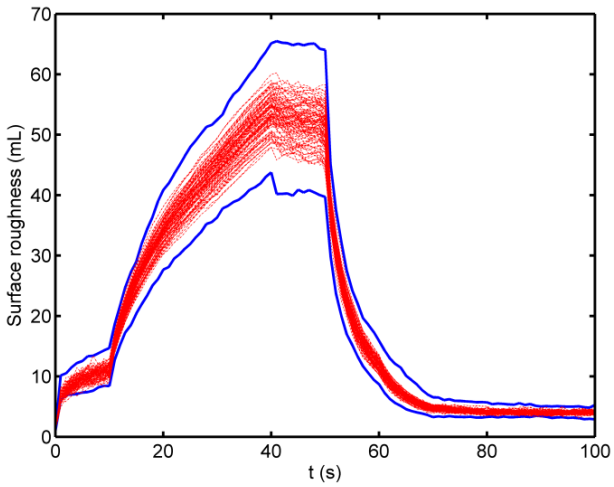

Figure 4-11. The upper and lower bounds estimated for surface roughness and open-loop simulations using the robust optimal temperature profile obtained under parametric uncertainty.

Figure 4-12 shows the corresponding open-loop variations of the final surface roughness and growth rate applying 100 Monte Carlo simulations using both the nominal temperature profile and the robust optimal temperature profile. As shown in this figure, open-loop simulations employing the robust temperature profile remained within the feasible operational limits specified for this process. On the other hand, the open-loop variations of the final surface roughness applying Monte Carlo simulations using the nominal temperature profile shows that the surface roughness at the end of the batch process does not meet the specification considered for this variable (r_{max}) most of the time, which results in a loss in performance.

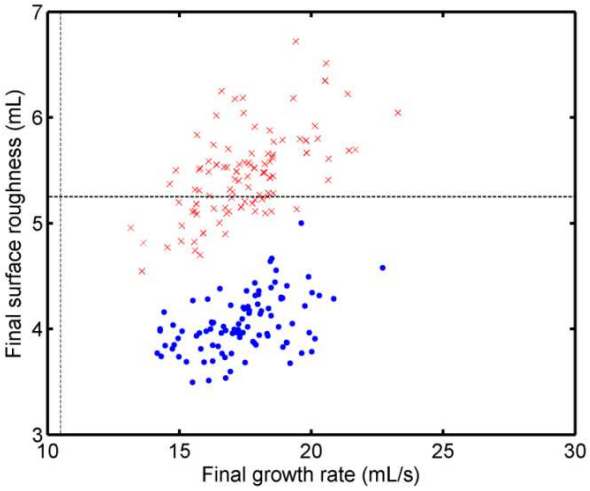

Figure 4-12. Final properties due to parameter uncertainties, obtained from the open-loop simulations applying various temperature profiles. The dots are for the robust temperature profile whereas the x-marks are for the nominal temperature profile; the dashed lines indicate the constraint on the final surface roughness and growth rate.

4.4. Summary

The main contribution of this research is to employ higher order PSEs for uncertainty analysis of multiscale systems. Although series expansions have been employed in the literature for sensitivity analysis of multiscale systems, PSEs have been employed in this part of the research for robust optimization of multiscale systems under uncertainty. The uncertainty analysis of the thin film deposition is performed applying worst-case and probabilistic-based approaches. The optimal temperature profile that maximizes the final thickness of the thin film under end-point product constraints and uncertainty in the model parameters was determined. The results show that employing the SSV analysis or probabilistic-based approach based on the prior assumption on type of the uncertainty affects the optimization results. Thus, inaccurate uncertainty description assumptions can lead to a loss in performance and therefore economic losses in the process.

A systematic framework was explored to analyze the time-varying model uncertainty propagation based on the PSE. The uncertainty in the parameters of the KMC simulations and in the boundary condition of the mass transfer equation is propagated into total rates of microscopic events using PSEs. That is, having the prior distribution of the uncertain parameters and estimating the sensitivities, the PDF of microscopic events are determined using the PSE.

Subsequently, upper and lower bounds on the outputs are estimated using the outputs distributions. The computational feasibility for robust optimization has been achieved using average of multiple multiscale models that apply reduced-order lattices in the KMC ion. This method has been used to obtain the optimal substrate temperature trajectory that maximized the endpoint thin film thickness while meeting constraints on the roughness and growth rate in the presence of uncertainty in the multiscale model's parameters. The proposed approach has been evaluated through simulations that show that the system's outputs remained within their corresponding feasible operational limits under uncertainty.

The implementation of the framework used in this chapter for online applications is still challenging and even prohibitive due to the computational costs associated with the simulations of the KMC model. The issue of computationally intensive KMC simulations is addressed in the next chapter by developing low-order models for online applications.

Chapter 5
Robust Estimation and Control of Surface Roughness and Growth Rate[†]

The production of high quality thin films is not feasible without a precise control framework. However, measurements are not available at a frequency that is required for effective control. Therefore, real-time estimators are required to estimate the desired thin film properties for control and optimization approaches. The controllability of the thin film growth process has been extensively studied in the literature. Most of the advanced microstructure controllers proposed in the literature for thin film deposition require measurements at fine scale, while in practice, thin film depositions are typically operated in open-loop. Moreover, model parameter uncertainty has been usually neglected in those methodologies. Thus, control approaches that can operate regardless of the measurements under model-plant mismatch are essential for the efficient operation of these processes. Methodologies for real-time estimation and control of thin film deposition process have been proposed based on multiple reduced-order lattices in KMC simulations (Lou and Christofides, 2003b). The implementation of KMC simulations for online applications is still challenging and even prohibitive due to the computational costs. The issue of computationally intensive KMC simulations is circumvented by developing low-order models that are identified offline based on data obtained from the multiscale model. This approach significantly reduces the simulation time over KMC and makes the online control and optimization feasible.

This chapter presents the development of an estimator to evaluate the surface roughness and growth rate based on the substrate temperature and the bulk precursor mole fraction during the growth process. Section 5.1 shows the open-loop responses in the deposition process and investigates the potential interactions between the manipulated variables and controlled outputs. Section 5.2 presents an algorithm to construct the multivariable robust estimator. In Section 5.3, the performance of the estimator is evaluated by coupling the estimator with PI controllers to simultaneously control the surface roughness and the growth rate under different scenarios. The outcomes obtained from this implementation are summarized at the end of this chapter.

[†] This chapter has been written based on: (Rasoulian and Ricardez-Sandoval, 2015b).

5.1. Interaction between the manipulated variables and controlled outputs

In order to design a multiple-input-multiple-output control scheme for the thin film deposition process, the effect of manipulated variables on the controlled outputs must be analyzed first. For this analysis, the multiscale model presented in Chapter 3 has been employed to mimic the actual process behavior. Eqs.(3-8)-(3-15) reveal the significant role of substrate temperature on the microscopic events that affect the surface microstructure, in thin film deposition, particularly roughness. Eq.(3-8) shows that the precursor mole fraction influences the deposition rate and accordingly the surface roughness and growth rate. Thus, the effect of bulk precursor mole fraction and substrate temperature on the surface roughness and growth rate, and their potential interactions, are studied through open-loop simulations. Figure 5-1 shows the surface roughness and growth rate when the bulk mole fraction is remained constant at 2×10^{-6} whereas the substrate temperature is changed from 1000 to 1100 K at $t = 50$ s. As illustrated in this figure, the growth rate shows an instantaneous decrease from approximately 17.3 to 16.5 mL/s, i.e., with a gain of -0.008 mL/(s.K). The surface roughness follows a typical step response to overdamped processes with a gain of -0.0125 mL/K, i.e., the roughness is decreased from 3.75 to 2.5 mL. Therefore, although the temperature affects both surface roughness and growth rate, the surface roughness is more sensitive to variations in temperature. In Figure 5-2, the roughness and growth rate profiles are shown when the bulk mole fraction is changed from 2×10^{-6} to 3×10^{-6} at $t = 50$ s while the temperature remained constant at 1000 K. As shown in this figure, the growth rate is instantaneously increased from approximately 17.3 to 26 mL/s with a gain of 8.7×10^{6} mL/s while the surface roughness follows a response typically observed for overdamped processes to step changes with a gain of 5.5×10^{5} mL, i.e., the roughness increased from 3.75 to 4.3 mL. Although the bulk precursor mole fraction affects both surface roughness and growth rate, growth rate is more sensitive to variations in this process variable. Therefore, the precursor mole fraction and temperature simultaneously affect the desired outputs and this interaction needs to be considered in multivariable estimation and control scheme.

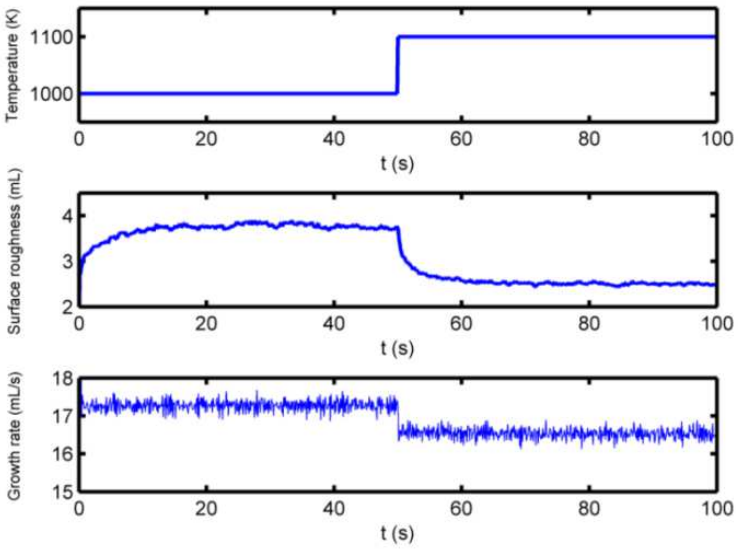

Figure 5-1. Surface roughness and growth rate for a step change in the substrate temperature from 1000 to 1100 K while $\mathcal{X} = 2 \times 10^{-6}$.

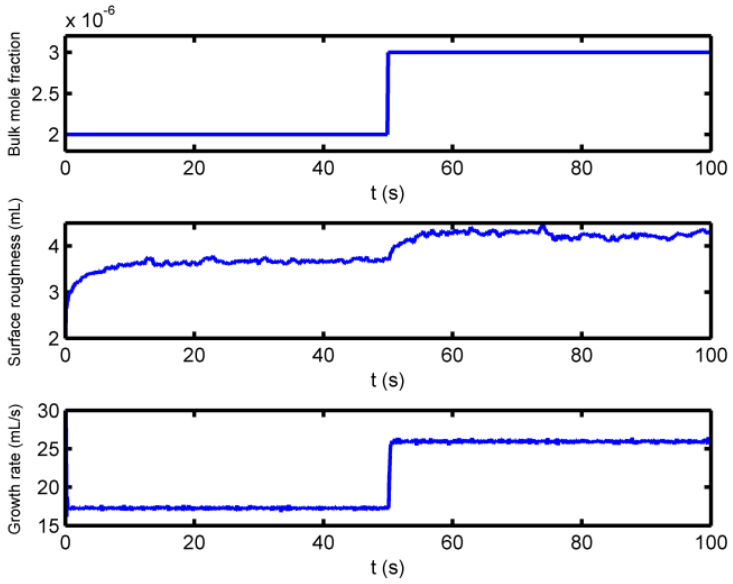

Figure 5-2. Surface roughness and growth rate for a step change in the bulk precursor mole fraction from 2×10^{-6} to 3×10^{-6} while $T = 1000$ K.

5.2. Real-time robust estimation of roughness and growth rate

In Section 4.3, some uncertainties were considered to be changing in time and an algorithm was proposed to estimate upper and lower bounds on the outputs under uncertainties. The

distributional uncertainty quantification was performed for the rates of the microscopic events using PSEs; upper and lower bounds of the outputs were then obtained using the PSE-based bounds on the rate of these events (Rasoulian and Ricardez-Sandoval, 2014). The main reason for uncertainty quantification of the states was the availability of a closed-form formulation between these rates and the uncertain parameters. Therefore, PSEs were employed to avoid the high computational load corresponding with simulation of the primary model for multiple realizations of the uncertain parameters. In the current research, however, the uncertainty is directly propagated into the outputs of the system where the closed-form model is not available. This approach provides the distribution of the outputs instead of only determining upper and lower bounds for the system's outputs. Uncertainty quantification is studied in this work employing PSEs to assess the variability resulted in the outputs of the system due to model parameter uncertainty.

5.2.1. Model construction

In this section, an algorithm is presented to develop a robust estimator that can mimic the multiscale process efficiently for online control and optimization purposes in the presence of model parameter uncertainty. As a result of the input/output interactions illustrated in Section 5.1, multivariable identification is considered. Offline system identification is performed to determine the parameters of a reduced-order model that describes the surface roughness and growth rate as a function of substrate temperature and bulk precursor mole fraction. The identified closed-form model is incorporated in an estimator that predicts the controlled outputs for online application. The algorithm comprises the following steps:

1. *Space discretization:* Discretize the operational region of temperature into equally spaced intervals ΔT, and the bulk precursor mole fraction region into equally spaced intervals $\Delta \mathcal{X}$.

$$T_i = \{T_{min} + i\Delta T | T_{min} \leq T_i \leq T_{max}, i = 0, 1, \dots, (T_{max} - T_{min})/\Delta T\},$$
$$\mathcal{X}_j = \{\mathcal{X}_{min} + j\Delta \mathcal{X} | \mathcal{X}_{min} \leq \mathcal{X}_j \leq \mathcal{X}_{max}, j = 0, 1, \dots, (\mathcal{X}_{max} - \mathcal{X}_{min})/\Delta \mathcal{X}\}, \quad (5\text{-}1)$$

   where T_{min} and T_{max} are respectively the minimum and maximum operating temperature while $\mathcal{X}_{min}$ and $\mathcal{X}_{max}$ are the minimum and maximum applicable bulk precursor mole fraction, respectively. The purpose of the discretization is to derive a finite-dimensional identification problem. Decreasing the discretization resolution reduces the computational costs but it also diminishes the model's ability to make accurate predictions whereas

increasing the number of discretization points improves the accuracy in the model predictions at the expense of higher computational costs.

2. *Batch time discretization:* Divide the batch time horizon $t \in [t_0, t_f]$ into equally spaced time intervals, Δt, with discrete time steps $t_k = t_0 + k\Delta t;\ k = 0,1,\dots,K$.
3. *Uncertainties description*: Define the vector of uncertain parameters $\boldsymbol{\theta} = \{\theta_1, \dots, \theta_q, \dots, \theta_Q\} \in \mathbb{R}^Q$, $\widehat{\boldsymbol{\theta}}$ as the vector of nominal model parameters, $\hat{y}$ as the output of the process using the nominal parameter vector, $\widehat{\boldsymbol{\theta}}$, and y as its value for the perturbed vector, $\boldsymbol{\theta}$. Specify the prior PDF of each uncertain parameter, $f_{p.d}(\theta_q)$.

$$\theta_q = \{\theta_q | \theta_q \in f_{p.d.}(\theta_q)\}. \tag{5-2}$$

Although this method takes advantage of the prior knowledge about the distribution of the uncertain parameters, the algorithm presented here is applicable regardless of the PDF assigned to the uncertain parameters.

4. *Sensitivity evaluation*: Evaluate the nominal outputs and sensitivities of the outputs with respect to the uncertain parameters for each pair of T_i and $\mathcal{X}_j$, at each discrete batch time, t_k, during the growth process. The sensitivities have to be estimated based on the average of multiple multiscale simulation runs using high-order lattices in the KMC models. The order of the sensitivities relies on the accuracy required by the PSE to approximate the outputs' PDFs of the primary multiscale model.
5. *Output's PDF approximation:* Estimate the PDF of y at each sampling time instance during the deposition for each pair of T_i and $\mathcal{X}_j$ using the following truncated PSE:

$$y_{i,j,k} = \hat{y}_{i,j,k} + \mathbf{L}_{1,i,j,k}\left(\boldsymbol{\theta} - \widehat{\boldsymbol{\theta}}\right) + \frac{1}{2}\left(\boldsymbol{\theta} - \widehat{\boldsymbol{\theta}}\right)^T \mathbf{L}_{2,i,j,k}\left(\boldsymbol{\theta} - \widehat{\boldsymbol{\theta}}\right) + \cdots, \tag{5-3}$$

where $\mathbf{L}_{1,i,j,k} = (dy/d\boldsymbol{\theta})_{\widehat{\boldsymbol{\theta}}} \in \mathbb{R}^Q$ and $\mathbf{L}_{2,i,j,k} = (d^2y/d\boldsymbol{\theta}^2)_{\widehat{\boldsymbol{\theta}}} \in \mathbb{R}^{Q\times Q}$ are respectively the Jacobian and Hessian evaluated at $T_i, \mathcal{X}_j$ and sampling time instance, t_k around the nominal values of the uncertain parameters ($\widehat{\boldsymbol{\theta}}$).

6. *Calculation of output's bounds*: Estimate the upper and lower bounds on y at a predefined confidence level, α, during the entire batch time for each pair of T_i and $\mathcal{X}_j$, $y_{i,j,k}^{PSE}$

$$y_{i,j,k}^{PSE} = F_{i,j,k}^{-1}(\mathbb{Pr}|y_{i,j,k}) = \{y_{i,j,k}: F_{i,j,k}(y_{i,j,k})\} \quad (5\text{-}4)$$

where the function $F^{-1}(\mathbb{Pr}|y)$ represents the inverse of CDF evaluated at a predefined probability, $\mathbb{Pr}$. Setting $\mathbb{Pr}$ in Eq.(5-4) to $\alpha/2$ and $1-\alpha/2$ yields respectively the lower bound and the upper bound on the output. Accordingly, y can be the upper or lower bound of any output of the process, i.e. surface roughness or growth rate.

7. *Model selection:* Select an appropriate model that can describe the evolution of the process outputs with respect to time. According to the trajectories depicted in Figure 5-1 and Figure 5-2 and the discussions provided in Section 5.1, the surface roughness can be interpreted as an overdamped process model whereas growth rate can be modeled as a steady-state gain process. Therefore, the following models are considered to describe the surface roughness and growth rate during the batch time for each pair of T_i and $\mathcal{X}_j$:

$$r(T_i, \mathcal{X}_j, t) = \beta_{1,i,j} T_i \mathcal{X}_j^{\beta_{2,i,j}} \left(1 - e^{-\frac{t}{\beta_{3,i,j}}}\right), \quad (5\text{-}5)$$

$$Gr(T_i, \mathcal{X}_j) = \beta_{4,i,j} T_i \mathcal{X}_j, \quad (5\text{-}6)$$

where $\beta_{l,i,j} (l = 1, \dots, 4)$ are the low-order model parameters that can be identified through the least-squares approach.

8. *Model identification:* Estimate the parameters of Eqs.(5-5)-(5-6) for the dataset obtained for each pair of T_i and $\mathcal{X}_j$ (i.e. $\beta_{l,i,j}$) through minimization of the following least-squares function:

$$\phi(\boldsymbol{\beta_{i,j}}) = \sum_{k=0}^{K} (y_{i,j,k}^{PSE} - y_{i,j,k}^{pred})^2, \quad (5\text{-}7)$$

where $y_{i,j,k}^{PSE}$ and $y_{i,j,k}^{pred}$ are respectively the bound on the process output obtained using the PSE-based approach and model prediction of the output at k^{th} sampling time instance and T_i and $\mathcal{X}_j$. The identified $\beta_{l,i,j} (l = 1, \dots, 4)$ represent the parameters of the models presented in Eqs.(5-5)-(5-6) for each pair of T_i and $\mathcal{X}_j$. That is, there exists one model for each pair of temperature and bulk mole fraction considered in the *Space discretization* step.

9. *Approximation of the low-order model parameters:* The aim of this step is to use the model parameters estimated from offline identification at each discrete point (i.e. $\beta_{l,i,j}$) to determine a polynomial function that can be used to estimate these parameters at any temperature or bulk mole fraction that is within the operational region, i.e., $\bar{\beta}_l (l = 1, \dots, 4)$. Regression can be

used to correlate the estimated parameters, $\bar{\beta}_l (l = 1, \dots, 4)$, to the independent variables T and $\mathcal{X}$:

$$\bar{\beta}_l = b_{0,l} + \sum_{d=1}^{D} b_{d,l} \Gamma_d(T, \mathcal{X}), \tag{5-8}$$

where Γ_d represents a polynomial function of temperature and bulk precursor mole fraction; $b_{0,l}$ and $b_{d,l}$ are the polynomial coefficients calculated using regression analysis and D is the number of independent terms considered in the analysis. These polynomial correlations can be used in closed-form models to predict the surface roughness and growth rate for online applications.

10. *Online robust estimator:* Once these polynomial correlations are obtained offline, they can be used for online estimation of roughness and growth rate. According to Eq.(5-6), measuring the temperature and bulk mole fraction is sufficient to estimate growth rate. On the other hand, surface roughness at any sampling time during the growth process depends not only on temperature and bulk precursor mole fraction but also on the roughness at a previous time instance; thus,

$$r_k = r_{k-1} + sgn\left(\bar{\beta}_1 T \mathcal{X}^{\bar{\beta}_2}\left(1 - e^{-\frac{t_k}{\bar{\beta}_3}}\right) - r_{k-1}\right)\left|\left(\bar{\beta}_1 T \mathcal{X}^{\bar{\beta}_2} - r_{ref}\right)\left(e^{-\frac{t_{k-1}-t_{ref}}{\bar{\beta}_3}} - e^{-\frac{t_k - t_{ref}}{\bar{\beta}_3}}\right)\right|, \tag{5-9}$$

where r_k is the estimated roughness at sampling time instance, t_k, while r_{k-1} is the estimated roughness at previous sampling time instance, t_{k-1}. It is important to note that, r_{k-1} is obtained from the estimator. r_{ref} and t_{ref} respectively denote the reference roughness and the reference time when the substrate temperature changes to the current temperature. sgn is the sign function while $\bar{\beta}_1$, $\bar{\beta}_2$ and $\bar{\beta}_3$ are the model parameters evaluated using the temperature and bulk mole fraction at time, t_k.

5.2.2. Application to thin film deposition process

To determine the order of the required PSEs for distributional uncertainty propagation, a comparison has been made between the PDFs obtained via uncertainty propagation in surface roughness using the primary multiscale model and PSEs. In this case, $\boldsymbol{\theta}^T = [E, E_d, E_m]$ is considered as the vector of uncertain parameter. It is assumed that the uncertainties are normally distributed around their nominal values listed in Table 3-1 with a standard deviation of 500 cal/mol. The standard deviation for the uncertain parameters is set based on the sensitivity of the model outputs to these parameters. Note that the PSE technique is applicable regardless of the

variability in the model parameters. Therefore, 1000 sample points were generated randomly for the vector of uncertain parameters from their corresponding prior PDFs. The roughness PDF at $t = 20$ s is obtained through the Monte Carlo technique employing these sample points in the multiscale model described in Chapter 3 at $T = 800$ K and $\mathcal{X} = 2 \times 10^{-6}$. This PDF is plotted in Figure 5-3 with the PDFs obtained using first and second-order PSE approximations. The normal distribution resulted from the first-order PSE can be estimated analytically whereas, for the second-order PSE, the Monte Carlo sampling method is applied (Nagy and Braatz, 2007). As illustrated in this figure, although first-order PSE can adequately describe the distribution of surface roughness, second-order PSE has captured the tails of the PDF more accurately.

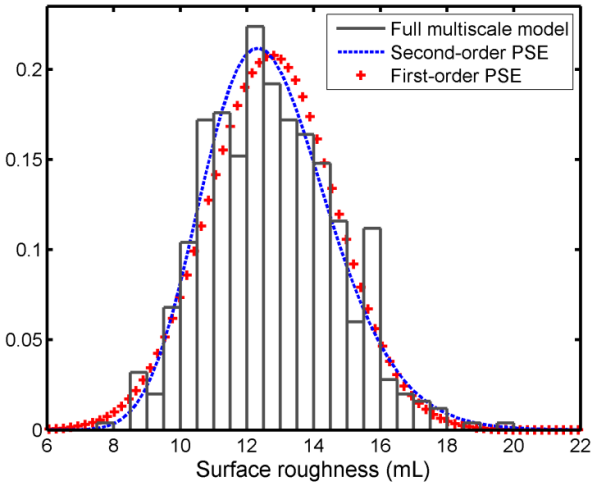

Figure 5-3. Roughness PDFs at $T = 800$ K and $\mathcal{X} = 2 \times 10^{-6}$ obtained using the multiscale model, first and second-order PSEs at $t = 20$ s.

The computational times for these approaches are depicted in Table 5-1. As shown in this table, the implementation of the Monte Carlo sampling technique for uncertainty propagation in the outputs using the multiscale model has a high computational cost compared to PSE-based approaches. Upper and lower bounds obtained at 68.2% confidence interval are also shown in Table 5-1. Comparing the bounds estimated using PSE-based approaches with those obtained from the multiscale model reveals that, although the bounds evaluated using first-order PSE are acceptable, the second-order PSE provides higher accuracy. As shown in Table 5-1, the error of the first-order PSE model is larger than 1% (i.e., 1.7% and 1.024%) whereas the errors in the second-order PSE are smaller than 1% (i.e., 0.2% and 0.7%). This confidence interval corresponds to the upper and lower bounds that lie within one standard deviation from the mean

value. It is important to note that these bounds can be calculated using any other value for the confidence interval.

Table 5-1. The probabilistic bounds of the surface roughness at 68.2% confidence interval from different approaches and the corresponding computational costs.

Approach	r^{low}**(mL)**	r^{up}**(mL)**	**Computational Time**
Monte Carlo using the multiscale model	10.81	14.71	28 hr
First-order PSE	10.62 (1.7%)	14.56 (1.02%)	16.6 min
Monte Carlo using the second-order PSE	10.83 (0.2%)	14.82 (0.7%)	38 min

Figure 5-4 shows the roughness PDFs obtained at a different operating point, i.e., $T = 1100$ K and $\mathcal{X} = 4 \times 10^{-6}$. Likewise, the second-order PSE is able to capture the tails of the output distribution more accurately. Although more accurate output distributions may be obtained using high-order expansions, the order of the PSE is mostly determined by the accuracy of the approximation required while performing the robustness analysis.

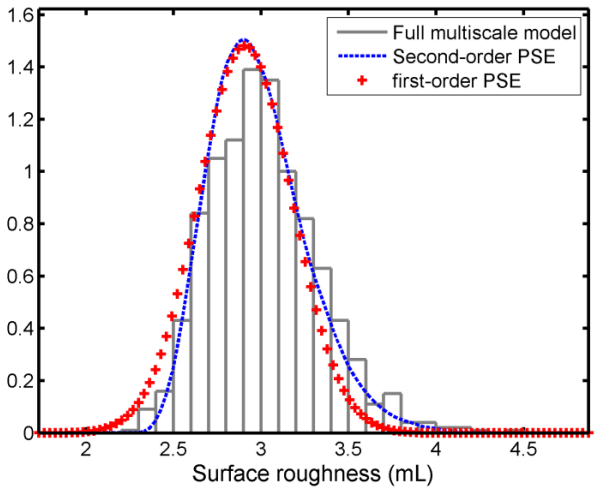

Figure 5-4. Roughness PDFs at $T = 1100$ K and $\mathcal{X} = 4 \times 10^{-6}$ obtained using the multiscale model, first and second-order PSEs at $t = 20$ s.

To investigate the effect of this set of uncertain parameters on growth rate, the distribution of growth rate is estimated using the Monte Carlo sampling method applied on 1000 sample points randomly generated from the corresponding PDFs of the uncertain parameters. Uncertainty is propagated into the growth rate employing the multiscale model, first and second-order PSE

approximations at $T = 800$ K and $\mathcal{X} = 2 \times 10^{-6}$. As shown in Figure 5-5, the variability in growth rate as a result of uncertainty is small and growth rate is not significantly sensitive to this set of uncertainties.

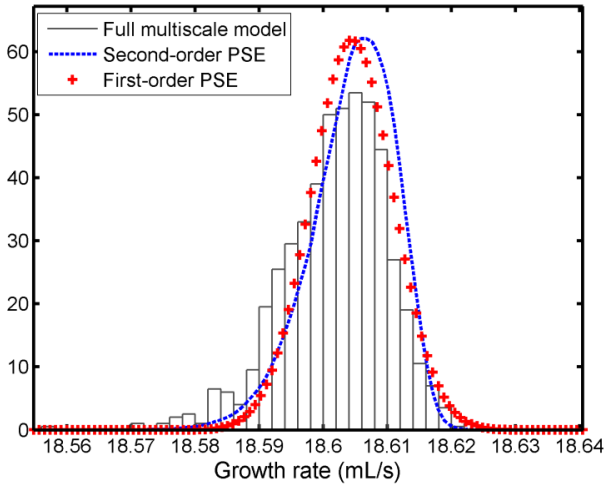

Figure 5-5. Growth rate PDFs at $T = 800$ K and $\mathcal{X} = 2 \times 10^{-6}$ obtained using the multiscale model, first and second-order PSEs at $t = 20$ s.

To develop the proposed robust estimator for the thin film deposition presented in Chapter 3, it is assumed that the substrate temperature can change from 600 K to 1400 K, $T_i (i = 1, \dots, 9)$, whereas precursor bulk mole fraction can vary from 1×10^{-6} to 7×10^{-6}, $\mathcal{X}_j (j = 1, \dots, 7)$. For this application, using more discrete points does not improve the accuracy of the estimations. To discretize the batch time, $t_f = 100$ s, 101 discretization points were used. As shown in Figure 5-3 and Figure 5-4, surface roughness is quite sensitive to these uncertain parameters. Despite that high-order PSEs provide more accurate distributions of roughness, the first-order PSE is applied here since it was accurate enough for control purposes. Therefore, first-order sensitivities of roughness with respect to the uncertain parameters are generated offline for each pair of temperature and bulk mole fraction along the batch time. Due to normally distributed uncertainties assumption in the parameters and using a first-order PSE, the uncertainty in the surface roughness will be normally distributed and its mean and variance can be calculated analytically (Nagy and Braatz, 2007). The mean and the variance of the corresponding normal distributions are used to obtain the lower and upper bounds on roughness at $\alpha = 0.5\%$. This data is used in *Model identification* step in the previous algorithm to estimate the model parameters for each pair of T_i and $\mathcal{X}_j$. The regression results for the upper bound on roughness at $T = 600$ K

and $T = 700\,\mathrm{K}$ are presented in Appendix A. To provide a general model for the whole operational region (step 9 in the previous algorithm), the operational substrate temperature region is divided into three regions and the parameters in Eq.(5-5) are estimated assuming that these parameters are functions of substrate temperature and bulk mole fraction as follows:

$$\bar{\beta}_l = b_{0,l} + b_{1,l}T + b_{2,l}T^2 + b_{3,l}T\mathcal{X} + b_{4,l}T^2\mathcal{X} + b_{5,l}T^2\mathcal{X}^2. \quad (5\text{-}10)$$

Figure 5-6 shows the model fittings obtained from regression for these parameters, which are used to estimate the upper bound on surface roughness when the operating temperature is between 1100 K and 1400 K. It is important to note that, for brevity, the regression results for other regions of temperature are provided in the Appendix A. Moreover, the narrow confidence bounds obtained for each regression is included in Appendix A demonstrating that the regression models are statistically significant. Although other polynomial functions or nonlinear functions can be used, the estimations obtained by the function shown in Eq.(5-10) are sufficiently accurate for online control purposes.

To examine the performance of the estimator, upper and lower bounds obtained for the surface roughness from the robust estimator are shown in Figure 5-7. In this case, the bulk precursor mole fraction is maintained constant at 3×10^{-6} whereas the substrate temperature is changed according to the profile shown in this figure. To show the effect of uncertainties, a set of 30 realizations were generated from the distributions of uncertain parameters and used in the multiscale model to calculate the surface roughness. As shown in Figure 5-7, these open-loop simulations are bounded within the lower and the upper bounds obtained by the robust estimator. It is important to note that, in the presence of model-plant mismatch, estimating the upper bound on roughness from the multiscale model is not applicable in online applications. That is, calculating the bounds employing PSE takes couple of hours while the closed-form models developed in this work predict the bounds in milliseconds.

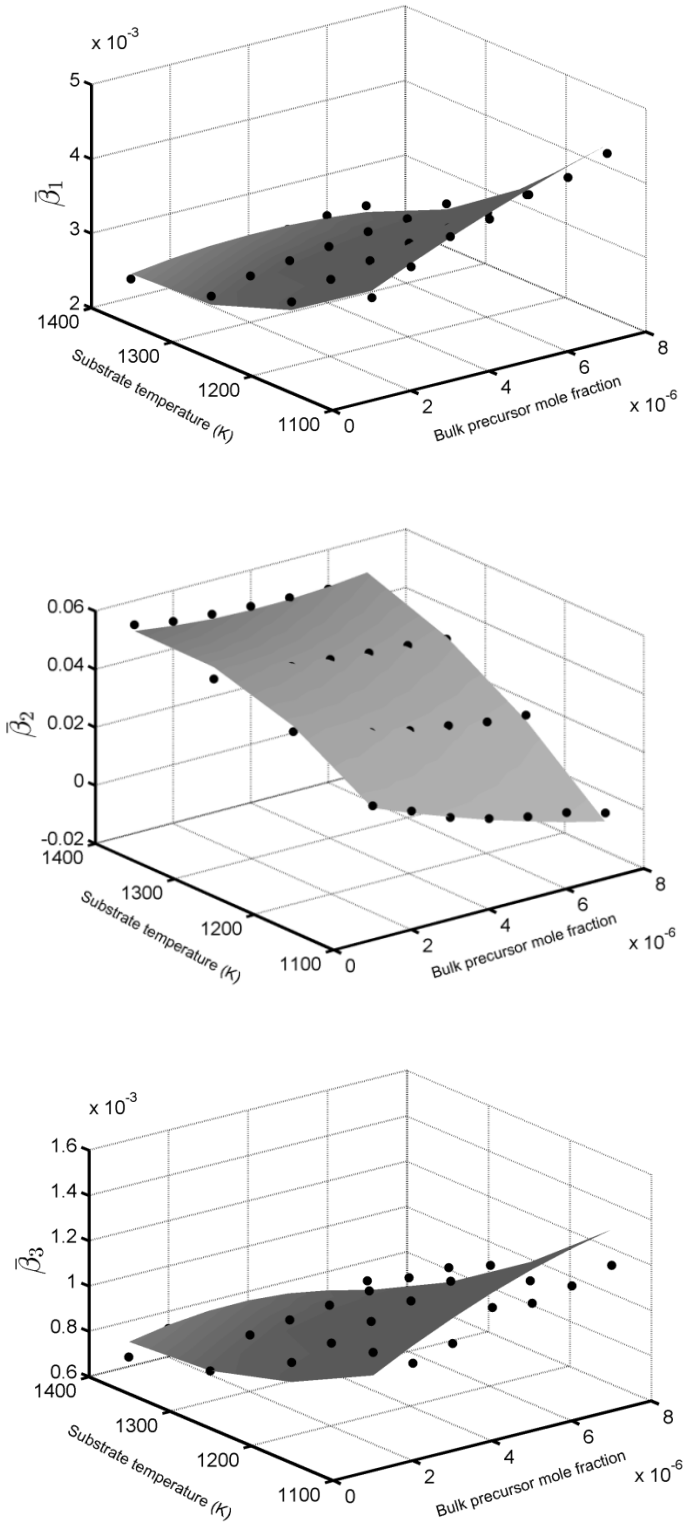

Figure 5-6. Polynomial models used to determine $\bar{\beta}_1, \bar{\beta}_2$ and $\bar{\beta}_3$ to estimate the upper bound on surface roughness while $1100\ \mathrm{K} < T < 1400\ \mathrm{K}$.

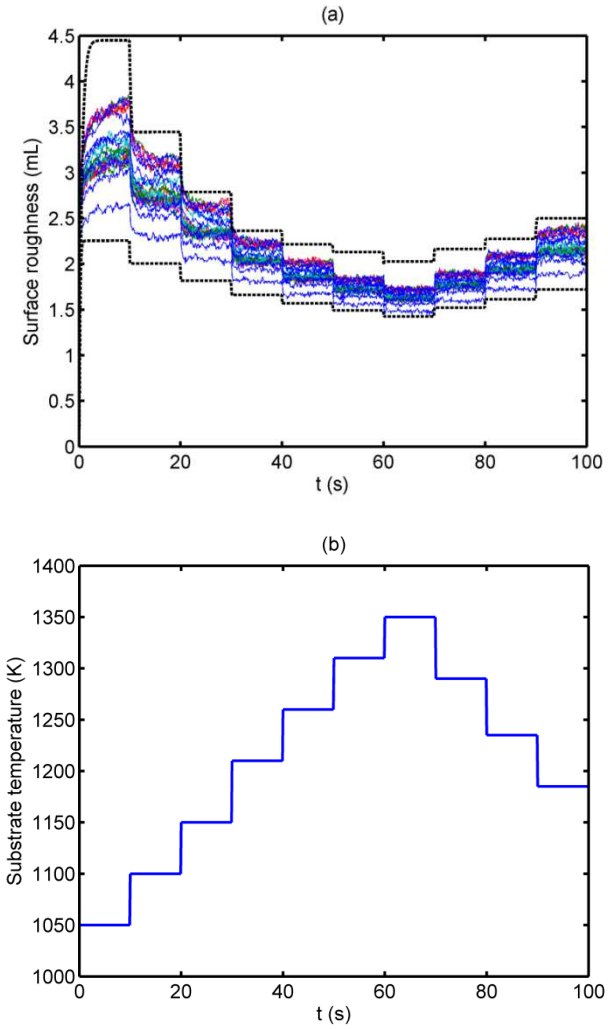

Figure 5-7. (a) Surface roughness due to parameter uncertainties, obtained by Monte Carlo simulation using 30 open-loop simulations (solid lines), the upper and lower bounds on surface roughness by robust estimator (dashed lines), (b) Substrate temperature profile.

To develop an estimator for growth rate, as shown in Figure 5-5, the uncertain parameters considered in the present analysis have no significant effect on this output of the process. Therefore, a nominal estimator was designed for growth rate from the data collected using open-loop multiscale simulations at each pair of T_i and $\mathcal{X}_j$. The input and output measurements along with the model proposed in Eq.(5-6) are used in least-squares minimization to obtain $\beta_{4,i,j}$ for each discrete point in the operational domain. Then, the following model is obtained for growth rate through regression:

$$Gr = (5.34 \times 10^4 - 99.1T + 4.92 \times 10^4 T\mathcal{X} + 7.5 \times 10^{-2} T^2 - 2.1 \times 10^{-5} T^3) T\mathcal{X}, \qquad (5\text{-}11)$$

where the term in the brackets is the polynomial function used to approximate $\bar{\beta}_4$ for any temperature and bulk mole fraction in the specified operating region.

To show the performance of the nominal estimator for growth rate, the bulk precursor mole fraction is maintained constant at 3×10^{-6} whereas the substrate temperature is changed according to the profile shown in Figure 5-7(b). The estimated profile and the growth rate obtained from the multiscale model under uncertainty in the parameters are shown in Figure 5-8. As shown in this figure, the estimator predicts the growth rate obtained from the multiscale model.

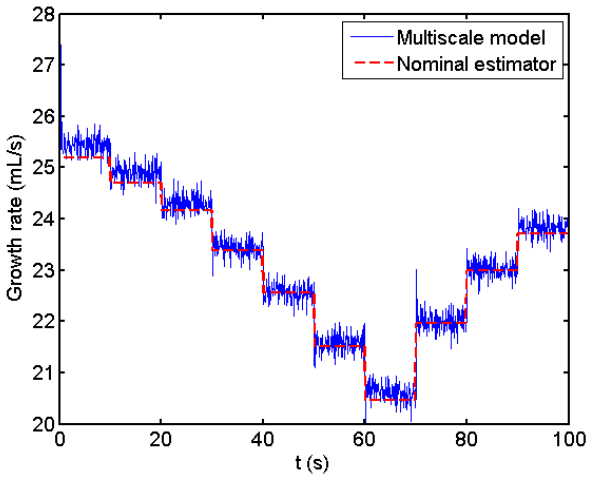

Figure 5-8. Comparison between the growth rate obtained by multiscale model and growth rate estimated using the estimator.

5.3. Control of surface roughness and growth rate

In this section, the multivariable control of surface roughness and growth rate is studied adopting the estimator proposed in Section 5.2 coupled with PI controllers. The control scheme block diagram is shown in Figure 5-9 and thin film deposition is modeled based on the multiscale model developed in Chapter 3 using a 100 × 100 lattice in the KMC simulation.

To justify the need for a robust estimator in the control applications and to demonstrate the effectiveness of the proposed estimator, three different case studies are investigated:

1. The nominal estimator is applied to control the nominal thin film deposition process.

2. The nominal estimator is employed to control the deposition process under model parameter uncertainty.
3. The robust estimator is applied to control the deposition process under model parameter uncertainty.

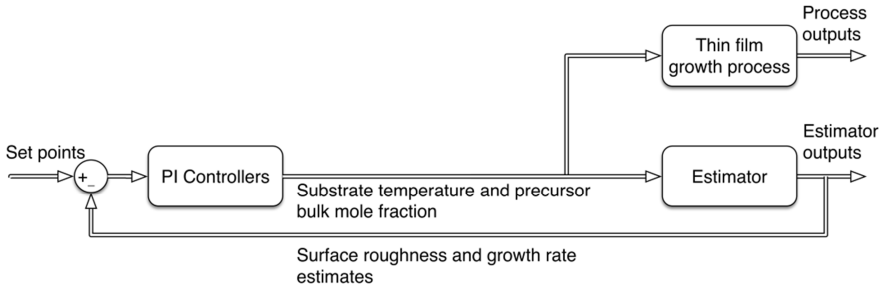

Figure 5-9. Block diagram of multivariable control of thin film growth process.

In the first case study, a nominal estimator would suffice to estimate the controlled outputs assuming that all the parameters of the process are perfectly known. To design the nominal estimator, step 4-6 in the algorithm proposed to design the estimator in Section 5.2.1 is modified as follows: instead of estimating bounds on the controlled outputs, the responses from multiple open-loop simulations are averaged for roughness and growth rate using the nominal model parameters shown in Table 3-1. According to the results shown in Figure 5-1 and Figure 5-2, the surface roughness is paired with substrate temperature whereas growth rate is paired with the bulk precursor mole fraction. The set point of the surface roughness in these simulations is 2 mL while the proportional gain in its PI controller is set to 1.7 K/mL and its integral gain is set to 1 K/(mL.s). The set point for the growth rate is set to 40 mL/s while the proportional gain and the integral gain in the growth rate PI controller are 1.4×10^{-9} mL^{-1} and 8×10^{-10} $(mL.s)^{-1}$, respectively. As shown in Figure 5-9, the controller uses the estimate of the outputs obtained from the estimator to determine the control actions including temperature and precursor mole fraction. The controlled surface roughness and growth rate from the deposition process, their corresponding estimations and also their control actions are illustrated in Figure 5-10. As shown in this figure, the estimator is able to follow the multiscale process resulting in a successful regulation of the surface roughness and growth rate around their desired set points.

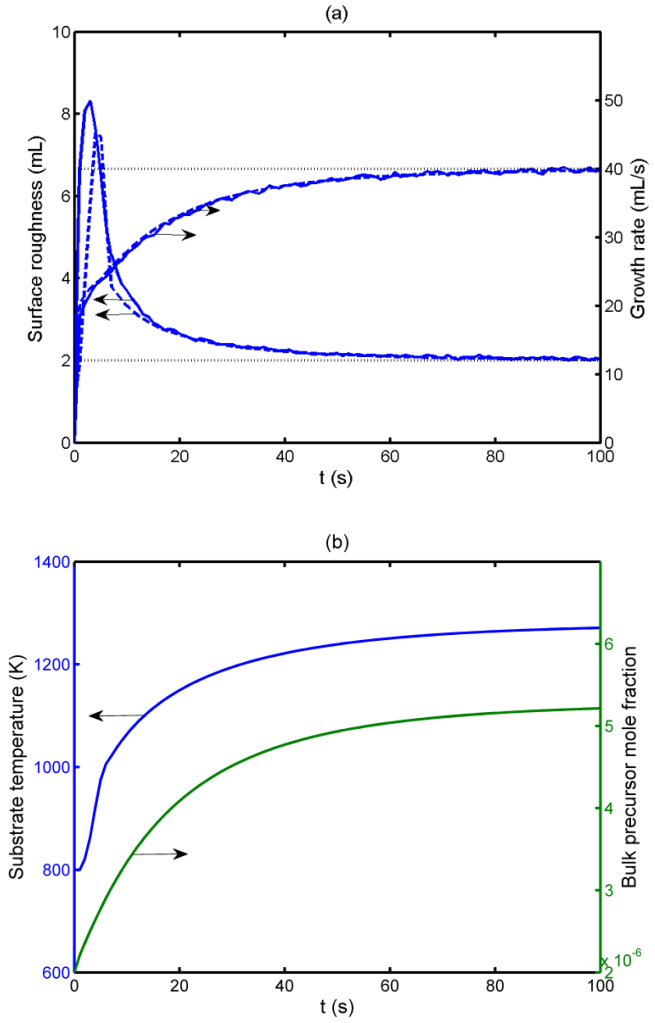

Figure 5-10. (a) Surface roughness and growth rate trajectories from the nominal process (solid line), the roughness and growth rate estimations from the nominal estimator (dashed line), (b) Substrate temperature and bulk precursor mole fraction trajectories.

In the second case study, to make the study more realistic, the performance of the nominal estimator is investigated when there is uncertainty in the model parameters of the system. To incorporate uncertainty in the process, it is assumed that $\boldsymbol{\theta}^T = [E, E_d, E_m]$ is the vector of uncertain parameters that are normally distributed around their nominal values with a standard deviation of 500 cal/mol. Since growth rate is not sensitive to these uncertain parameters, the results are only shown for surface roughness. In thin film manufacturing, the surface roughness has to be less than a certain value since higher roughness can deteriorate the conductivity of the semiconductor. As shown in Figure 5-11, the surface roughness is sensitive to these uncertainties and the estimated roughness is smaller than the surface roughness obtained from the multiscale

model. Accordingly, underestimating the surface roughness by the nominal estimator has hindered the performance of the control framework. This result motivates the development of a robust estimator for this process.

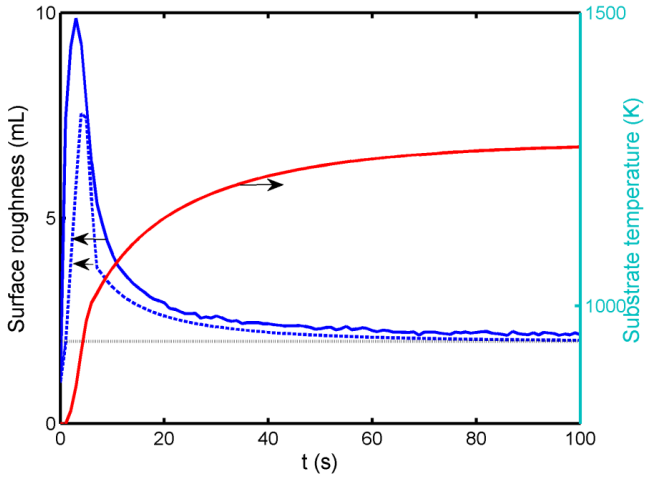

Figure 5-11. Surface roughness trajectory from process under uncertainty (solid line), the roughness estimation from the nominal estimator (dashed line) and the substrate temperature.

Based on the above, in the third case study, the algorithm presented in the previous section is implemented to design a robust estimator. To ensure the control objective at the end of the batch, the robust estimator is designed such that it predicts the upper bound on surface roughness. As shown in Figure 5-12, the estimated roughness is larger than the roughness obtained from multiple multiscale simulations. Therefore, the robust estimator is able to ensure that the surface roughness at the end of the batch is always below its set point limit under uncertainty in the system parameters, which is a desirable feature given the robust approach pursued in this work. The multiscale simulations shown in Figure 5-12 were generated under multiple realizations in the uncertain parameters that follow the PDF descriptions defined for these parameters.

To further investigate the performance of the robust estimator, the set points for surface roughness and growth rate were changed to 2.5 mL and 50 mL/s, respectively. As shown in Figure 5-13, the coupled robust estimator and PI controllers have successfully regulated the process outputs around their corresponding set points in the presence of uncertainty in the multiscale model parameters.

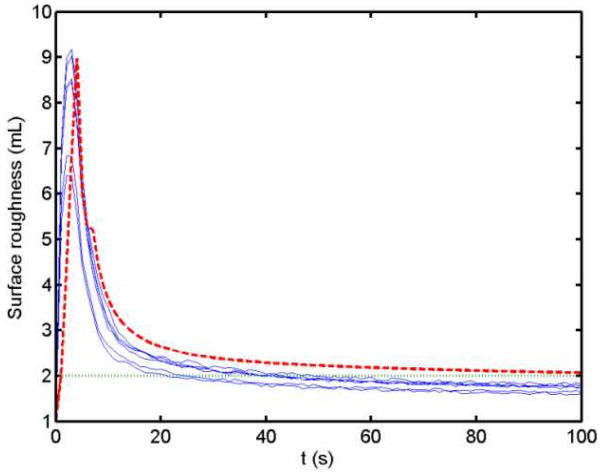

Figure 5-12. Surface roughness trajectories from process under uncertainty (solid lines), the roughness estimation from the robust estimator (dashed lines).

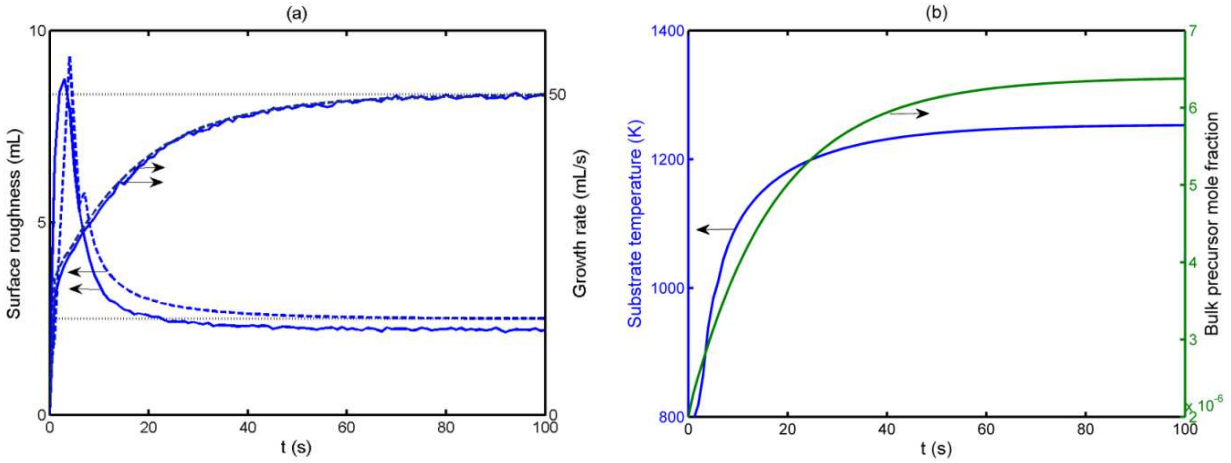

Figure 5-13. (a) Surface roughness and growth rate trajectories from the process under uncertainty (solid line), the roughness and growth rate estimations from the robust estimator (dashed line), (b) Substrate temperature and bulk precursor mole fraction trajectories.

5.4. Summary

Although the cutting-edge sensors that are able to perform measurements online at the fine-scale level can improve monitoring and control, in practice, most of the industrial thin film deposition processes are still operated in open-loop. Motivated by this, a methodology to design a robust multivariable estimator has been presented in this chapter to assess the surface roughness and growth rate efficiently under uncertainty in a thin film deposition process. To that end, the uncertainty in the outputs of the system is quantified through the PSEs while the

coefficients of these expansions are identified offline based on the output data collected from the multiscale model. Uncertainty in a few of the multiscale model parameters has been added to account for plant-model mismatch. To demonstrate the performance of the estimator in multivariable process control applications, the proposed estimator is coupled with PI controllers. To provide a robust control of surface roughness, the robust estimator predicts the upper bound on this controlled output. As shown in the simulation results, the predicted surface roughness at the end of the batch bounds the multiple realizations from the multiscale model under parameter uncertainties and prevents a loss in performance. Although the developed low-order model is used to design a robust estimator, it is also applicable for robust optimization purposes, or as a basis for the design of an MPC algorithm.

Chapter 6
Robust NMPC for a Thin Film Deposition Process[‡]

The economics in the microelectronics industry highly depend on the operating policies adopted in the plant. Non-optimal strategies may result in undesired plant performance leading to economic loss or environmental and safety hazards. Model-plant mismatch, actuator constraints and sporadic sensor data can potentially drive the process far from the optimum. Unlike conventional feedback controllers, the main advantage of the MPC framework is the ability to cope with the safety, operational or economic constraints in the presence of model-plant mismatch (Mayne et al., 2000). MPC provides an effective control framework employing the system model to predict the control actions which optimize a performance index in the presence of constraints (Allgöwer et al., 2004; García et al., 1989; Qin and Badgwell, 2003). Therefore, in practice, a closed-form model is essential for efficient and accurate forecasting of the process behavior (Morari and H. Lee, 1999). To guarantee closed-loop performance under deterministic parameter uncertainty, robust formulations have been proposed in the literature based on the worst-case deviation in product quality (Gunawan et al., 2004; Ma et al., 1999; Ma and Braatz, 2001). Robust MPC addresses optimal control problems with hard constraints that must be satisfied for all realizations of the parameter uncertainty. Such a control design, however, can become overly conservative when the realizations in the uncertain parameters that produce the worst-case scenario have a low frequency of occurrence (Nagy and Braatz, 2004). Therefore, distributional uncertainty analysis have been proposed where the restriction imposed by the bounded uncertainty description is relaxed using probabilistic-based uncertainties (Nagy and Braatz, 2003a, 2003b; Ricardez-Sandoval, 2012). In addition to probabilistic descriptions for the uncertain parameters, the MPC formulation can be solved with probabilistic constraints (Mesbah et al., 2014; Nagy, 2009). Adopting a chance constrained approach, stochastic MPC allows an acceptable level of risk where the constraints are satisfied with a specific probability of occurrence (Cannon et al., 2011; Li et al., 2008; Schwarm and Nikolaou, 1999).

Although the advent of multiscale modeling has significantly improved the prediction capabilities in the thin film deposition process, this type of models are not appropriate for advanced control strategies. Multiscale models are not available in closed-form and are

[‡] This chapter has been written based on (Rasoulian and Ricardez-Sandoval, 2015c) and S. Rasoulian, L.A. Ricardez-Sandoval, Stochastic nonlinear model predictive control applied to a thin film deposition process under uncertainty, Submitted to the Chemical Engineering Science, CES-D-15-01118.

computationally prohibitive for online applications. Particularly, in an MPC framework, which has been the most prominent advanced control strategy, an online optimization-based technique is adopted where extensive online calculations are required. Nevertheless, the detailed multiscale models can be employed to derive low-order models that are practical for an MPC framework. In this chapter, the development of closed-form models is presented that can predict the control objectives in the presence of model-plant mismatch. These models will be efficient for online applications, while being able to capture the multiscale nature of the thin film deposition process under uncertainty. Although PSE can be employed to analyse the distributional uncertainties in the controlled outputs under model parameter uncertainties, the evaluation of the sensitivities is not straightforward. Sensitivities change in time and online estimation of these sensitivities through the multiscale model is not practical. Thus, offline identification is performed to identify the parameters of the closed-form model.

This chapter presents an algorithm to develop a closed-from model that is identified offline to predict the controlled outputs at a predefined specific probability for a robust NMPC application. The identification is performed for a fixed confidence level and hard constraints are imposed in the robust MPC framework. In another approach, to improve the robust performance using probabilistic constraints, closed-form models are developed to estimate the first and second-order statistical moments of the thin film properties under uncertainty in the multiscale model parameters. Since, the closed-form models enable the prediction of outputs at any probability limit, the probabilistic (soft) constraints in the stochastic MPC framework can be reformulated as deterministic constraints. In Section 6.1, a PSE-based framework is presented to identify a closed-form model that can predict the controlled outputs based on the substrate temperature at a predefined probability in the presence of model parameter uncertainties. The model is employed in an NMPC framework to minimize the final surface roughness while satisfying the hard constraints on the temperature profile and final film thickness. Section 6.2 provides the algorithm used in this work to develop a closed-form model that predicts the statistical moments of the controlled outputs as a function of the control actions during the deposition process. This model enables the reformulation of the stochastic NMPC as a computationally tractable NMPC framework. The performance of the stochastic NMPC is evaluated under different scenarios.

6.1. Robust NMPC with hard constraints for thin film deposition process

As mentioned previously, PSE is applied in this work as a practical tool for uncertainty analysis since it only requires the computation of the sensitivities of the controlled outputs with respect to the uncertain parameters. An approach to circumvent the inherent noise included in the multiscale model due to the KMC simulations is averaging the estimates obtained from multiple simulations which increases the computational costs (Drews et al., 2003). Since this approach is not practical for online applications, in the current work, the required sensitivities in the expansions are assessed offline by central finite differences through average of multiple multiscale simulations describing the thin film deposition process. Subsequently, closed-form models that can efficiently predict the probabilistic bounds on the controlled outputs under model parameter uncertainty are developed for online control applications. The algorithm developed to identify the closed-form model from a multiscale process system is described next.

6.1.1. Model construction procedure

Specify the vector of uncertain parameters $\boldsymbol{\theta} = \{\theta_1, \dots, \theta_q, \dots, \theta_Q\} \in \mathbb{R}^Q$, $\widehat{\boldsymbol{\theta}}$ as the vector of nominal model parameters; $\hat{y}$ as the process output obtained from the nominal parameter vector, $\widehat{\boldsymbol{\theta}}$, and y as the output for the perturbed vector, $\boldsymbol{\theta}$. From a control point of view, the purpose of this study is to manipulate the thin film properties using the substrate temperature. The PSE-based algorithm to estimate the controlled outputs as a function of the substrate temperature at any time during the process under model parameter uncertainty can be outlined as follows:

1. *Space discretization:* Discretize the operational region of substrate temperature into equally spaced intervals ΔT, i.e.,

   $$T_i = \{T_{min} + i\Delta T | T_{min} \leq T_i \leq T_{max}, i = 0, 1, \dots, (T_{max} - T_{min})/\Delta T\}, \quad (6\text{-}1)$$

   where T_{min} and T_{max} are respectively the minimum and maximum operating substrate temperatures.
2. *Batch time discretization:* Divide the batch time horizon $t \in [t_0, t_f]$ into equally spaced time intervals, Δt, as follows:

   $$t_k = \{t_0 + k\Delta t | t_0 \leq t_k \leq t_f, k = 0, 1, \dots, K\}, K = (t_f - t_0)/\Delta t. \quad (6\text{-}2)$$

3. *Uncertainties description*: Define the prior PDF of each uncertain parameter, $f_{p.d}(\theta_q)$, as follows:

$$\theta_q = \{\theta_q | \theta_q \in f_{p.d.}(\theta_q)\}. \quad (6\text{-}3)$$

The prevalent assumption in distributional uncertainty analysis is that uncertainty is distributed around the nominal parameter with a specific variability. When the nominal value changes during the process, the variance can also change proportional to the nominal value.

4. *Sensitivity evaluation*: For every T_i, evaluate the nominal outputs and sensitivities of the outputs with respect to the uncertain parameters at each discrete batch time, t_k, during the growth process around the nominal parameters ($\widehat{\boldsymbol{\theta}}$).

5. *Output's PDF approximation*: Evaluate the PDF of y at each sampling time instance during the growth process for each temperature using the following truncated PSE:

$$y_{i,k} = \hat{y}_{i,k} + \mathbf{L}_{1,i,k}\left(\boldsymbol{\theta} - \widehat{\boldsymbol{\theta}}\right) + \frac{1}{2}\left(\boldsymbol{\theta} - \widehat{\boldsymbol{\theta}}\right)^T \mathbf{L}_{2,i,k}\left(\boldsymbol{\theta} - \widehat{\boldsymbol{\theta}}\right) + \cdots, \quad (6\text{-}4)$$

where $\mathbf{L}_{1,i,k} = (dy/d\boldsymbol{\theta})_{\widehat{\boldsymbol{\theta}}} \in \mathbb{R}^Q$ and $\mathbf{L}_{2,i,k} = (d^2y/d\boldsymbol{\theta}^2)_{\widehat{\boldsymbol{\theta}}} \in \mathbb{R}^{Q\times Q}$ are respectively the Jacobian and Hessian at each temperature T_i evaluated at the time instance, t_k, and consist of the sensitivities estimated from the previous step.

6. *Calculation of output's bounds*: Evaluate the upper (lower) bound on the process output at a specific confidence level, α, during the entire batch time for each T_i, $\mathbf{Y}_i^{PSE} \in \mathbb{R}^K$. Thus, $\mathbf{Y}_i^{PSE}$ represents the upper or lower bound of any output of the process and each element of this vector is calculated as follows:

$$y_{i,k}^{PSE} = F_{i,k}^{-1}\left(\mathbb{Pr}\middle|y_{i,k}\right) = \{y_{i,k} : F_{i,k}(y_{i,k})\}, \quad (6\text{-}5)$$

where the function $F_{i,k}^{-1}\left(\mathbb{Pr}\middle|y_{i,k}\right)$ represents the inverse of the CDF at time instance, t_k and temperature, T_i evaluated at a predefined probability, $\mathbb{Pr}$. Setting $\mathbb{Pr}$ in Eq.(6-5) to $\alpha/2$ and $1-\alpha/2$ yields respectively the lower and the upper bound for the output, y. The bounds on the controlled outputs can be directly determined at each sampling time during the growth process by evaluating the sensitivities through multiple multiscale models and applying Monte Carlo sampling on the PSEs. However, that approach is not efficient for online applications and motivates identification of closed-form models that can predict these bounds at a time-scale that is practical for online applications.

7. *Model selection:* Select a model that can describe the time evolution of the process output. In the current study, the thin film properties of interest are the film thickness and surface roughness. According to the trajectories depicted in Figure 3-10 and Figure 3-13, the surface roughness can be described as an overdamped process model whereas thickness is linear with respect to time. Therefore, the models considered to describe the surface roughness and film thickness during the batch time for each T_i are as follows:

$$r(T_i, t) = \lambda_{1,i} T_i \left(1 - e^{-\frac{t}{\lambda_{2,i}}}\right), \tag{6-6}$$

$$H(T_i, t) = \lambda_{3,i} T_i t, \tag{6-7}$$

where $\lambda_{l,i} (l = 1, \dots, 3)$ are the parameters of the closed-form model that can be identified via least-squares.

8. *Model identification:* Estimate the parameters of Eqs.(6-6)-(6-7)for the data set obtained for each T_i through minimization of the following least-squares function:

$$\Lambda(\boldsymbol{\lambda}_i) = \sum_{k=0}^{K} (y_{i,k}^{PSE} - y_{i,k}^{pred})^2, \tag{6-8}$$

where $y_{i,k}^{PSE}$ and $y_{i,k}^{pred}$ are respectively the bound on the process output calculated using the PSE-based approach and the model prediction from the closed-form models shown in Eqs.(6-6)-(6-7) at the k^{th} sampling time instance and T_i. The identified $\boldsymbol{\lambda}_i{}^T = [\lambda_{1,i}, \lambda_{2,i}, \lambda_{3,i}]$ represent the set of parameters of the models presented in Eqs.(6-6)-(6-7) for each discrete temperature T_i, i.e., there exist one set of model parameters for each temperature considered in the *Space discretization* step.

9. *Approximation of the closed-form model parameters:* For model-based process control applications, it is required to estimate the parameters at any temperature within the specified operating region. Therefore, a polynomial function is required to correlate the estimated parameters to the independent variable T using the model parameters estimated for each discrete temperature in the previous step, i.e.,

$$\bar{\lambda}_l = b_{0,l} + \sum_{d=1}^{D} b_{d,l} \Gamma_d(T), \tag{6-9}$$

where $\Gamma_d(T)$ represents a temperature-dependent polynomial function while $b_{0,l}$ and $b_{d,l}$ are the coefficients of the polynomial calculated through regression; D is the number of independent terms considered in the analysis. Once these polynomial correlations are

obtained offline, they can be used to predict the surface roughness and film thickness in online applications.

10. *Closed-form model:* As shown in Eq.(6-6), surface roughness at any sampling time during the deposition process depends on temperature and the roughness at a previous time step. Thus,

$$r_k = r_{k-1} + sgn(\delta)\left|\frac{\bar{\lambda}_1 T - r_{ref}}{\bar{\lambda}_1 T}\right|\delta, \tag{6-10}$$

where,

$r_0 = 1$ mL

$\delta = \bar{\lambda}_1 T(e^{-\frac{t_{k-1}-t_{ref}}{\bar{\lambda}_2}} - e^{-\frac{t_k - t_{ref}}{\bar{\lambda}_2}})$,

where r_k is the estimated roughness at sampling time instance, t_k, while r_{k-1} is the estimated roughness at sampling time instance, t_{k-1}. In the present analysis, r_{k-1} is evaluated from the closed-form model since it is assumed there is no measurement available for surface roughness during the process. r_{ref} and t_{ref} respectively denote the reference roughness and the time when the substrate temperature changes to the current temperature. sgn is the sign function while $\bar{\lambda}_1$ and $\bar{\lambda}_2$ are the model parameters evaluated based on the temperature at time, t_k, obtained from the polynomial function shown in Eq.(6-9). Following Eq.(6-7), thickness depends on temperature and the thickness evaluated at the previous time instance; thus, this output can be calculated as follows:

$$H_k = H_{k-1} + \bar{\lambda}_3 T(t_k - t_{k-1}), \quad H_0 = 0 \text{ mL}, \tag{6-11}$$

where $\bar{\lambda}_3$ is the model parameter estimated from Eq.(6-9) using the substrate temperature at time, t_k.

The models developed in this section can be used to design a robust estimator for an effective feedback control wherever the measurements are not available and they can also be used for model-based control applications, e.g., to design an NMPC algorithm. Moreover, this approach is applicable in analyzing the effects of measurement noise.

6.1.2. Application of robust NMPC to the thin film deposition process

To determine the order of the series expansions for uncertainty analysis of surface roughness and film thickness, a comparison has been made between the PDFs obtained by uncertainty

propagation in these outputs applying the primary multiscale model and PSEs. Monte Carlo technique adopting the primary multiscale model is a trivial method with no truncation error caused by the PSE. However, due to high computational cost, this approach is applied as an index to validate the accuracy of the PSE method. In this case, $\boldsymbol{\theta}^T = [E, T]$ is the vector of uncertain parameters that are normally distributed with mean $\widehat{\boldsymbol{\theta}}^T = [17000\ \text{cal/mol}, 800\ \text{K}]$, and a standard deviation of 2% of their mean values. The uncertainty analysis through the Monte Carlo method was performed employing 500 sample points generated randomly for the vector of uncertain parameters from their prior normal distribution functions and uncertainty is propagated into surface roughness using the model described in Chapter 3. This PDF is shown in Figure 6-1 with the PDFs obtained using first and second-order PSE approximations. As shown in this figure, while first-order PSE can adequately describe the distribution of surface roughness, second-order PSE captures the tails of the PDF more accurately.

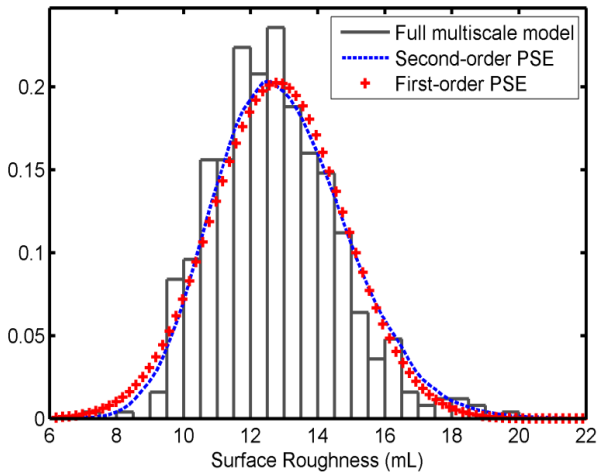

Figure 6-1. Roughness PDFs at $T = 800$ K obtained through the multiscale model, first and second-order PSEs at $t = 20$ s.

Likewise, the PDF obtained for film thickness employing 500 data points in the multiscale model at $T = 800$ K is presented in Figure 6-2. The variability is also assessed using a first-order PSE and the fitted normal distribution is shown in this figure. As illustrated in this figure, thickness is not significantly sensitive to the uncertainties in E and T, i.e., these uncertainties resulted in small variability in the film thickness (+/-2%) whereas large variability was observed in surface roughness due to these uncertainties (+/-50%).

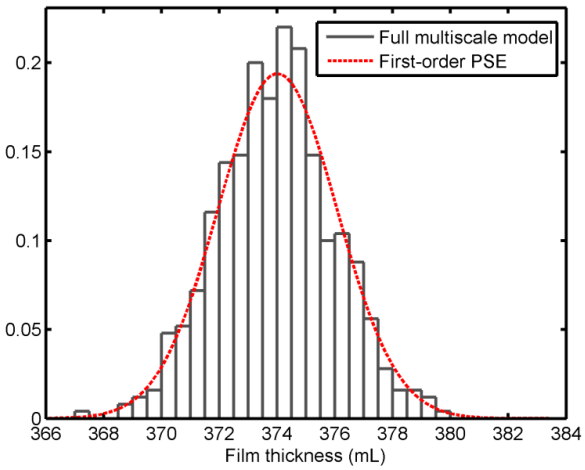

Figure 6-2. Thickness PDFs at $T = 800$ K obtained through the multiscale model and first-order PSE at $t = 20$ s.

To develop a closed-form model for the deposition process presented in Chapter 3, the operational region for the substrate temperature is considered from 600 to 1400 K and is discretized into 9 equally spaced temperatures, $T_i (i = 1, \dots, 9)$. For this application, finer discretization did not improve the accuracy of the estimations. The batch time, $t_f = 100$ s, is discretized into 101 points, $t_k (k = 0, \dots, 100)$. As mentioned above, $\boldsymbol{\theta}^T = [E, T]$ is the set of uncertain parameters that are normally distributed around their nominal values with the standard deviations of 2% of their corresponding nominal values. Therefore, since the substrate temperature is the control action and is time varying, the variability will be considered as 2% of the control action predicted by the controller. As shown in Figure 6-1, second-order PSE is accurate enough to capture the variability in the surface roughness; thus, first and second-order sensitivities of roughness with respect to the uncertain parameters are generated offline for each temperature T_i during the batch time. Then, uncertainty is propagated in surface roughness using the Monte Carlo sampling method applied to the second-order PSE to obtain the lower and upper bounds on roughness using a confidence level: $\alpha = 0.5\%$. The data collected for each temperature, T_i, is then employed to identify the parameters of the model shown in Eq.(6-9) using the least-squares formulation shown in Eq.(6-8). This results in a set of model parameters, each corresponding to a particular temperature. To approximate the parameters of the closed-form model presented in Eq.(6-10), the operational substrate temperature region is divided into two regions. The parameters of the closed-form model shown in Eq.(6-10) are estimated assuming that they are functions of the substrate temperature as follows:

$$\bar{\lambda}_l = b_{0,l} + b_{1,l}T + b_{2,l}T^2 + b_{3,l}T^3. \quad (6\text{-}12)$$

The corresponding polynomial functions obtained from regression for $\bar{\lambda}_1$ and $\bar{\lambda}_2$ to estimate the upper and lower bounds on roughness for the two temperature regions are shown in Figure 6-3 and Figure 6-4, respectively. Although other polynomials or nonlinear functions can also be adopted, the estimations obtained by the function shown in Eq.(6-12) are sufficiently accurate for online control of the surface roughness as it will be shown in the next section.

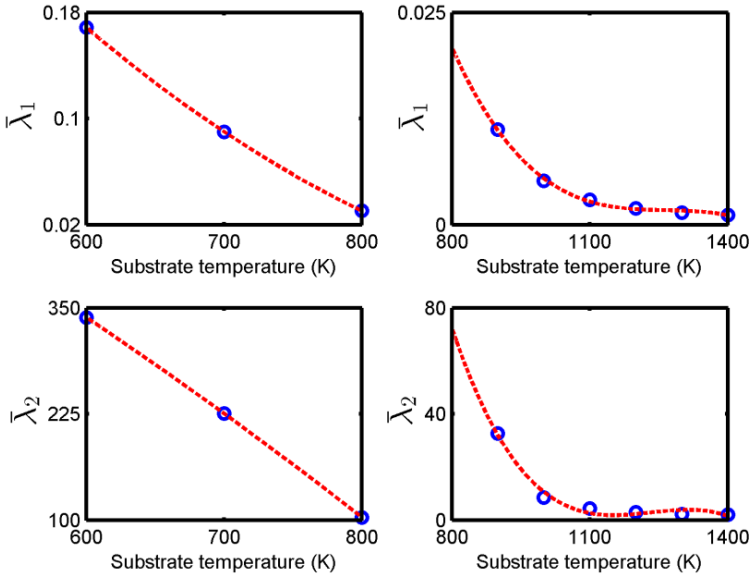

Figure 6-3. Polynomial models used to determine $\bar{\lambda}_1$ and $\bar{\lambda}_2$ to estimate the upper bound on surface roughness.

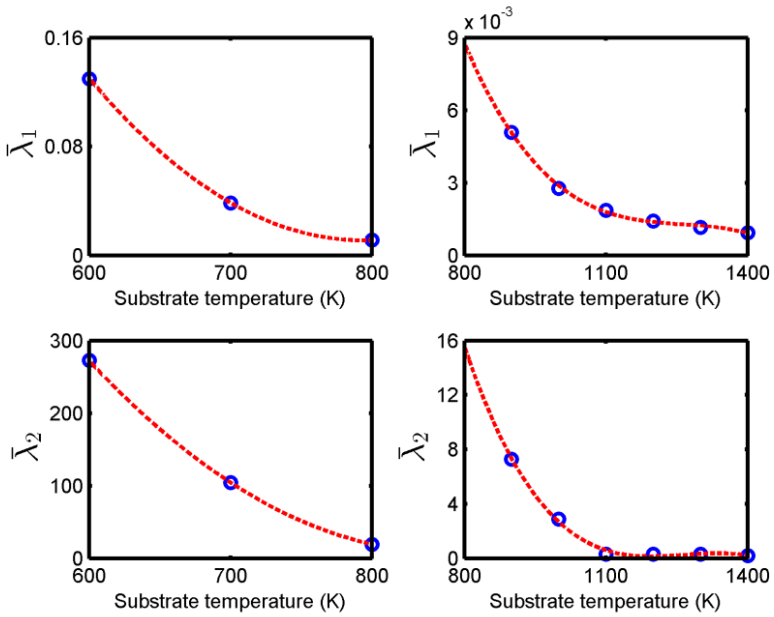

Figure 6-4. Polynomial models used to determine $\bar{\lambda}_1$ and $\bar{\lambda}_2$ to estimate the lower bound on surface roughness.

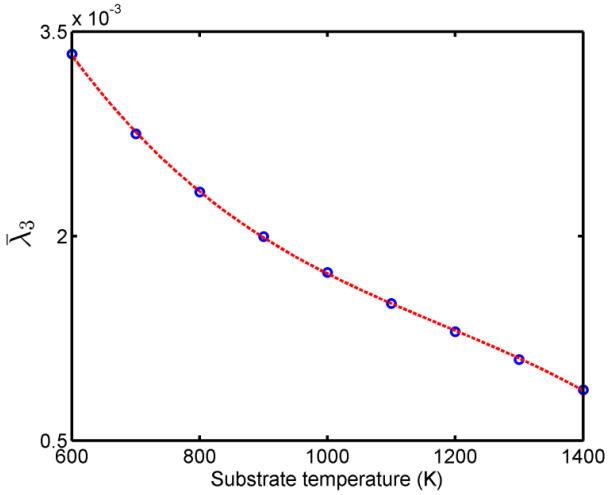

Figure 6-5. Polynomial model used to determine $\bar{\lambda}_3$ to estimate the film thickness.

As shown in Figure 6-2, thickness is not sensitive to the uncertainties considered in this work and accordingly a nominal model is sufficient to estimate the film thickness. To provide a closed-form model for thickness, the nominal thickness is calculated for each temperature, T_i, at each sampling time, t_k. Subsequently, steps 3 to 6 in the algorithm presented in Section 6.1.1 are not required and identification is performed using the nominal thickness to obtain the parameters of the model at each temperature, T_i. Using these data points in regression analysis, a model is

identified as a function of the substrate temperature. The model obtained to determine the parameter of the film thickness in Eq.(6-11), $\bar{\lambda}_3$, is shown in Figure 6-5.

To show the accuracy of the closed-form model in prediction of surface roughness, upper and lower bounds obtained for the surface roughness are shown in Figure 6-6. The substrate temperature profile used in this validation step is also shown in this figure. The dashed lines correspond to the bounds evaluated using the closed-form model presented in Section 6.1.1 and the solid lines are obtained by calculating the bounds using the PSE-based approach. The sensitivities are estimated by averaging the solutions from three multiscale model applying 100×100 lattices in the KMC simulations. The bounds are estimated properly using the closed-form model in 140 ms whereas the other approach took approximately 7 hrs on a Core i7-2600 with 8GB of RAM. This demonstrates the benefit of the approach proposed in this work to address the online control of the thin film deposition process while explicitly considering model parameter uncertainty.

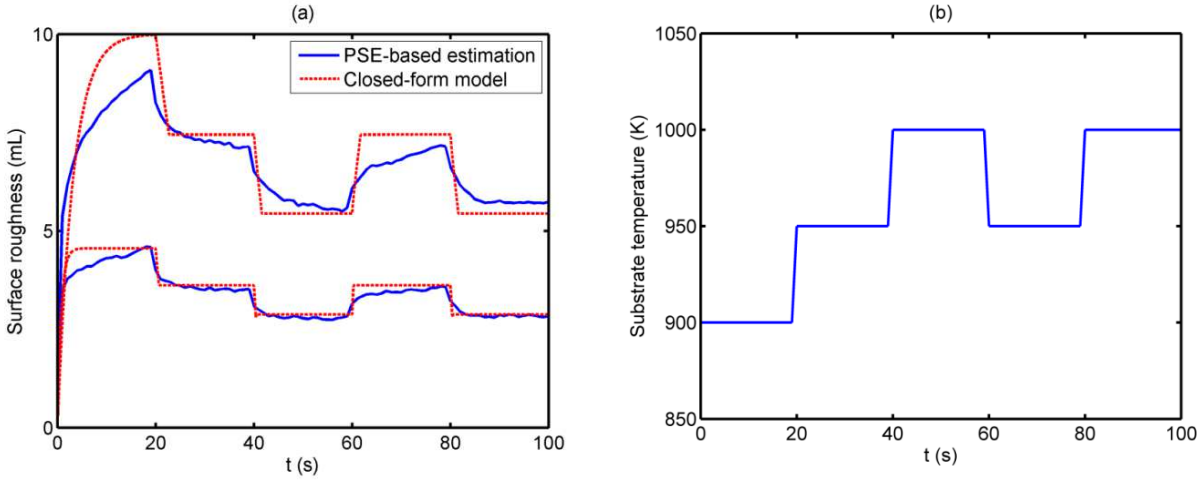

Figure 6-6. (a) The upper and lower bounds on surface roughness, and (b) Substrate temperature profile.

6.1.3. NMPC applied in a thin film deposition process

The development of advanced sensors has provided the potential of feedback control for smart operation of the deposition processes in the semiconductor industry. Despite the application of spectroscopic ellipsometry for thickness and composition control, precise control of the microscopic properties such as roughness is not still practical since these sensors cannot provide frequent measurements needed for online applications (Xiong and Grover, 2012). In the current work, it is assumed that thickness can be measured in practice while measurements are not

available for the surface roughness during the process. Whenever a measurement is available for the film thickness, the predictions of this film property are corrected. Employing the proposed closed-form models, model-based control approaches can be readily applied to improve the closed-loop performance in the thin film deposition process. Particularly, an NMPC technique can be designed to simultaneously address performance considerations and process constraints, e.g., actuator constraints, while using nonlinear dynamic models. To illustrate the benefits of the approach presented in this study, the closed-form model developed in the previous section is used as the internal model in an NMPC algorithm as shown in Figure 6-7. Moreover, due to lack of roughness measurements, the closed-form model is considered as an estimator for this property of the thin film. The thin film deposition process is assumed to be the multiscale model presented in Chapter 3 using a 100×100 lattice in the KMC simulations.

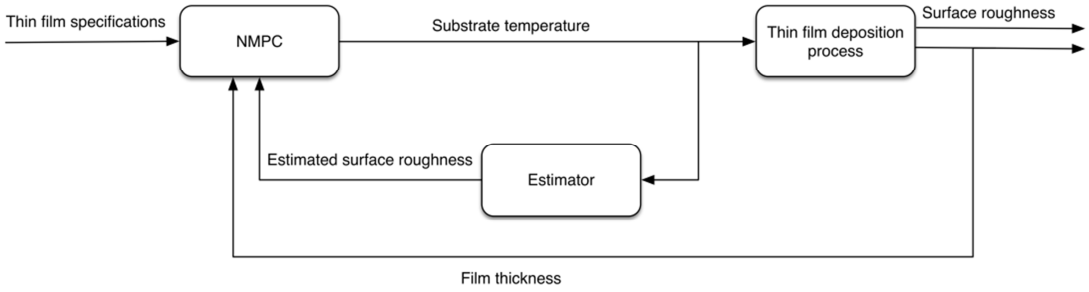

Figure 6-7. Block diagram of an NMPC structure coupled with the estimator.

In the present study, the NMPC algorithm was set-up such that it minimizes the final surface roughness while complying with a minimum film thickness constraint requirement at the end of the batch. In addition, temperature constraints are included to ensure the feasible operation of this process. Hence, the optimal control problem solved at every sampling time interval in the NMPC framework is as follows:

$$\min_{T(j)} r(t_f)$$

Subject to:

Closed-form model, Eqs. (6-10)-(6-11)

$$h_1 = H(t_f) - H_{min} \geq 0$$

$$h_2(j) = T_{min} - T(j) \leq 0 \qquad (6\text{-}13)$$

$$h_3(j) = T(j) - T_{max} \leq 0$$

$$h_4(j) = \mathcal{R}_{min} - \frac{dT(j)}{dt} \leq 0$$

$$h_5(j) = \frac{dT(j)}{dt} - \mathcal{R}_{max} \leq 0$$

$$j = 1,2,\dots,J$$

where $T_{min}, T_{max}, \mathcal{R}_{min}$ and $\mathcal{R}_{max}$ are respectively the minimum and maximum allowed temperature and temperature ramp rates during the batch process. The end-point constraint h_1 ensures that the minimum thickness is satisfied at the end of the batch time whereas constraints $h_2 - h_5$ ensure that the temperature profile remains within the feasible operating region for the deposition process.

Thin film deposition is a batch process and according to problem (6-13), the objective is to minimize the surface roughness at the end of the batch. Therefore, a shrinking horizon approach is implemented to calculate the control actions from the NMPC algorithm. The optimal set of substrate temperatures is obtained from the solution of the optimization problem of Eq.(6-13) and only the first value of the temperature trajectory is implemented on the thin film deposition process until the next sampling time when the NMPC problem is solved to obtain the updated temperature trajectory. The batch time is discretized into 20 equal intervals considering the temperatures at each sampling time interval as the decision variables. Moreover, the temperature profile is described as a constant piecewise trajectory between successive time intervals. In this study, $\mathcal{R}_{max}$ and $\mathcal{R}_{min}$ were set to 25 K/s while T_{min} and T_{max} were set to 600 and 1400 K, respectively. For closed-loop simulations, it is assumed that the measurements for thickness are available at every iteration of the NMPC algorithm which is 5 s in these simulations.

The overall performance of the NMPC algorithm depends on the accuracy of the model describing the process. Therefore, to show the efficiency of the control approach and the importance of the robust model, three different scenarios are presented and compared in this study:

1. Nominal models are employed for surface roughness and film thickness and control action is applied to the nominal thin film deposition process.
2. The nominal models are used to control the deposition process under model parameter uncertainty.
3. The robust model for surface roughness and nominal model for film thickness are applied to control the deposition process under model parameter uncertainty.

In the first scenario, the nominal model is used to predict the controlled outputs, assuming that the nominal closed-form model provides an accurate representation of the process. In the NMPC algorithm the nominal surface roughness is minimized while the nominal minimum allowed thickness is constrained to be at least 1700 mL at the end of the deposition process. The surface roughness predicted from the estimator is shown in Figure 6-8 along with the roughness trajectory obtained from the multiscale thin film process. As shown in this figure, the roughness estimator has followed the process accurately. The corresponding temperature profile is also shown in this figure.

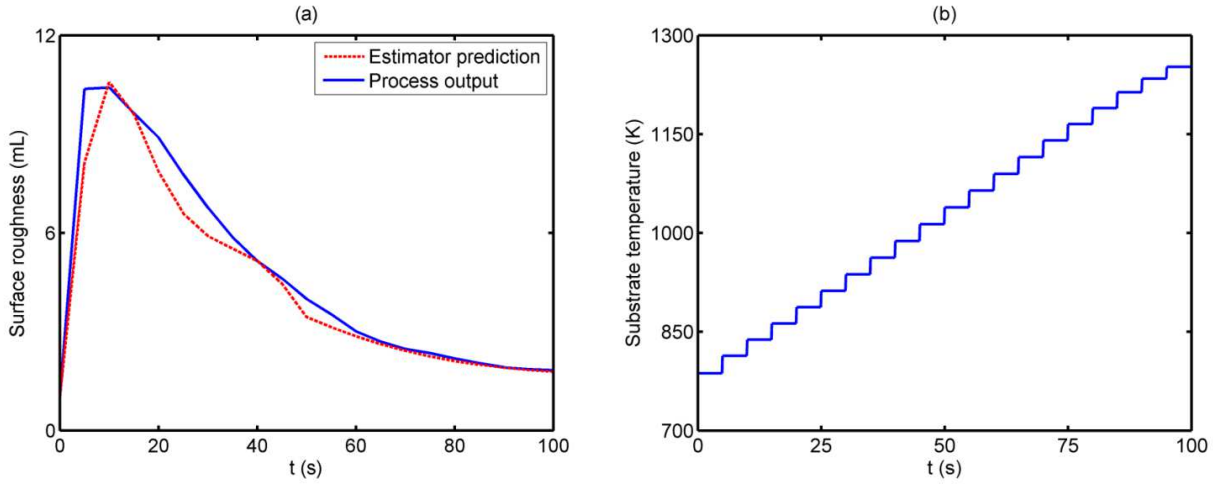

Figure 6-8. (a) Surface roughness trajectory from the nominal process (solid line), the roughness estimation from the nominal estimator (dashed line), and (b) Substrate temperature trajectory applying the nominal NMPC.

To assess the effect of the thickness measurements, the open-loop optimal control of the process is also performed and the results are compared to the nominal NMPC. Figure 6-9 shows

the final properties of the thin film from 20 simulations using the open-loop optimal control and NMPC. As shown in this figure, when the optimal open-loop control is used, the constraint on film thickness is violated in 35% of cases. In contrast, when the nominal NMPC approach is employed, the thickness constraint is always satisfied.

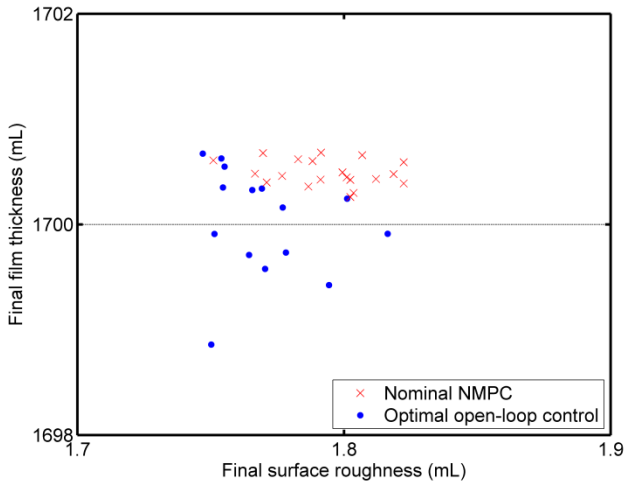

Figure 6-9. Surface roughness and thickness at the end of the batch for 20 simulations obtained from the open-loop optimal control and nominal NMPC. The dashed line corresponds to the constraint on final thickness.

To illustrate the importance of the robust estimator, in the second scenario, the nominal model is incorporated in the NMPC algorithm in the presence of model-plant mismatch. To incorporate uncertainty in the process, it is assumed that $\boldsymbol{\theta}^T = [E, T]$ is the vector of uncertain parameters that are normally distributed around their nominal values with standard deviations of 2% of their nominal values. Since E is a time-invariant parameter of the system, to assess the performance of the estimator, Monte Carlo simulations were performed with 20 random parameters generated from the corresponding normal distribution. Substrate temperature, on the other hand, is the control action and changes during the process. Therefore, to account for the model-plant mismatch, the applied temperature on the multiscale model is selected randomly from the normal distribution around the control actions determined by the NMPC. These trajectories are shown in Figure 6-10 with the roughness estimated from the nominal estimator. As shown in this figure, the trajectories obtained from the process deviate significantly from the nominal surface roughness estimator.

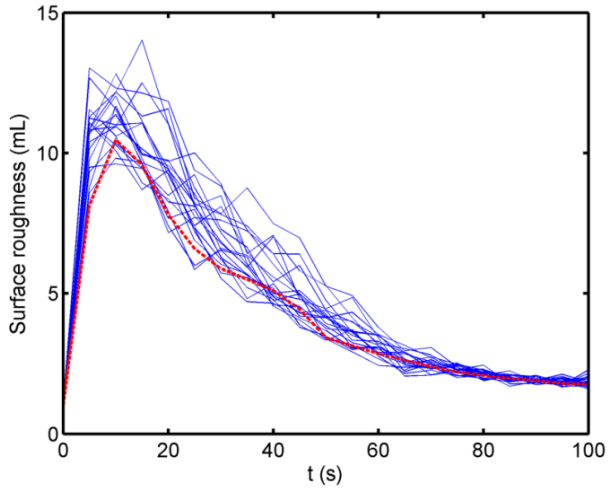

Figure 6-10. Surface roughness trajectories from 20 simulations using the process under model parameter uncertainty (solid line), the roughness estimation from the nominal estimator (dashed line).

To assess the performance of the nominal NMPC under model-plant mismatch, the final properties of the thin films obtained under uncertainty are compared to the properties obtained from the nominal multiscale model. As shown in Figure 6-11, the variance in surface roughness and thickness is two orders of magnitude larger under uncertainty and the nominal NMPC cannot meet the end-point constraint on the film thickness. These results show the importance of developing robust strategies for this process that can account for process variability under model parameter uncertainty.

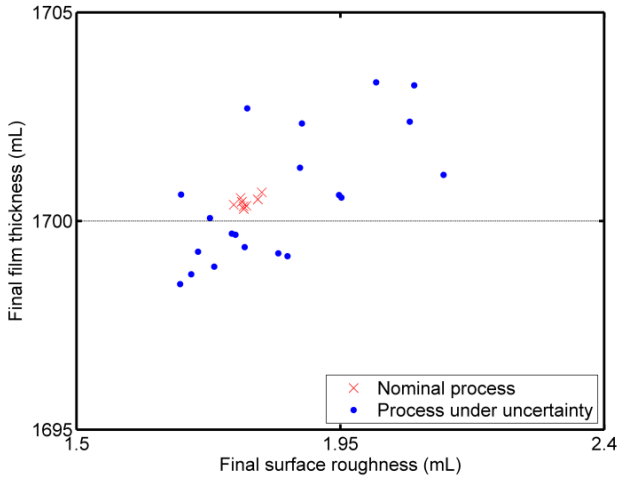

Figure 6-11. Surface roughness and thickness at the end of the batch for 20 simulations obtained from the nominal process and under model-plant mismatch applying the nominal NMPC.

To provide a robust control strategy under model parameter uncertainty, in the third scenario, the roughness model in the NMPC is implemented such that it predicts the upper bound on the surface roughness. The roughness trajectories obtained from 20 multiscale simulations under model parameter uncertainty are shown in Figure 6-12; the surface roughness calculated from the robust estimator is shown as a dashed line. As shown in this figure, the estimated roughness bounds surface roughness trajectories obtained from the process under uncertainty. The substrate temperature profile is also shown in this figure.

The performance of the robust NMPC and nominal NMPC are compared under model-plant mismatch based on the end-point properties obtained from 20 simulations using the multiscale model. As shown in Figure 6-13, the robust NMPC has improved the control performance since the constraint on the film thickness is met for all the simulations whereas violations to that end-point constraint were obtained using the nominal NMPC.

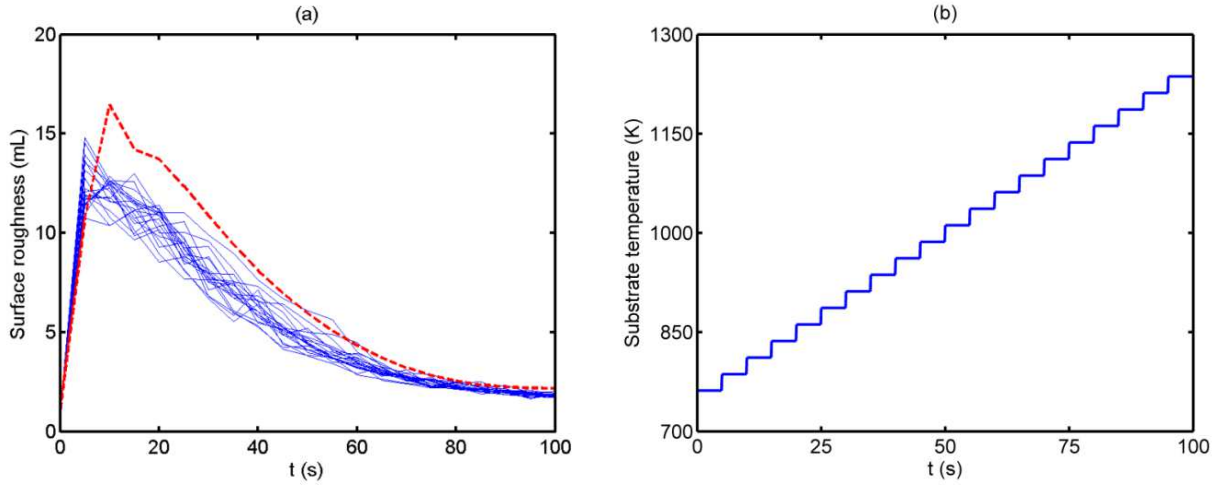

Figure 6-12. (a) Surface roughness trajectories from 20 simulations using the process under model parameter uncertainty (solid lines), the roughness estimation from the robust estimator (dashed line), (b) Substrate temperature trajectory applying the robust estimator.

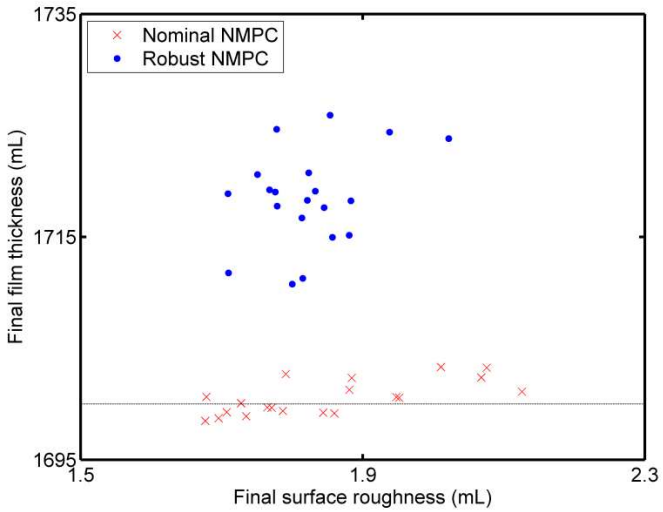

Figure 6-13. Surface roughness and thickness at the end of the batch for 20 simulations obtained from the nominal and robust NMPC under model-plant mismatch.

6.2. Stochastic NMPC with soft constraints applied to thin film deposition

In Section 6.1, to ensure the robust performance, hard constraints were imposed on the MPC framework. The internal model used in the MPC algorithm is a closed-form model that was identified offline to represent the dynamic behaviour of system under uncertainty in the model parameters. The identification of this model was performed such that it predicts bounds on the outputs for a narrow confidence level, which must be specified a priori. To that end, new offline identification is required in that approach to be able to estimate the outputs at a different confidence level.

In this section, a systematic framework is presented that enables the identification of a closed-form model to estimate the first and second-order statistical moments of the thin film properties. The parameters of the closed-form model are determined offline through PSEs developed for the multiscale model under uncertainty in the model parameters. The conservatism imposed by the hard constraints is reduced by imposing probabilistic (soft) constraints in the MPC. The closed-form model identified from the algorithm proposed in this work enables the prediction of outputs at any probability of satisfaction. Moreover, employing this model the probabilistic constraints in the stochastic MPC framework can be reformulated as deterministic constraints, thus allowing

the implementation of this control framework for the thin film deposition process under uncertainty in the model parameters.

6.2.1. Statistical moments of the outputs using PSE

An advantage of the PSE is that it can be employed directly to assess the statistical moments of the outputs. When a multivariate normal distribution with the covariance matrix, $\mathbf{V_\theta}$ can represent the uncertain parameters:

$$f_{p.d}(\boldsymbol{\theta}) = \frac{1}{\sqrt{(2\pi)^Q \mathbf{V_\theta}}} \exp\left(-\frac{1}{2}\left(\boldsymbol{\theta} - \widehat{\boldsymbol{\theta}}\right)^T \mathbf{V_\theta}\left(\boldsymbol{\theta} - \widehat{\boldsymbol{\theta}}\right)\right). \quad (6\text{-}14)$$

PSE can be used to estimate the mean and the variance of the output. For a first-order PSE, the expected value, ε_y, and the variance of the output, V_y can be determined as follows:

$$\varepsilon_y = \hat{y}, \quad (6\text{-}15)$$

$$V_y = \mathbf{L}_1 \mathbf{V_\theta} \mathbf{L}_1^T. \quad (6\text{-}16)$$

First-order PSE relates the output to the uncertain parameters linearly; thus, the PDF of the output can be estimated analytically. Accordingly, the PDF of the output will take the form of a normal distribution with mean and variance obtained from Eqs.(6-15)-(6-16), respectively. Applying a second-order PSE, the expected value and variance of the output y, can be obtained as follows (Nagy, 2009; Nagy and Allgöwer, 2007):

$$\varepsilon_y = \hat{y} + \frac{1}{2}\mathrm{tr}(\mathbf{L}_2 \mathbf{V_\theta}), \quad (6\text{-}17)$$

$$V_y = \mathbf{L}_1 \mathbf{V_\theta} \mathbf{L}_1^T + \frac{1}{2}[\mathrm{tr}(\mathbf{L}_2 \mathbf{V_\theta})]^2, \quad (6\text{-}18)$$

where $\mathrm{tr}(.)$ is the trace of matrix. For higher order PSEs, a similar approach can be applied to analytically determine the expected value and the variance of output.

To analyse the effect of distributional parameter uncertainties on the thin film deposition process, the uncertainty propagation into surface roughness and film thickness is assessed using PSE. The Monte Carlo method applied to the multiscale model is used as an index to determine the order of the truncated PSE. For the present deposition model, $\boldsymbol{\theta}^T = [E, E_m, \mathcal{X}]$ is the vector of uncertain parameters that are normally distributed around their nominal values listed in Table 3-1 with the following covariance matrix:

$$\mathbf{V_\theta} = \begin{pmatrix} 7.2\times10^5 & 2.6\times10^5 & 0 \\ 2.6\times10^5 & 2.6\times10^5 & 0 \\ 0 & 0 & 10^{-14} \end{pmatrix} \tag{6-19}$$

For the Monte Carlo method, 1,000 sample points are randomly generated for the vector of uncertain parameters from the prior multivariate normal distribution. The PDF of the surface roughness is obtained by using these realizations in the multiscale model at $T = 1000$ K. The PDF obtained at $t = 20$ s is shown in Figure 6-14 along with the PDFs estimated using first and second-order PSE approximations. The normal distribution resulted from the first-order PSE is estimated analytically using Eqs.(6-15)-(6-16) whereas for the second-order PSE, the Monte Carlo method is applied to the series expansion. As shown in this figure, the uncertainty propagation in surface roughness using the full multiscale model has resulted in a PDF that follows a lognormal distribution. The first-order PSE cannot describe the nonlinearity of this PDF while the second-order PSE has captured the distribution more accurately.

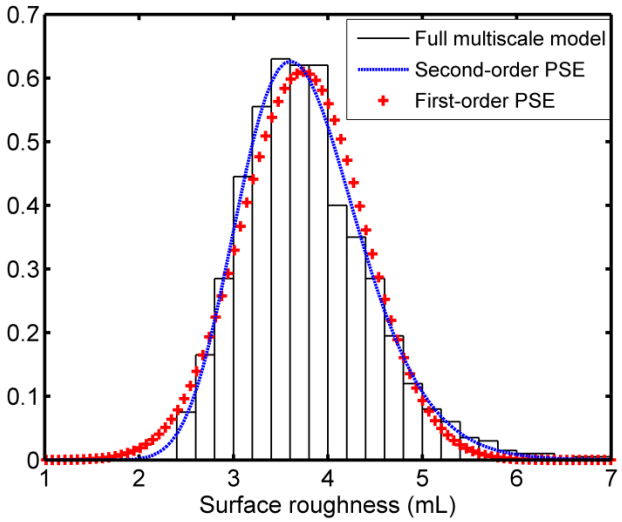

Figure 6-14. Roughness PDFs obtained using the multiscale model, first and second-order PSEs.

The statistical moments of surface roughness obtained from Eqs.(6-15)-(6-18) and the required computational times are listed in Table 6-1. Comparing the moments estimated from PSEs with those evaluated using Monte Carlo method applied to the multiscale model implies that the second-order PSE provides more accurate results. As shown in this table, the relative errors of the mean and the variance of the first-order PSE are respectively 0.8% and 8%, whereas the relative errors of the second-order PSE are respectively 0.2% and 4%. The computational times listed in Table 6-1 indicate that both first and second-order PSEs are computationally efficient

compared to the Monte Carlo method applied to the full multiscale model. However, due to the second-order sensitivities required in higher order PSE, first-order PSE is more computationally efficient than second-order PSE.

Table 6-1. The statistical moments of the surface roughness from different approaches and the corresponding computational costs.

Approach	Mean (mL)	Variance (mL^2)	Computational Time (hr)
Monte Carlo applied to the multiscale model	3.7824	0.4669	29.4
First-order PSE	3.7517 (0.8%)	0.4288 (8%)	0.6
Monte Carlo applied to the second-order PSE	3.7720 (0.2%)	0.4482 (4%)	1.9

Figure 6-15 shows the PDF obtained for film thickness at $t = 20$ s employing 1,000 realizations in the uncertain parameters and propagating those through the multiscale model at $T = 1000$ K. The PDF is also approximated using a first-order PSE; the fitted normal distribution shown in this figure has successfully captured the variability in the film thickness. As shown in Table 6-2, using first-order PSE, the mean and the variance of thickness are assessed with respectively 0.02% and 0.6% errors. Thus, first-order PSE estimates the moments of thickness with negligible errors at low computational costs. Similar results were observed for the surface roughness and thickness at other operating conditions and are not shown here for brevity.

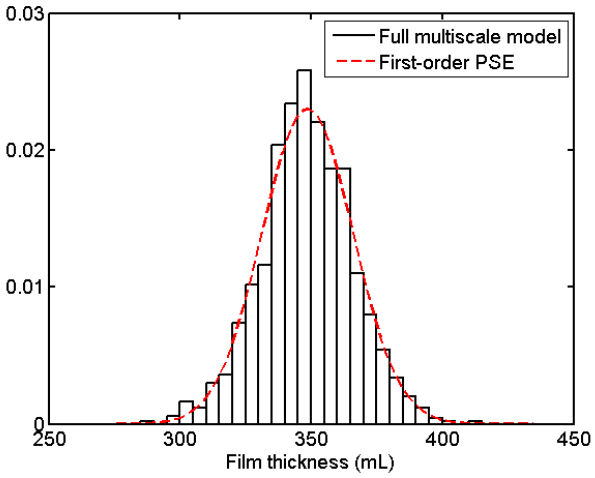

Figure 6-15. Thickness PDFs at $T = 1000$ K obtained using the multiscale model and first-order PSE at $t = 20$ s.

Table 6-2. The statistical moments of the film thickness from different approaches and the corresponding computational costs.

Approach	Mean (mL)	Variance (mL^2)	Computational Time (hr)
Monte Carlo applied to the multiscale model	348.4	304.4	29.4
First-order PSE	348.5 (0.02%)	302.6 (0.6%)	0.6

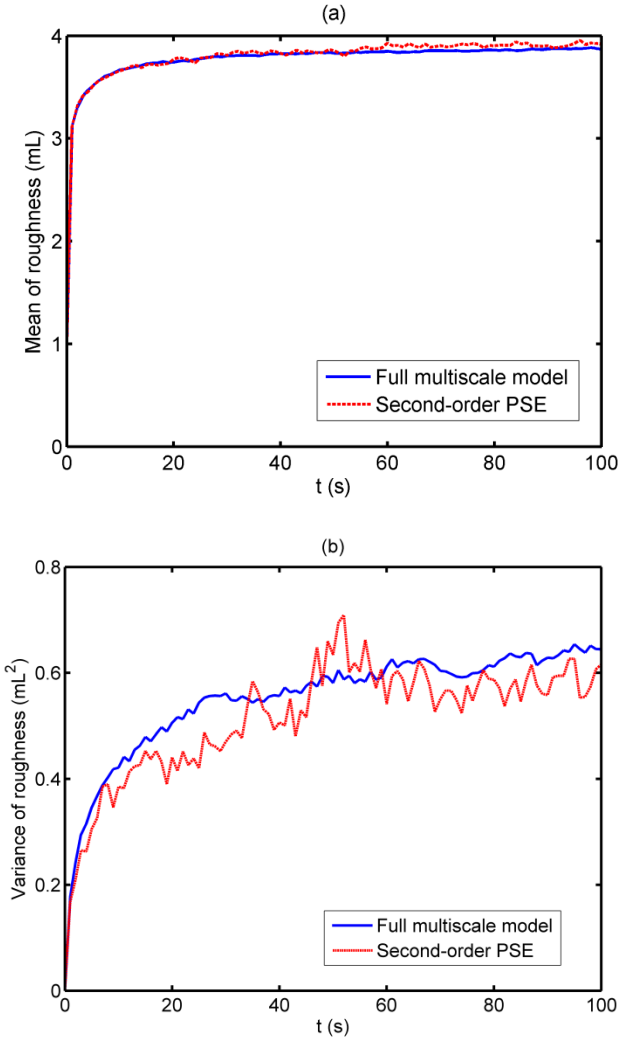

Figure 6-16. The evolution of roughness moments during the deposition process at $T = 1000$ K from Monte Carlo applied to the multiscale model and second-order PSE (a) Mean, (b) Variance.

The variation in the mean and variance in these output variables during the deposition process has also been investigated using both the Monte Carlo method applied to the full multiscale model and PSE. For the Monte Carlo approach, 1,000 sample points are applied to generate the

PDF of the surface roughness during the deposition process and then the moments of those distributions with respect to time have been recorded. The moments were also estimated using the second-order PSE shown in Eqs.(6-17)-(6-18). The sensitivities needed in the PSE were obtained using the average from multiple multiscale models. As shown in Figure 6-16(a), using the second-order PSE, the roughness mean is estimated accurately during the deposition process. The variance of surface roughness has also been estimated with a small deviation from that obtained from the Monte Carlo method. The largest deviation between two trajectories for roughness variance is about 0.12 mL^2 which is observed at $t = 26$ s. Considering the mean value at this point (3.78 mL), this deviation results in 8% error in estimation. Although this error may be negligible for control applications, a more accurate estimation for variance of surface roughness can be obtained using higher order PSEs.

The changes in mean and variance of thickness obtained from the Monte Carlo applied to the full multiscale model and a first-order PSE are depicted in Figure 6-17. As shown in this figure, the PSE has estimated the mean accurately while the variance estimated using the PSE method follows the variance obtained from Monte Carlo approach with a small discrepancy. The deviation observed at the end of the deposition is about 580 mL^2; considering the mean value at this point (1732 mL) the deviation in variance results in 1.4% error in estimation of thickness PDF. Therefore, the error observed in variance estimation for thickness through the PSE method is negligible.

The computational time required to estimate the variances shown in Figure 6-16 and Figure 6-17 using the Monte Carlo approach was about 150 hrs. However, the PSE method needed 10 hrs to assess the variances using the average of multiple multiscale simulations for the computation of the sensitivities. While the PSE method presents a more computationally efficient approach for uncertainty analysis compared to the Monte Carlo method, this method is still impractical for real-time applications in multiscale systems. Therefore, in the next section, a PSE-based algorithm is presented to develop a closed-form model that predicts the statistical moments of the outputs as a function of substrate temperature at minimum computational cost for online applications.

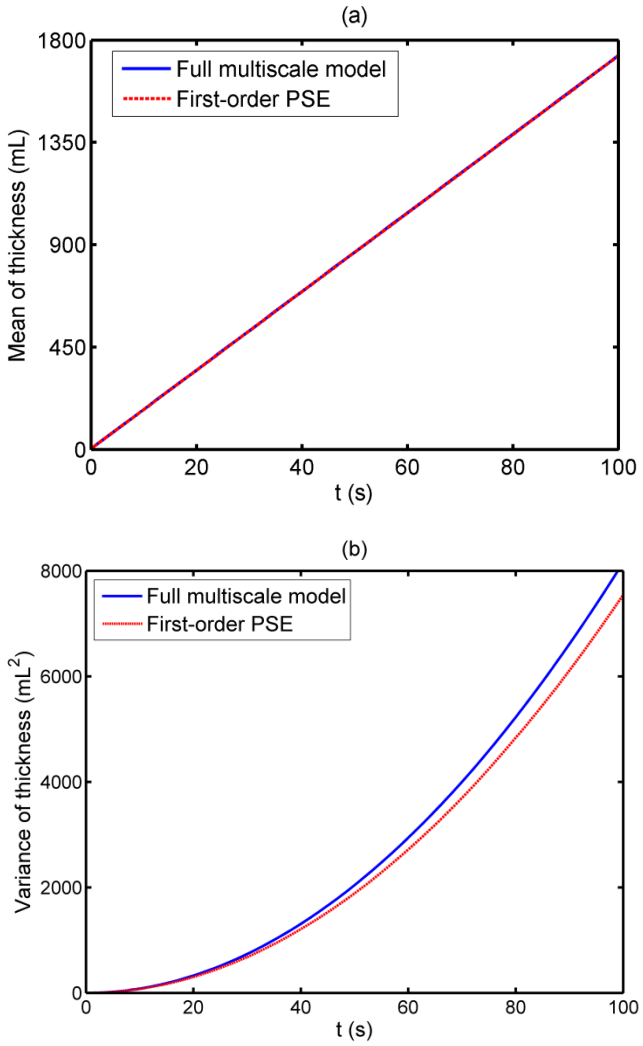

Figure 6-17. The evolution of thickness moments during deposition at $T = 1000$ K from Monte Carlo applied to the multiscale model and second-order PSE (a) Mean, (b) Variance.

6.2.2. Stochastic NMPC formulation

In this study, it is assumed that thickness, which is a macroscopic characteristic of the thin film, can be measured online while measurements for the surface roughness are not available during the deposition process. Microelectronic market imposes tight requirements upon thin film properties including specific thickness and surface roughness. To assemble high-performance electronic devices, optimal control strategies that can accommodate actuator and economic constraints in the presence of model-plant mismatch are required. Therefore, an MPC framework is designed to minimize the surface roughness at the end of the batch by manipulating substrate temperature in the presence of uncertainty in the multiscale model parameters. Thus, the control

objective is to minimize the surface roughness at the end of the batch while the film thickness meets a minimum specification at a desired probability.

The closed-loop optimal control formulation to be solved at every sampling instant in a shrinking horizon stochastic MPC with probabilistic constraint is as follows:

$$\min_{\mathbf{K}(t)} r(t_f)$$

Subject to:

Multiscale model presented in Chapter 3

$$T(t) = T_{ref}(t) + \mathbf{K}(t)(H(t) - H_{ref}(t)) \tag{6-20}$$

$$\mathbb{P}\mathrm{r}\left[H_{min} - H\left(t_f\right) \leq 0\right] \geq \beta$$

$$T_{min} \leq T(t) \leq T_{max}$$

$$\mathcal{R}_{min} \leq \frac{dT(t)}{dt} \leq \mathcal{R}_{max}$$

In the above formulation, the performance objective is the surface roughness at the end of the batch, i.e. $r(t_f)$. As shown in Figure 6-14, in the presence of distributional parameter uncertainty, a distribution can be determined for roughness. Therefore, in the optimization formulation, the performance index is the roughness determined at a specific probability limit. In the feedback law, similar to the approach presented in (Nagy and Braatz, 2004), $H(t)$ is the measured thickness, $H_{ref}(t)$ is the thickness reference vector obtained using the nominal open-loop optimal substrate temperature trajectory $T_{ref}(t)$, and $\mathbf{K}(t)$ is the time-varying gain vector of the feedback controller. H_{min} is the minimum allowed thickness at the end of the batch which will be specified by market considerations. To reduce conservatism, the probabilistic form of this constraint is considered in the present MPC formulation where $\mathbb{P}\mathrm{r}$ denotes probability and β is the desired probability of satisfaction of the constraint. Moreover, $T_{min}, T_{max}, \mathcal{R}_{min}$ and $\mathcal{R}_{max}$ represent respectively the minimum and maximum allowed temperatures and temperature ramp rates during the batch process.

To identify an optimal temperature profile in problem (6-13), the PDFs of thickness and roughness at the end of the batch are required. Theses PDFs can be obtained through either by Monte Carlo method applied to the full multiscale model or employing the PSEs that describe roughness and thickness as a function of the uncertain parameters during the deposition process.

As discussed in the previous section, even though the PSE method is less intensive than the Monte Carlo method, this approach is still computationally intractable for online applications. Therefore, it is desired to reformulate the probabilistic constraint and performance objective function to deterministic expressions that can be immediately evaluated. To achieve this goal, a low-order model that can efficiently assess the statistical moments of surface roughness and film thickness is employed in this work. The algorithm to identify such a model is presented in the next section.

6.2.3. Closed-form model identification

Online identification of a closed-form model during the deposition process is computationally challenging. Thus, an algorithm has been developed in this work to obtain the parameters of the closed-form model offline. This PSE-based algorithm estimates the parameters of the model that predicts the statistical moments of surface roughness and film thickness. This model predicts the statistical moments efficiently as a function of the substrate temperature at any sampling instant during the process under model parameter uncertainty. The algorithm is outlined as follows:

1. *Space discretization:* Discretize the operational region of substrate temperature, T, into equally spaced intervals, ΔT, to construct a finite-dimensional identification problem.

   $$T_i = \{T_{min} + i\Delta T | T_{min} \leq T_i \leq T_{max}, i = 0, 1, \dots, (T_{max} - T_{min})/\Delta T\}. \quad (6\text{-}21)$$

   It is important to note that the discretization resolution determines the offline computational costs.
2. *Temporal discretization:* Divide the batch time horizon into equally spaced time intervals, Δt, as follows:

   $$t_k = \{t_0 + k\Delta t | t_0 \leq t_k \leq t_f, k = 0, 1, \dots, (t_f - t_0)/\Delta t\}. \quad (6\text{-}22)$$

3. *Uncertainties description*: Define the multivariate normal distribution of uncertain parameters based on Eq.(6-14).
4. *Sensitivity evaluation*: Evaluate the nominal outputs and sensitivities of the outputs with respect to the uncertain parameters for each T_i at each discrete batch time, t_k, during the deposition process. According to Figure 6-14 and Figure 6-15, to capture the uncertainty propagation in surface roughness, a second-order PSE is required while film thickness can be accurately approximated using a first-order PSE. Therefore, first and second-order

sensitivities of roughness and first-order sensitivities of film thickness with respect to the uncertain parameters need to be estimated for the present deposition process.

5. *Approximation of the statistical moments*: Using the PSEs, evaluate the statistical moments of the output y at each sampling time instance t_k, during the process for each discrete point in the temperature domain T_i. To assess the mean and the variance of surface roughness, Eqs.(6-17)-(6-18) are employed whereas for the film thickness Eqs.(6-15)-(6-16) are used.
6. *Model selection:* Select a model that can describe the time evolution of the statistical moments of each output, i.e. the surface roughness and thickness. According to the trajectories shown in Figure 6-16, the evolution of the surface roughness and its variance during the deposition process can be described as an overdamped process model. Therefore, the models considered to describe the expected value and the variance of roughness during the batch time for each T_i can be described as follows:

$$\varepsilon_r(T_i,t) = \lambda_{1,i}T_i\left(1 - e^{-\frac{t}{\lambda_{2,i}}}\right), \tag{6-23}$$

$$V_r(T_i,t) = \lambda_{3,i}T_i\left(1 - e^{-\frac{t}{\lambda_{4,i}}}\right). \tag{6-24}$$

Based on the trajectories depicted in Figure 6-17, the expected value of thickness is linear with respect to time while its variance has an exponent form. Therefore, the models considered to describe the mean and the variance of thickness during the deposition process for each discrete point in the temperature domain are as follows:

$$\varepsilon_H(T_i,t) = \lambda_{5,i}T_i t, \tag{6-25}$$

$$V_H(T_i,t) = \lambda_{6,i}T_i t^{\lambda_{7,i}}, \tag{6-26}$$

where $\lambda_{l,i}(l = 1,\dots,7)$ represent the model parameters for each T_i that can be identified using least-squares.

7. *Model identification:* Estimate the parameters of Eqs.(6-23)-(6-26) for the data set obtained for each discrete point in the *Space discretization* step through minimization of the following least-squares function:

$$\Lambda(\boldsymbol{\lambda}_i) = \sum_{k=0}^{K}\left(\mu_{i,k}^{PSE} - \mu_{i,k}^{pred}\right)^2, \quad (6\text{-}27)$$

where $\mu_{i,k}^{PSE}$ and $\mu_{i,k}^{pred}$ are respectively the statistical moment of the process output calculated using the PSEs in step 5 and the model prediction obtained from Eqs.(6-23)-(6-26) at the k^{th} sampling time instance and for a specific discrete temperature, T_i. The identified $\boldsymbol{\lambda}_i$ represent the vector of parameters for each discrete temperature, T_i, i.e., there exist one set of model parameters for each discrete point considered in the *Space discretization* step.

8. *Approximation of the closed-form model parameters:* The identified model parameters $\boldsymbol{\lambda}_i$ are only valid for a discretized set of temperatures. However, for model-based control applications, it is required to estimate the statistical moments of the process outputs at any temperature within the specified operating region. Therefore, a polynomial function is employed here to correlate the model parameters to the manipulated variable, T, using the model parameters, $\boldsymbol{\lambda}_i$, estimated for each discrete T_i in the previous step, i.e.,

$$\bar{\lambda}_l = b_{0,l} + \sum_{d=1}^{D} b_{d,l}\Gamma_d(T)\,, l = 1,2,\dots,7, \quad (6\text{-}28)$$

where $\Gamma_d(T)$ represents a temperature-dependent polynomial function while $b_{0,l}$ and $b_{d,l}$ are the coefficients of the polynomial calculated through least-squares regression; D is the number of terms considered in the analysis. Once these correlations are obtained offline, they can be used to predict the statistical moments of each output for online applications.

9. *Closed-form model:* As shown in Eqs.(6-23)-(6-24), the statistical moments of surface roughness at any sampling time during the deposition process depend on the substrate temperature and the statistical moments of roughness at the previous time step. Thus,

$$\varepsilon_{r,k} = \varepsilon_{r,k-1} + sgn\left(\bar{\lambda}_{1,k}T\left(1 - e^{-\frac{t_k}{\bar{\lambda}_{2,k}}}\right) - \varepsilon_{r,k-1}\right)\left|\left(\bar{\lambda}_{1,k}T - \varepsilon_{r,ref}\right)\left(e^{-\frac{t_{k-1}-t_{ref}}{\bar{\lambda}_{2,k}}} - e^{-\frac{t_k-t_{ref}}{\bar{\lambda}_{2,k}}}\right)\right|; \quad (6\text{-}29)$$

$\varepsilon_{r,0} = 1$ mL,

$$V_{r,k} = V_{r,k-1} + sgn\left(\bar{\lambda}_{3,k}T\left(1 - e^{-\frac{t_k}{\bar{\lambda}_{4,k}}}\right) - V_{r,k-1}\right)\left|\left(\bar{\lambda}_{3,k}T - V_{r,ref}\right)\left(e^{-\frac{t_{k-1}-t_{ref}}{\bar{\lambda}_{4,k}}} - e^{-\frac{t_k-t_{ref}}{\bar{\lambda}_{4,k}}}\right)\right|; \quad (6\text{-}30)$$

$V_{r,0} = 0$ mL^2,

where $\varepsilon_{r,k}$ and $V_{r,k}$ are respectively the estimated mean and variance of roughness at sampling time instance, t_k, while $\varepsilon_{r,k-1}$ and $V_{r,k-1}$ are the estimated values at sampling time instance, t_{k-1}. $\varepsilon_{r,ref}, V_{r,ref}$ and t_{ref} respectively denote the reference roughness mean, the reference roughness variance and the reference time when the substrate temperature changes

to the current temperature. sgn is the sign function while $\bar{\lambda}_{l,k}(l = 1,..4)$ are the model parameters evaluated employing the temperature at time, t_k, in the model obtained in step 8. Following Eq.(6-25), the expected value of thickness depends on the temperature and the mean thickness evaluated at the previous time instance, i.e.

$$\begin{aligned} &\varepsilon_{H,k} = \varepsilon_{H,k-1} + \bar{\lambda}_{5,k} T(t_k - t_{k-1}); \\ &\varepsilon_{H,0} = 0 \text{ mL}, \end{aligned} \tag{6-31}$$

where $\bar{\lambda}_{5,k}$ is the model parameter estimated using the polynomial obtained in Eq.(6-28) and the substrate temperature at time, t_k. The variance of the film thickness at any time during the deposition process can be estimated as follows:

$$\begin{aligned} &V_{H,k} = V_{H,k-1} + \bar{\lambda}_{6,k} T\left(\bar{\lambda}_{7,k} - 1\right) t_k^{\bar{\lambda}_{7,k}} (t_k - t_{k-1}); \\ &V_{H,0} = 0 \text{ mL}^2, \end{aligned} \tag{6-32}$$

where $\bar{\lambda}_{l,k}(l = 6,7)$ are the model parameters estimated from Eq.(6-28) using the substrate temperature at time, t_k.

Based on the above, a nonlinear discrete closed-form model can be obtained to determine the statistical moments of roughness and thickness during the deposition process for optimization and control applications:

$$\mu_k = g(\mu_{k-1}, T), \tag{6-33}$$

where $\mu_k^T = \left[\varepsilon_{r,k}, V_{r,k}, \varepsilon_{H,k}, V_{H,k}\right]$ is the vector of statistical moments at sampling time t_k, while $\mu_{k-1}^T = \left[\varepsilon_{r,k-1}, V_{r,k-1}, \varepsilon_{H,k-1}, V_{H,k-1}\right]$ is the vector of statistical moments at sampling time t_{k-1}.

To show the effectiveness of this approach, the developed model has been applied to estimate the upper and lower bounds on surface roughness and film thickness at a predefined confidence level, α, during the deposition process. Taking advantage of the form of PDFs, thickness and roughness can be estimated at a specific probability limit. That is, as shown in Figure 6-14 and Figure 6-15, the variability in surface roughness and film thickness can be described respectively using lognormal and normal distributions. The surface roughness can be evaluated at a specific probability $\mathbb{P}\mathbb{r}$, as follows:

$$r_k^b = F_r^{-1}\left(\mathbb{Pr}\middle|\varepsilon_{r,k}, V_{r,k}\right) = \left\{r_k^b : F_r\left(r_k^b|\varepsilon_{r,k}, V_{r,k}\right) = \mathbb{Pr}\right\}, \tag{6-34}$$

$$\mathbb{Pr} = F_r\left(r_k^b|\varepsilon_{r,k}, V_{r,k}\right) = \frac{1}{\sqrt{2\pi V_{r,k}}}\int_0^{r_k^b} \frac{e^{-\frac{\left(\ln z - \varepsilon_{r,k}\right)^2}{2V_{r,k}}}}{z} dz, \tag{6-35}$$

where $b \in \{low, up\}$ and F_r^{-1} represents the inverse CDF of surface roughness. Setting $\mathbb{Pr}$ in Eq.(6-35) to $\alpha/2$ and $1-\alpha/2$ yields respectively the lower bound, r_k^{low}, and the upper bound, r_k^{up}, for the surface roughness at t_k. Likewise, the bounds on thickness can be obtained at any sampling time, t_k as follows:

$$H_k^b = F_H^{-1}\left(\mathbb{Pr}\middle|\varepsilon_{H,k}, V_{H,k}\right) = \left\{H_k^b : F_H\left(H_k^b|\varepsilon_{H,k}, V_{H,k}\right) = \mathbb{Pr}\right\}, \tag{6-36}$$

$$\mathbb{Pr} = F_H\left(H_k^b|\varepsilon_{H,k}, V_{H,k}\right) = \frac{1}{\sqrt{2\pi V_{H,k}}}\int_{-\infty}^{H_k^b} e^{-\frac{\left(z-\varepsilon_{H,k}\right)^2}{2V_{H,k}}} dz. \tag{6-37}$$

For the present deposition process, the operational region for the substrate temperature is from 600 to 1400 K that is discretized into 9 equally spaced temperatures, $T_i (i = 1, \dots, 9)$. The batch time, $t_f = 100$ s, is discretized into 101 equally spaced points, $t_k (k = 0, \dots, 100)$. $\boldsymbol{\theta}^T = [E, E_m, \mathcal{X}]$ is the set of uncertain parameters that are normally distributed around their nominal values listed in Table 3-1 with the covariance matrix shown in Eq.(6-19). The first and second-order sensitivities of surface roughness with respect to the uncertain parameters and the nominal surface roughness are generated offline for each discrete temperature during the deposition process. These estimates are then applied in Eqs.(6-17)-(6-18) to approximate the mean and the variance of surface roughness during the batch time for each temperature, T_i. Likewise, the nominal film thickness and first-order sensitivities of thickness with respect to the uncertain parameters are generated offline during the deposition process for each T_i. Then using Eqs.(6-15)-(6-16), the mean and the variance of film thickness is estimated during the batch time for each temperature, T_i. The data collected for each statistical moment is then used in least-squares approach as shown in Eq.(6-8) to estimate the parameters of the models shown in Eqs.(6-23)-(6-26) for each temperature, T_i. To find a correlation between the model parameters and the substrate temperature, regression analyses are performed for the vector of closed-form model parameters $\bar{\boldsymbol{\lambda}}^T = \left[\bar{\lambda}_1, \dots, \bar{\lambda}_7\right]$. These polynomials can be used to determine the coefficients of Eqs.(6-29)-(6-32) during the deposition process as a function of substrate temperature.

To obtain a general model for $\bar{\lambda}_l(l = 1, \ldots, 4)$, the temperature operational region is divided into two regions. The polynomial functions obtained from regression to estimate the mean and variance of surface roughness for the two temperature regions are shown in Figure 6-18 and Figure 6-19, respectively.

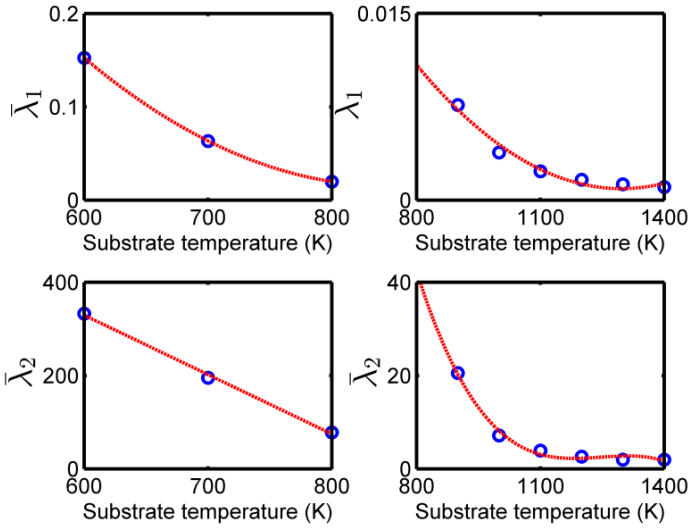

Figure 6-18. Polynomial models used to determine $\bar{\lambda}_1$ and $\bar{\lambda}_2$ to estimate the surface roughness mean.

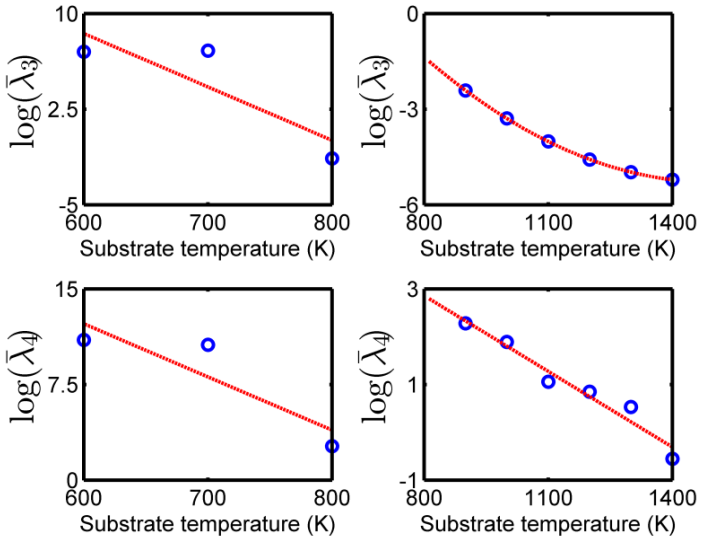

Figure 6-19. Polynomial models used to determine $\bar{\lambda}_3$ and $\bar{\lambda}_4$ to estimate the surface roughness variance.

The polynomial models obtained using regression for $\bar{\lambda}_l(l = 5,6,7)$ are shown in Figure 6-20 and Figure 6-21.

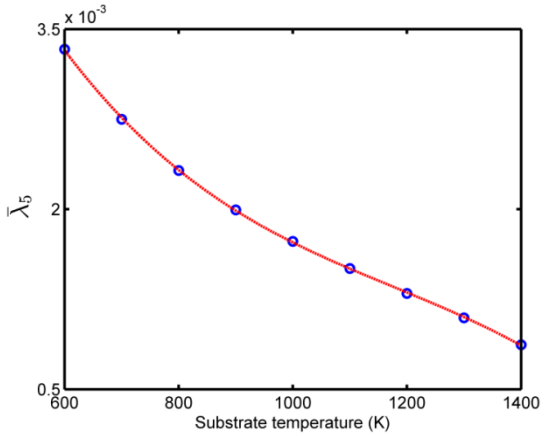

Figure 6-20. Polynomial model used to determine $\bar{\lambda}_5$ to estimate the film thickness mean.

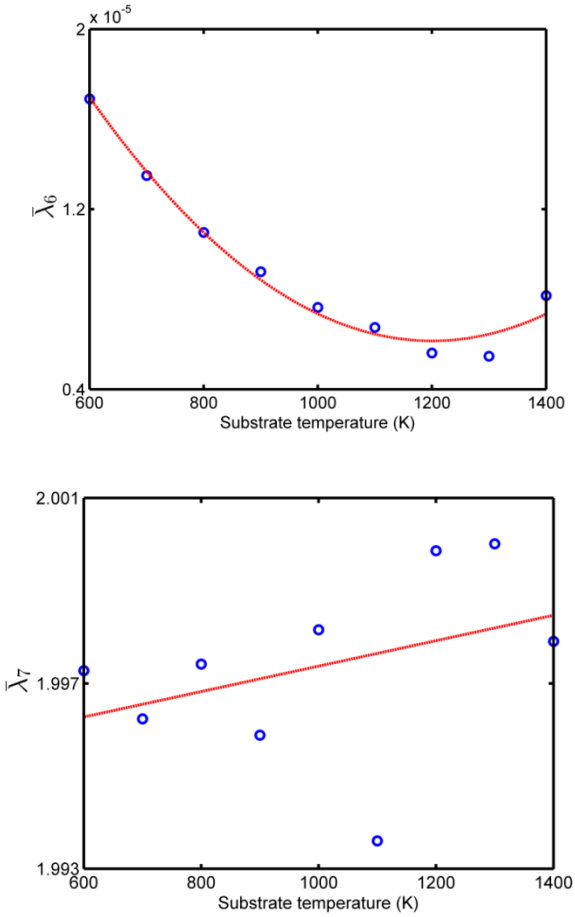

Figure 6-21. Polynomial model used to determine $\bar{\lambda}_6$ and $\bar{\lambda}_7$ to estimate the film thickness variance.

Upper and lower bounds estimated using the closed-form model on surface roughness at $\alpha = 0.5\%$ are shown in Figure 6-22(a) as dashed lines using the temperature profile shown in Figure 6-22(b). As shown in this figure, the open-loop responses obtained from 20 simulations

using random realizations in the uncertain parameters are bounded within the estimated upper and lower bounds. Likewise, Figure 6-23 shows the open-loop simulations for the film thickness and the corresponding bounds (dashed lines). While the upper and lower bounds are estimated using the closed-form model in milliseconds, each open-loop simulation using a 100×100 lattice in the KMC model takes approximately an hour.

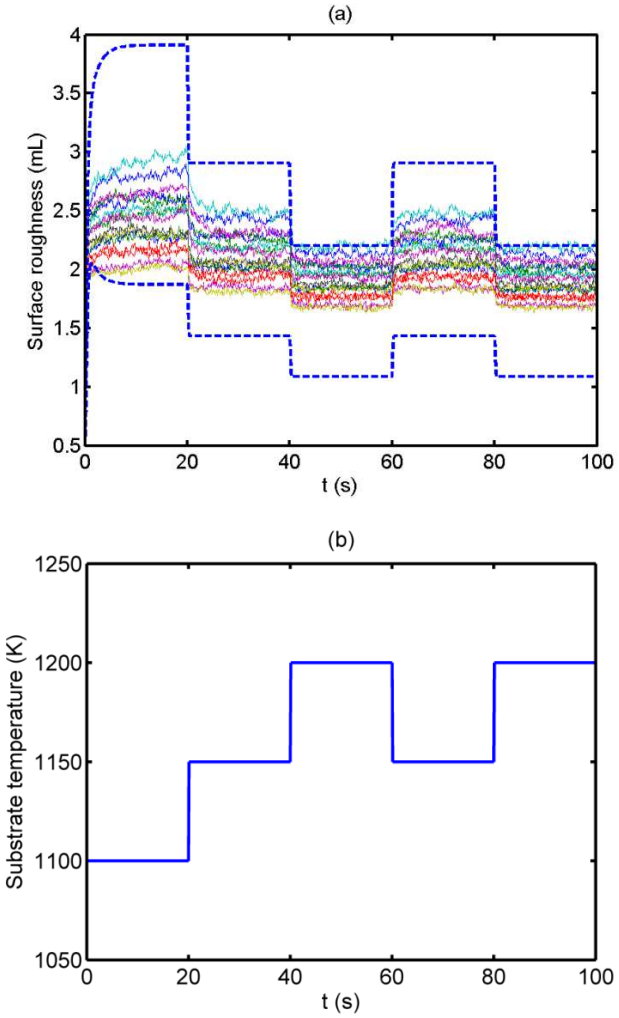

Figure 6-22. (a) Surface roughness due to parameter uncertainties, obtained by Monte Carlo simulation using 20 open-loop simulations (solid lines), the upper and lower bounds estimated on surface roughness by closed-form model (dashed lines), (b) Substrate temperature profile.

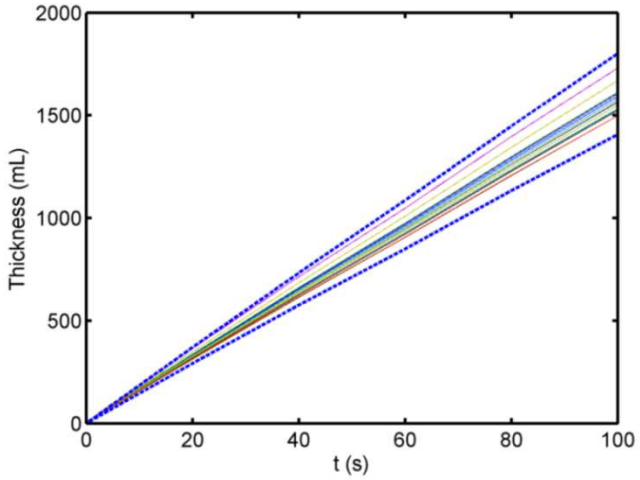

Figure 6-23. Thickness due to parameter uncertainties obtained by Monte Carlo simulation using 20 open-loop simulations (solid lines), the upper and lower bounds estimated on thickness by closed-form model (dashed lines).

6.2.4. Deterministic surrogate formulation of stochastic NMPC

Figure 6-22 and Figure 6-23 demonstrate the accuracy of the developed closed-form model and its efficiency for online control of the deposition process under uncertainty in the model parameters. Motivated by this, the computationally tractable deterministic surrogate of the stochastic NMPC scheme shown in Eq.(6-20) can be developed by replacing the probabilistic constraint on film thickness with the following deterministic constraint:

$$H_{min} - F_H^{-1}\left(1-\beta\middle|\varepsilon_H(t_f), V_H(t_f)\right) \leq 0, \tag{6-38}$$

where $\varepsilon_H(t_f)$ and $V_H(t_f)$ are respectively estimated using Eqs.(6-11)-(6-32). This formulation has been derived considering that, the probabilistic constraint in problem (6-20) is a linear function of final thickness, and the film thickness can be described using a normal distribution as shown in Eq.(6-36). The conversion of probabilistic constraints for efficient optimization has been studied for a wide class of PDFs (Calafiore and Ghaoui, 2006). Using Eq.(6-38), the shrinking horizon stochastic NMPC scheme shown in Eq.(6-20) can be reformulated as follows:

$$\min_{\mathbf{K}(j)} F_r^{-1}\left(\mathcal{B}\middle|\varepsilon_r(t_f), V_r(t_f)\right)$$

Subject to:

Closed-form model, Eqs.(6-29)-(6-32)

$$\begin{aligned} &T(j) = T_{ref}(j) + \mathbf{K}(j)(H(j) - H_{ref}(j)) \\ &H_{min} - F_H^{-1}\left(1-\beta\middle|\varepsilon_H(t_f), V_H(t_f)\right) \leq 0 \\ &T_{min} \leq T(j) \leq T_{max} \\ &\mathcal{R}_{min} \leq T(j) - T(j-1) \leq \mathcal{R}_{max} \\ &j = 1, \dots, J. \end{aligned} \tag{6-39}$$

The performance index in this optimization problem is the surface roughness evaluated at a specific probability, $\mathcal{B}$. To provide a finite-dimensional optimization problem, the batch time, t_f has been discretized into 20 equally spaced time intervals. Accordingly, the feedback gain vector, $\mathbf{K}(t)$, which is the optimization variable for this problem, is considered to be piecewise constant between the sampling time intervals t_j and t_{j+1}. In this study, $\mathcal{R}_{max}$ and $\mathcal{R}_{min}$ were set to 25 K while T_{min} and T_{max} were respectively set to 600 and 1400 K, which correspond to the operational limits at which the closed-form models were identified. The nominal open-loop optimization problem was solved offline to determine the reference trajectory of the substrate temperature and the reference thickness. The measurements for thickness are available at every iteration of the NMPC algorithm, which has been set to 5 s in these simulations. The closed-form model shown in Eq.(6-33) is modified to estimate the states of the system for the NMPC framework. Although this model performs successfully under model-plant mismatch, its performance can be deteriorated in the presence of unmeasured disturbances. To improve the predictions, a linear correction term has been added to the model shown in Eq.(6-33) as follows:

$$\mu_j = g\left(\mu_{j-1}, T\right) + \mathbf{G}\,(\varepsilon_{H,j} - H(j)), \tag{6-40}$$

where $\mathbf{G}$ is the gain vector.

To evaluate the performance of the NMPC algorithm shown in (6-39), the following four different scenarios are considered:

1. $\mathcal{B} = 50\%$ and $\beta = 50\%$.
2. $\mathcal{B} = 70\%$ and $\beta = 70\%$.

3. $\mathcal{B} = 90\%$ and $\beta = 80\%$.
4. $\mathcal{B} = 90\%$ and $\beta = 80\%$ under disturbance.

In the first scenario, the NMPC scheme minimizes the final surface roughness estimated at 50% probability while the minimum allowed film thickness, H_{min}, has to be at least 1,700 mL in more than 50% of the runs. To assess the effectiveness of the control framework, Monte Carlo simulations of the closed-loop control have been performed using 50 random realizations in the uncertain parameters obtained from the joint multivariable normal distribution previously described in Eq.(6-19). The PDFs of the surface roughness and film thickness at the end of the batch are shown in Figure 6-24. The mean value of the thickness PDF is 1,708 mL indicating that the thickness obtained in more than 50% of the closed-loop simulations at the end of the batch are more than almost 1,700 mL. Therefore, the NMPC scheme successfully complies with the constraint defined on final film thickness for this scenario. The PDF of surface roughness at the end of the batch is also shown in this figure and has the mean value of 1.78 mL.

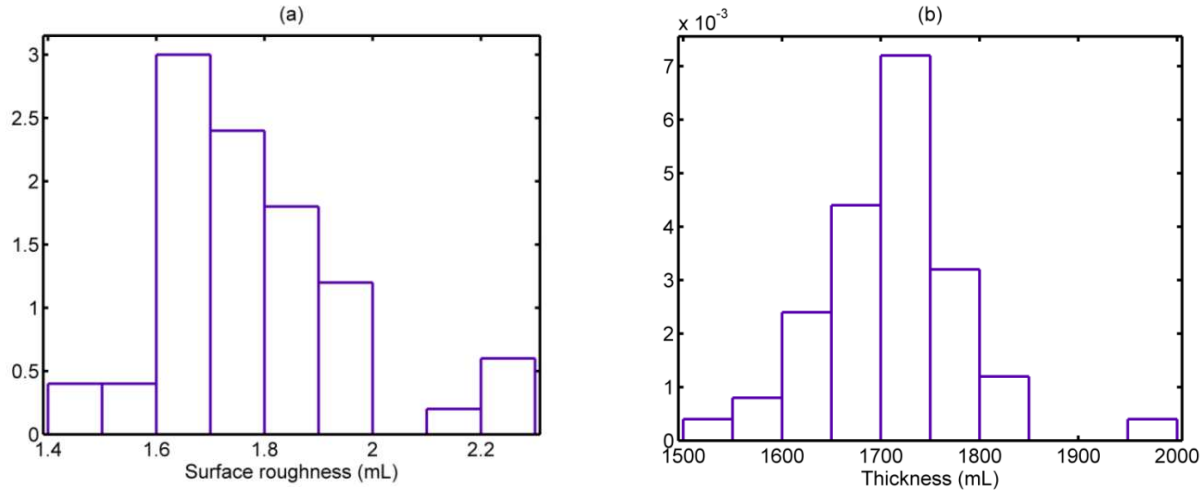

Figure 6-24. PDFs obtained at the end of the batch from 50 Monte Carlo simulations for $\mathcal{B} = 50\%$ and $\beta = 50\%$ (a) Surface roughness, and (b) Thickness.

In the second scenario, the final surface roughness is estimated at 70% probability while the film thickness has to be more than 1,700 mL in at least 70% of the runs. Figure 6-25 shows final thin film properties obtained from 50 closed-loop simulations for the first and second scenarios. Since in the second scenario, a higher probability of satisfaction has been enforced on the film thickness constraint, the number of thin films that has a thickness that is more than 1,700 mL is 14% more than the first scenario. The average thickness in this scenario is 1,742 mL which is

larger compared to the mean thickness obtained in the first scenario. As shown in this figure, due to requirements to achieve a thickness larger than 1,700 mL in 70% of the runs, the controller has resulted in higher surface roughness at the end of the batch with the mean value of 1.99 mL.

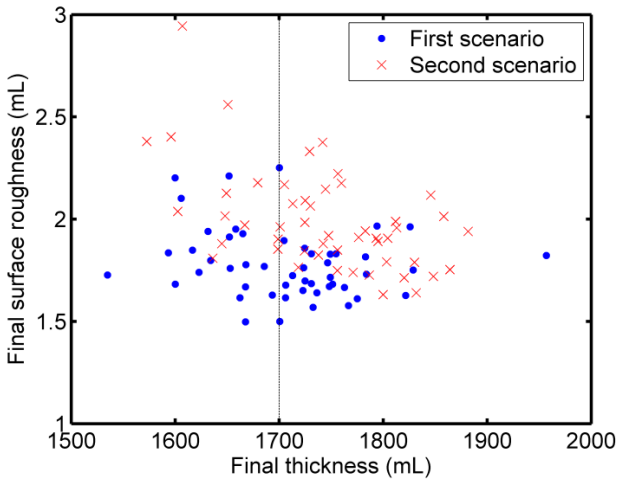

Figure 6-25. Final properties at the end of the batch from 50 Monte Carlo simulations for the first and second scenarios.

The substrate temperature trajectory for the second scenario is compared to the trajectory obtained in the first scenario in Figure 6-26 using the same realization in the uncertain multiscale model parameters. As shown in this figure, a low temperature profile in the second scenario promotes adsorption on the surface to comply with the film thickness constraint. The penalty of the lower temperature is the larger average surface roughness obtained at the end of the deposition process as indicated in Figure 6-25.

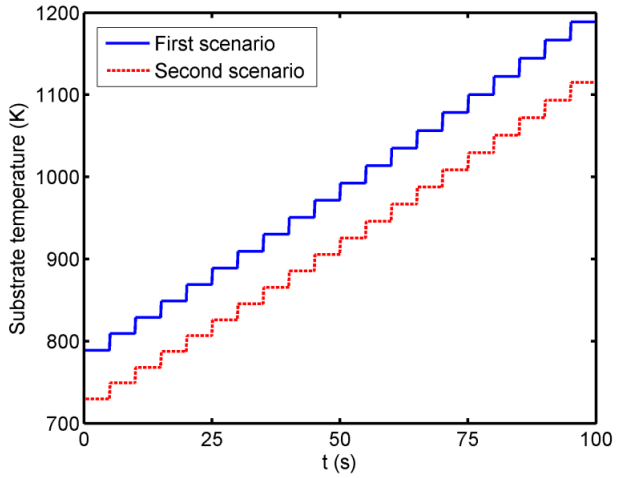

Figure 6-26. The substrate temperature trajectory applying the first and the second scenarios in the stochastic NMPC.

To further demonstrate the applicability of the NMPC scheme, in the third scenario, the control objective is to minimize the final surface roughness evaluated at 90% probability while the film thickness is required to be more than 1,700 mL in at least 80% of the runs. Figure 6-27 shows the variation of the PDFs of surface roughness and film thickness during the deposition process for the first and third scenarios. As shown in Figure 6-27(a), the variability in surface roughness is described by lognormal PDFs during the process. The mean and the variance of the PDFs are changing during the batch due to variation in the temperature trajectories. As shown in Figure 6-27(b), the film thickness is normally distributed during the process in the first and third scenarios; however, their mean and the variances are slightly different since different confidence levels were imposed in the stochastic MPC framework. In the third scenario, the average roughness at the end of the batch is 2.25 mL while the average film thickness is 1,770 mL.

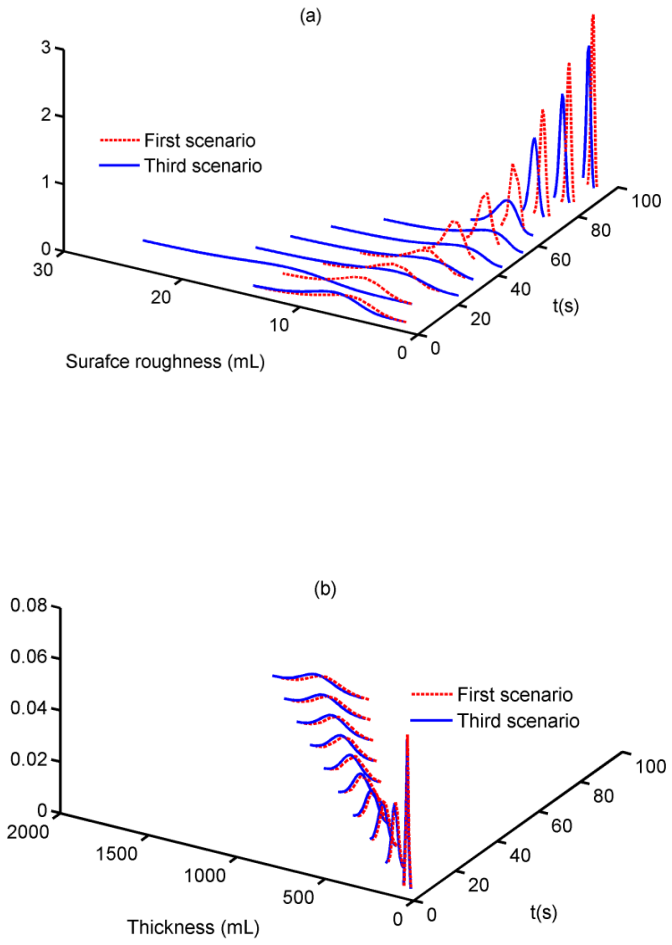

Figure 6-27. Variations of the PDFs along the batch for the first and third scenarios (a) Surface roughness, and (b) Thickness.

To show the effectiveness of the control scheme in the presence of disturbances, in the last scenario, a step change of -5% has been inserted in the sticking coefficient, S_0, at $t = 50$ s. As shown in Eq.(3-8), the sticking coefficient directly affects the adsorption rate on the surface, and consequently affects the surface roughness and film thickness. The final properties from 50 closed-loop simulations are shown in Figure 6-28 for the third and fourth scenarios. The disturbance introduced in the fourth scenario lowers the adsorption rate on the surface that can lead to a low thickness at the end of the batch. However, as shown in Figure 6-28, the film thickness at the end of the batch is more than 1,700 mL in more than 80% of the runs, which satisfies the requirement specified in the stochastic NMPC framework. The average roughness at

the end of the batch is 2.22 mL while the average film thickness is 1,766 mL. Thus, these values are similar to the means obtained in the third scenario for the surface roughness and thickness, which demonstrates the effectiveness of the proposed control scheme.

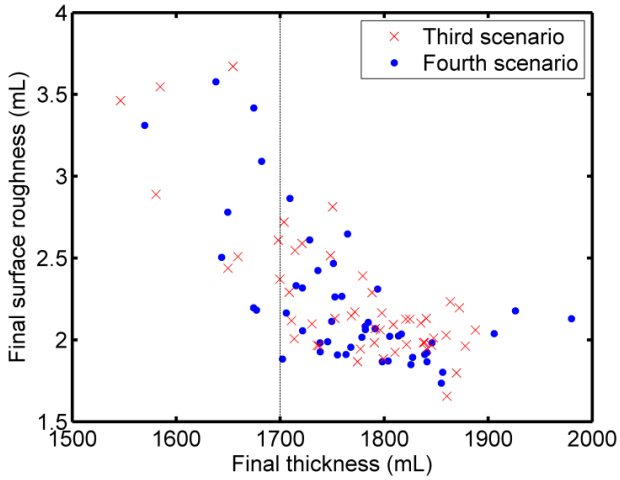

Figure 6-28. Final properties at the end of the batch from 50 Monte Carlo simulations for the third and fourth scenarios.

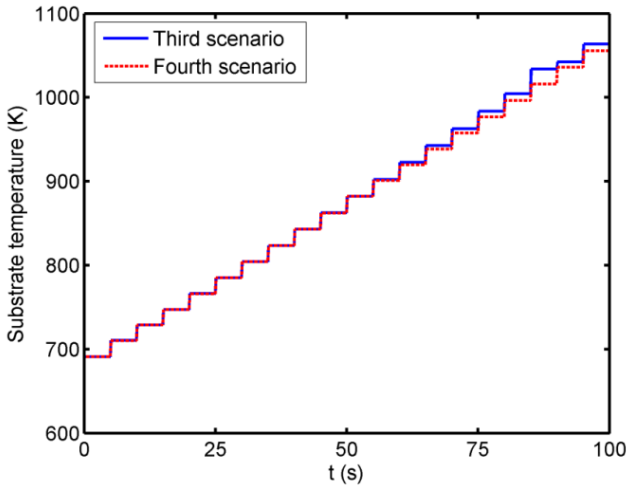

Figure 6-29. Substrate temperature trajectory applying the third and the fourth scenarios in the stochastic NMPC.

The optimal substrate temperature trajectories for the third and fourth scenarios are compared in Figure 6-29. To provide a fair comparison between these scenarios, the temperature trajectories are obtained for a specific realization of the uncertain multiscale model parameters. As shown in this figure, the temperature profile for the fourth scenario is slightly lower in the second half of the batch to meet the constraint on thickness. This decrease in the temperature

profile is performed by NMPC to compensate for the sudden drop in the adsorption rate due to the step change in the sticking coefficient at $t = 50$ s.

6.3. Summary

A robust NMPC algorithm has been presented in this chapter to minimize the surface roughness in a thin film deposition process while satisfying the constraints on applied substrate temperature and the minimum film thickness required at the end of the process. To provide a model that is efficient for NMPC, model identification is performed through data collected from a multiscale thin film deposition model. A series expansion of the surface roughness is used to estimate the distribution of this controlled output in the growth process. A closed-form model is developed to predict the surface roughness and film thickness during the growth process under model parameter uncertainty. Subsequently, this model is applied in the NMPC to provide a robust control strategy under uncertainties in the KMC parameter and the control actions. As shown in the simulation results, significant variability in the film deposition process due to model uncertainty can lead to economic losses, since the process cannot meet the desired product specifications. Considering the uncertainties in the model have shown to significantly improve the performance of the control approach; hence, motivating the need to develop robust strategies for the thin film deposition process.

Moreover, a closed-form model has been developed that is able to accurately predict the statistical moments of surface roughness and film thickness during the deposition under model parameter uncertainty. Employing PSEs, the expected value and the variance of the surface roughness and film thickness are estimated as a function of substrate temperature. This collected data is used for offline identification of the closed-form model parameters. The developed model can efficiently predict the statistical moments for online control and optimization applications. Thus, the model is applied in a stochastic NMPC to provide a robust control strategy for the deposition process under uncertainties in the multiscale model parameters. The stochastic shrinking horizon NMPC minimizes the surface roughness in a thin film deposition process while complying with the constraints on applied substrate temperature and the minimum film thickness required at the end of the process at a desired probability limit.

Chapter 7
Conclusions and Recommendations

The focus of this research is on uncertainty analysis of the thin film deposition process using PSE for robust optimization and control applications. The disparity in length and time scales of the physicochemical events occurring in thin film deposition is described using a multiscale model that couples nonlinear PDEs with lattice-based KMC simulations. Unlike continuum models, the KMC model does not provide a closed-form expression and is also computationally prohibitive for uncertainty analysis. Therefore, for robust control and optimization applications in this research, the controlled objectives are described as a series expansion of the uncertain model parameters. The Monte Carlo sampling method is employed in this work as an index to validate the accuracy of the approximations and to determine the order of the truncated PSEs. The analytical expressions obtained using the PSE method can be used for an efficient uncertainty propagation using Monte Carlo method or to determine the statistical moments of the controlled outputs.

7.1. Conclusions

A fundamental step to design a robust optimization or control strategy is the characterization of uncertainty in model parameters. However, when there is no access to data from the process, the common assumption is that the uncertainties are either normally distributed or bounded. The probabilistic approach based on normal distribution leads to optimistic estimates whereas the worst-case scenario via bounded uncertainties might include realizations in the parameters that will be very unlikely thus leading to overly conservative results. The uncertainty analysis on the thin film deposition is performed in Chapter 4 applying worst-case and probabilistic-based approaches. To provide a computationally tractable optimization, the required sensitivities in the PSEs are obtained from average of multiple multiscale simulations employing reduced-order lattices in the KMC simulations. The optimal temperature profile that maximizes the final thickness of the thin film under end-point product constraints and uncertainty in the model parameters has been identified. The results show that the prior assumption on type of the uncertainty affects the optimization results. Thus, inaccurate uncertainty description assumptions can lead to a loss in performance and therefore economic losses in the process.

Sensitivity analysis of the stochastic computationally intensive KMC simulations is not trivial. However, closed-form expressions that describe the states of the thin film deposition as a function of KMC parameters are available. In Chapter 4, to accelerate the distributional uncertainty analysis of the rate of microscopic events using PSE, the sensitivities are calculated analytically. The probabilistic bounds on these rates are employed to determine the probabilistic bounds on outputs for optimization purposes. Moreover, an algorithm is developed to provide less conservative bounds for time-varying parameter uncertainties. The method is used to obtain the optimal substrate temperature trajectory that maximizes the endpoint thin film thickness while meeting constraints on the roughness and growth rate in the presence of model-plant mismatch. The proposed approach is evaluated through simulations that show that the system's outputs remained within their corresponding feasible operational limits under uncertainty. To that end, neglecting the model-plant mismatch in optimization strategies may result in undesired plant performance that is far from the optimum.

Offline optimization of the thin film deposition process through multiscale model simulation is computationally intensive. This motivates the development of data-driven models that can efficiently predict the controlled outputs for online applications. The identified models can be used either as an estimator in the lack of sensors or as a basis of the MPC framework. Therefore, a robust estimator is developed in Chapter 5 to predict the surface roughness and growth rate as a function of substrate temperature and bulk precursor mole fraction in the lack of measurements and under uncertainty in the system parameters. To provide a computationally efficient estimator for online applications, an algorithm is presented for offline identification of a closed-form model that describes the controlled outputs based on transient changes in the manipulated variables. This algorithm is applicable regardless of the probability distribution assigned to the uncertain parameters. To provide robust estimations, the estimator is designed to evaluate the upper and lower bounds on the outputs under model parameter uncertainties. The closed-form model is developed based on data collected from the multiscale model. The sensitivities of the outputs with respect to the uncertain parameters are assessed offline at different substrate temperatures and bulk precursor mole fractions. Accordingly, upper and lower bounds on the outputs are determined at a specific confidence level and employed to identify a closed-form model for online applications. To assess the performance of the estimator in multivariable process control applications, the proposed estimator is coupled with PI controllers. To provide a

robust control of surface roughness, the robust estimator estimates the upper bound on this controlled output. Results from this implementation have shown that the robust estimator has successfully predicted the process for control multivariable control under model-plant mismatch.

Effective control of thin film deposition processes involves accounting for model-plant mismatch, operating under constraints and in the lack of key process measurements. Therefore, a robust NMPC algorithm has been developed in Chapter 6 to minimize the surface roughness in a thin film deposition process while satisfying constraints on the applied substrate temperature and the minimum film thickness required at the end of the process. A series expansion of the surface roughness is used to estimate the distribution of this controlled output in the growth process. A closed-form model is developed to predict the surface roughness and film thickness during the growth process at a predefined probability. Subsequently, this model is applied in the NMPC to provide a robust control strategy under uncertainties in the KMC parameters and the control actions. Moreover, to improve the robust performance of the NMPC framework, a closed-form is developed to estimate the statistical moments of the surface roughness and film thickness during the deposition process. The closed-form model predicts the expected value and the variance of the thin film properties based on the substrate temperature during the deposition process. The parameters of the closed-form model are determined offline employing power series expansion (PSE). The closed-form model allows the reformulation of probabilistic constraints into their corresponding deterministic expressions thus enabling the design of a computationally feasible stochastic NMPC. To show the effectiveness of the approach, a shrinking horizon stochastic NMPC framework is devised to minimize the final surface roughness while complying with actuator constraints and a probabilistic constraint on the final film thickness.

In process modeling and analysis, the discrepancy between the actual process and the model is expected. The performance of model-based control and optimization approaches can be deteriorated due to inappropriate assumptions applied in the model development and model uncertainty. Specifically, when the system's performance objective is sensitive to unpredictable or sudden changes in the system's physical parameters, this model-plant mismatch can lead to loss in performance. This research provides insight regarding the qualitative and quantitative effects of parameter uncertainty in multiscale process systems. The methods developed in this research enable accurate online control of the key properties of a multiscale system in the presence of model-plant mismatch.

7.2. Recommendations

The current research can potentially be extended in different ways as explained below.

Control thin film porosity in the presence of model-plant mismatch: A key assumption in modeling of the thin film deposition process in this research is SOS approximation. Based on this assumption, overhangs and vacancies are not allowed and atoms are located on top of other atoms on the surface. Porosity can adversely affect the electrical properties of microelectronic devices. Employing a triangular lattice in the KMC simulation, control of porosity under model parameter uncertainty can be analysed.

Evaluate the methodologies in heterogeneous multiscale process systems: In the present research, thin film deposition is considered as a simple yet effective case study for a multiscale process system to evaluate the proposed methods. Although the thin film deposition process is spatially homogeneous, the application of the methods presented in this work can be explored in spatially heterogeneous systems. For instance, these methods can be applied to investigate the effect of model parameter uncertainties on product concentration in catalytic reactors.

Sensitivity analysis using other methods: Efficient and accurate estimation of sensitivities for stochastic KMC simulations is challenging. In this work, the sensitivity analysis has been performed using the average of results from multiple multiscale simulations in finite differences. Moving forward, the sensitivity analysis of the system can be conducted using other approaches.

Uncertainty analysis using other methods: Despite its importance, uncertainty analysis is still an open problem for optimization and control of multiscale process systems. The difficulties in considering uncertainty in such systems arise due to the computational intensity, the inherent stochastic behavior and the lack of closed-form model. In the current research, the uncertainty analysis has been performed applying PSE. Moving forward, the results can be compared to other uncertainty quantification methods such as PCE.

Online identification of the closed-form model: The closed-form models presented in this work for online applications have been developed using PSE-based algorithms. Sensitivity analysis required for these expansions is computationally intensive, and online estimation of these sensitivities through the multiscale model used in this work is not practical. Thus, offline identification is performed to identify the parameters of the closed-form model. Having an

efficient sensitivity evaluation approach, the algorithm can be modified as an adaptive model, where the parameters of the closed-form model can be identified online.

Extend the stochastic NMPC to other distributional uncertainties: The algorithm presented in Chapter 6 to predict the statistical moments of the controlled outputs assumed a normal distribution for uncertain parameters. The development of the closed-form model and the stochastic NMPC can be extended to a general case regardless of the form of distributional uncertainty. This will strengthen the foundations of the algorithms presented in this research.

Bibliography

Albo, S.E., Broadbelt, L.J., Snurr, R.Q., 2006. Multiscale modeling of transport and residence times in nanostructured membranes. AIChE J. 52, 3679–3687.

Allgöwer, F., Findeisen, R, Nagy, Z.K., 2004. Nonlinear model predictive control: From theory to application. J Chin Inst Chem Engrs 35, 299–315.

Armaou, A., Baker, J., D. Christofides, P., 2001. Feedback control of plasma etching reactors for improved etching uniformity. Chem. Eng. Sci. 56, 1467–1475.

Armaou, A., Christofides, P.D., 1999. Plasma enhanced chemical vapor deposition: Modeling and control. Chem. Eng. Sci. 54, 3305–3314.

Armaou, A., I. Siettos, C., G. Kevrekidis, I., 2004. Time-steppers and "coarse" control of distributed microscopic processes. Int. J. Robust Nonlinear Control 14, 89–111.

Bahakim, S.S., Rasoulian, S., Ricardez-Sandoval, L.A., 2014. Optimal design of large-scale chemical processes under uncertainty: A ranking-based approach. AIChE J. 60, 3243–3257.

Baumann, F. h., Chopp, D. l., de la Rubia, T.D., Gilmer, G. h., Greene, J. e., Huang, H., Kodambaka, S., O'Sullivan, P., Petrov, I., 2001. Multiscale modeling of thin-film deposition: Applications to Si device processing. MRS Bull. 26, 182–189.

Beck, J.V., Arnold, K.J., 1977. Parameter estimation in engineering and science. James Beck.

Behrens, C.M., Armaou, A., 2010. Optimal design and operation of a spatially distributed multiscale process, with regard to layered heterostructure growth. Ind. Eng. Chem. Res. 49, 7891–7900.

Birge, J.R., Louveaux, F., 2011. Introduction to Stochastic Programming. Springer Science & Business Media.

Braatz, R.D., Alkire, R.C., Rusli, E., Drews, T.O., 2004. Multiscale systems engineering with applications to chemical reaction processes. Chem. Eng. Sci. 59, 5623–5628.

Braatz, R.D., Alkire, R.C., Seebauer, E.G., Drews, T.O., Rusli, E., Karulkar, M., Xue, F., Qin, Y., Jung, M.Y.L., Gunawan, R., 2006a. A multiscale systems approach to microelectronic processes. Comput. Chem. Eng. 30, 1643–1656.

Braatz, R.D., Alkire, R.C., Seebauer, E., Rusli, E., Gunawan, R., Drews, T.O., Li, X., He, Y., 2006b. Perspectives on the design and control of multiscale systems. J. Process Control 16, 193–204.

Braatz, R.P., Young, P.M., Doyle, J.C., Morari, M., 1994. Computational complexity of mu; calculation. IEEE Trans. Autom. Control 39, 1000–1002.

Buzea, C., Robbie, K., 2005. State of the art in thin film thickness and deposition rate monitoring sensors. Rep. Prog. Phys. 68, 385.

Calafiore, G.C., Ghaoui, L.E., 2006. On distributionally robust chance-constrained linear programs. J. Optim. Theory Appl. 130, 1–22.

Cannon, M., Kouvaritakis, B., Raković, S.V., Cheng, Q., 2011. Stochastic tubes in model predictive control with probabilistic constraints. IEEE Trans. Autom. Control 56, 194–200.

Chatterjee, A., Vlachos, D.G., 2007. An overview of spatial microscopic and accelerated kinetic Monte Carlo methods. J. Comput.-Aided Mater. Des. 14, 253–308.

Christofides, P.D., Armaou, A., 2006. Control and optimization of multiscale process systems. Comput. Chem. Eng. 30, 1670–1686.

Christofides, P.D., Armaou, A., Lou, Y., Varshney, A., 2008. Control and optimization of multiscale process systems. Springer Science & Business Media.

Christofides, P.D., Davis, J.F., El-Farra, N.H., Clark, D., Harris, K.R.D., Gipson, J.N., 2007. Smart plant operations: Vision, progress and challenges. AIChE J. 53, 2734–2741.

Crose, M., Sang-Il Kwon, J., Nayhouse, M., Ni, D., Christofides, P.D., 2015. Multiscale modeling and operation of PECVD of thin film solar cells. Chem. Eng. Sci.

Datta, M., Landolt, D., 2000. Fundamental aspects and applications of electrochemical microfabrication. Electrochimica Acta 45, 2535–2558.

Dollet, A., 2004. Multiscale modeling of CVD film growth—a review of recent works. Surf. Coat. Technol. 177–178, 245–251.

Dooling, D.J., Broadbelt, L.J., 2001. Generic Monte Carlo tool for kinetic modeling. Ind. Eng. Chem. Res. 40, 522–529.

Drews, T.O., Braatz, R.D., Alkire, R.C., 2004a. Coarse-grained kinetic Monte Carlo simulation of copper electrodeposition with additives. Int. J. Multiscale Comput. Eng. 2, 313–327.

Drews, T.O., Braatz, R.D., Alkire, R.C., 2003. Parameter sensitivity analysis of Monte Carlo simulations of copper electrodeposition with multiple additives. J. Electrochem. Soc. 150, C807–C812.

Drews, T.O., Webb, E.G., Ma, D.L., Alameda, J., Braatz, R.D., Alkire, R.C., 2004b. Coupled mesoscale—continuum simulations of copper electrodeposition in a trench. AIChE J. 50, 226–240.

Fichthorn, K.A., Weinberg, W.H., 1991. Theoretical foundations of dynamical Monte Carlo simulations. J. Chem. Phys. 95, 1090–1096.

Freund, L.B., Suresh, S., 2004. Thin film materials: stress, defect formation and surface evolution. Cambridge University Press.

Gadgil, P.N., 1993. Single wafer processing in stagnation point flow CVD reactor: Prospects, constraints and reactor design. J. Electron. Mater. 22, 171–177.

Gallivan, M.A., 2005. An estimation study for control of a lattice model of thin film deposition. Comput. Chem. Eng., Control of Multiscale and Distributed Process Systems 29, 761–769.

Gallivan, M.A., 2003. Optimization, estimation, and control for kinetic Monte Carlo simulations of thin film deposition. Presented at the 42nd IEEE Conference on Decision and Control, 2003. Proceedings, pp. 3437–3442 vol.4.

Gallivan, M.A., Murray, R.M., 2004. Reduction and identification methods for Markovian control systems, with application to thin film deposition. Int. J. Robust Nonlinear Control 14, 113–132.

Gallivan, M.A., Murray, R.M., 2003. Model reduction and system identification for master equation control systems, in: American Control Conference, 2003. Proceedings of the 2003. pp. 3561–3566 vol.4.

García, C.E., Prett, D.M., Morari, M., 1989. Model predictive control: Theory and practice—A survey. Automatica 25, 335–348.

Gear, C.W., Li, J., Kevrekidis, I.G., 2003. The gap-tooth method in particle simulations. Phys. Lett. A 316, 190–195.

Ghanem, R.G., Spanos, P.D., 2003. Stochastic finite elements: A spectral approach. Courier Corporation.

Gillespie, D.T., 2001. Approximate accelerated stochastic simulation of chemically reacting systems. J. Chem. Phys. 115, 1716–1733.

Gilmer, G.H., Bennema, P., 1972. Simulation of crystal growth with surface diffusion. J. Appl. Phys. 43, 1347–1360.

Gilmer, G.H., Huang, H., de la Rubia, T.D., Dalla Torre, J., Baumann, F., 2000. Lattice Monte Carlo models of thin film deposition. Thin Solid Films 365, 189–200.

Gilmer, G.H., Huang, H., Roland, C., 1998. Thin film deposition: fundamentals and modeling. Comput. Mater. Sci. 12, 354–380.

Gorman, J.J., Shapiro, B., 2011. Feedback control of MEMS to atoms. Springer Science & Business Media.

Granneman, E.H.A., 1993. Thin films in the integrated circuit industry: requirements and deposition methods. Thin Solid Films 228, 1–11.

Grover, M.A., Xiong, R., 2009. A modified moving horizon estimator for in situ sensing of a chemical vapor deposition process. IEEE Trans. Control Syst. Technol. 17, 1228–1235.

Gunawan, R., Cao, Y., Petzold, L., Doyle III, F.J., 2005. Sensitivity analysis of discrete stochastic systems. Biophys. J. 88, 2530–2540.

Gunawan, R., Jung, M.Y.L., Seebauer, E.G., Braatz, R.D., 2004. Optimal control of rapid thermal annealing in a semiconductor process. J. Process Control 14, 423–430.

Halemane, K.P., Grossmann, I.E., 1983. Optimal process design under uncertainty. AIChE J. 29, 425–433.

Huang, J., Hu, G., Orkoulas, G., Christofides, P.D., 2011. Dynamics and lattice-size dependence of surface mean slope in thin-film deposition. Ind. Eng. Chem. Res. 50, 1219–1230.

Huang, J., Hu, G., Orkoulas, G., Christofides, P.D., 2010. Dependence of film surface roughness and slope on surface migration and lattice size in thin film deposition processes. Chem. Eng. Sci. 65, 6101–6111.

Hu, G., Lou, Y., Christofides, P.D., 2008. Dynamic output feedback covariance control of stochastic dissipative partial differential equations. Chem. Eng. Sci. 63, 4531–4542.

Hu, G., Orkoulas, G., Christofides, P.D., 2009. Regulation of film thickness, surface roughness and porosity in thin film growth using deposition rate. Chem. Eng. Sci. 64, 3903–3913.

Jensen, K.F., Rodgers, S.T., Venkataramani, R., 1998. Multiscale modeling of thin film growth. Curr. Opin. Solid State Mater. Sci. 3, 562–569.

Kampen, N.G.V., 1992. Stochastic processes in physics and chemistry. Elsevier.

Katsoulakis, M.A., Majda, A.J., Vlachos, D.G., 2003. Coarse-grained stochastic processes and Monte Carlo simulations in lattice systems. J. Comput. Phys. 186, 250–278.

Kwon, J.S., 2015. Multiscale modeling and control of crystal shape and size distributions: accounting for crystal aggregation, evaluation of continuous crystallization systems and run-to-run control. eScholarship.

Lam, R., Vlachos, D.G., 2001. Multiscale model for epitaxial growth of films: Growth mode transition. Phys. Rev. B 64, 035401.

Li, P., Arellano-Garcia, H., Wozny, G., 2008. Chance constrained programming approach to process optimization under uncertainty. Comput. Chem. Eng. 32, 25–45.

Liu, C., Erdmann, J., Macrander, A., 1999. In situ spectroscopic ellipsometry as a surface-sensitive tool to probe thin film growth. Thin Solid Films 355–356, 41–48.

Lou, Y., Christofides, P.D., 2006. Nonlinear feedback control of surface roughness using a stochastic PDE: Design and application to a sputtering process. Ind. Eng. Chem. Res. 45, 7177–7189.

Lou, Y., Christofides, P.D., 2004. Feedback control of surface roughness of GaAs (0 0 1) thin films using kinetic Monte Carlo models. Comput. Chem. Eng. 29, 225–241.

Lou, Y., Christofides, P.D., 2003a. Estimation and control of surface roughness in thin film growth using kinetic Monte-Carlo models. Chem. Eng. Sci. 58, 3115–3129.

Lou, Y., Christofides, P.D., 2003b. Feedback control of growth rate and surface roughness in thin film growth. AIChE J. 49, 2099–2113.

Ma, D.L., Braatz, R.D., 2003. Robust identification and control of batch processes. Comput. Chem. Eng. 27, 1175–1184.

Ma, D.L., Braatz, R.D., 2001. Worst-case analysis of finite-time control policies. IEEE Trans. Control Syst. Technol. 9, 766–774.

Ma, D.L., Chung, S.H., Braatz, R.D., 1999. Worst-case performance analysis of optimal batch control trajectories. AIChE J. 45, 1469–1476.

Majumder, D., Broadbelt, L.J., 2006. A multiscale scheme for modeling catalytic flow reactors. AIChE J. 52, 4214–4228.

Makov, G., Payne, M.C., 1995. Periodic boundary conditions in ab initio calculations. Phys. Rev. B 51, 4014–4022.

Mandur, J., Budman, H., 2014. Robust optimization of chemical processes using Bayesian description of parametric uncertainty. J. Process Control, ADCHEM 2012 Special Issue 24, 422–430.

Mayne, D.Q., Rawlings, J.B., Rao, C.V., Scokaert, P.O.M., 2000. Constrained model predictive control: Stability and optimality. Automatica 36, 789–814.

McGill, J.A., Ogunnaike, B.A., Vlachos, D.G., 2012. Efficient gradient estimation using finite differencing and likelihood ratios for kinetic Monte Carlo simulations. J. Comput. Phys. 231, 7170–7186.

Mesbah, A., Streif, S., Findeisen, R., Braatz, R.D., 2014. Stochastic nonlinear model predictive control with probabilistic constraints. Presented at the American Control Conference (ACC), 2014, pp. 2413–2419.

Morari, M., H. Lee, J., 1999. Model predictive control: past, present and future. Comput. Chem. Eng. 23, 667–682.

Nagy, Z.K., 2009. Model based robust control approach for batch crystallization product design. Comput. Chem. Eng. 33, 1685–1691.

Nagy, Z.K., Allgöwer, F., 2007. A nonlinear model predictive control approach for robust end-point property control of a thin-film deposition process. Int. J. Robust Nonlinear Control 17, 1600–1613.

Nagy, Z.K., Braatz, R.D., 2010. Distributional uncertainty analysis using polynomial chaos expansions. Presented at the 2010 IEEE International Symposium on Computer-Aided Control System Design (CACSD), pp. 1103–1108.

Nagy, Z.K., Braatz, R.D., 2007. Distributional uncertainty analysis using power series and polynomial chaos expansions. J. Process Control 17, 229–240.

Nagy, Z.K., Braatz, R.D., 2004. Open-loop and closed-loop robust optimal control of batch processes using distributional and worst-case analysis. J. Process Control 14, 411–422.

Nagy, Z.K., Braatz, R.D., 2003a. Robust nonlinear model predictive control of batch processes. AIChE J. 49, 1776–1786.

Nagy, Z.K., Braatz, R.D., 2003b. Worst-case and distributional robustness analysis of finite-time control trajectories for nonlinear distributed parameter systems. IEEE Trans. Control Syst. Technol. 11, 694–704.

Najm, H.N., 2009. Uncertainty quantification and polynomial chaos techniques in computational fluid dynamics. Annu. Rev. Fluid Mech. 41, 35–52.

Nayar, V., Pickering, C., Pidduck, A.J., Carline, R.T., Leong, W.Y., Robbins, D.J., 1993. The surface roughness and optical properties of high quality Si epitaxial layers. Thin Solid Films 233, 40–45.

Ni, D., Christofides, P.D., 2005a. Dynamics and control of thin film surface microstructure in a complex deposition process. Chem. Eng. Sci. 60, 1603–1617.

Ni, D., Christofides, P.D., 2005b. Multivariable predictive control of thin film deposition using a stochastic PDE model. Ind. Eng. Chem. Res. 44, 2416–2427.

Ni, D., Lou, Y., Christofides, P.D., Sha, L., Lao, S., Chang, J.P., 2004. Real-time carbon content control for PECVD ZrO2 thin-film growth. IEEE Trans. Semicond. Manuf. 17, 221–230.

Niederreiter, H., 1978. Quasi-Monte Carlo methods and pseudo-random numbers. Bull. Am. Math. Soc. 84, 957–1041.

Nieminen, R.M., 2002. From atomistic simulation towards multiscale modelling of materials. J. Phys. Condens. Matter 14, 2859.

Oguz, C., Gallivan, M.A., 2008. Optimization of a thin film deposition process using a dynamic model extracted from molecular simulations. Automatica 44, 1958–1969.

Pickering, C., 2001. Spectroscopic ellipsometry for monitoring and control of surfaces, thin layers and interfaces. Surf. Interface Anal. 31, 927–937.

Prasad, V., Vlachos, D.G., 2008. Multiscale model and informatics-based optimal design of experiments: Application to the catalytic decomposition of ammonia on ruthenium. Ind. Eng. Chem. Res. 47, 6555–6567.

Qin, S.J., Badgwell, T.A., 2003. A survey of industrial model predictive control technology. Control Eng. Pract. 11, 733–764.

Raimondeau, S., Aghalayam, P., Mhadeshwar, A.B., Vlachos, D.G., 2003. Parameter optimization of molecular models: Application to surface kinetics. Ind. Eng. Chem. Res. 42, 1174–1183.

Raimondeau, S., Vlachos, D.G., 2002. Recent developments on multiscale, hierarchical modeling of chemical reactors. Chem. Eng. J. 90, 3–23.

Raimondeau, S., Vlachos, D.G., 2000. Low-dimensional approximations of multiscale epitaxial growth models for microstructure control of materials. J. Comput. Phys. 160, 564–576.

Rasoulian, S., Ricardez-Sandoval, L.A., 2015a. Worst-case and distributional robustness analysis of a thin film deposition process. Presented at the 9th International Symposium on Advanced Control of Chemical Processes, Whistler, Canada.

Rasoulian, S., Ricardez-Sandoval, L.A., 2015b. Robust multivariable estimation and control in an epitaxial thin film growth process under uncertainty. Journal of Process Control, http://dx.doi.org/10.1016/j.jprocont.2015.07.002.

Rasoulian, S., Ricardez-Sandoval, L.A., 2015c. A robust nonlinear model predictive controller for a multiscale thin film deposition process. Chem. Eng. Sci, http://dx.doi.org/10.1016/j.ces.2015.02.002i.

Rasoulian, S., Ricardez-Sandoval, L.A., 2014. Uncertainty analysis and robust optimization of multiscale process systems with application to epitaxial thin film growth. Chem. Eng. Sci. 116, 590–600.

Reese, J.S., Raimondeau, S., Vlachos, D.G., 2001. Monte Carlo Algorithms for Complex Surface Reaction Mechanisms: Efficiency and Accuracy. J. Comput. Phys. 173, 302–321.

Renaud, G., Lazzari, R., Revenant, C., Barbier, A., Noblet, M., Ulrich, O., Leroy, F., Jupille, J., Borensztein, Y., Henry, C.R., Deville, J.-P., Scheurer, F., Mane-Mane, J., Fruchart, O., 2003. Real-time monitoring of growing nanoparticles. Science 300, 1416–1419.

Ricardez-Sandoval, L.A., 2012. Optimal design and control of dynamic systems under uncertainty: A probabilistic approach. Comput. Chem. Eng. 43, 91–107.

Ricardez-Sandoval, L.A., 2011. Current challenges in the design and control of multiscale systems. Can. J. Chem. Eng. 89, 1324–1341.

Rodgers, S.T., Jensen, K.F., 1998. Multiscale modeling of chemical vapor deposition. J. Appl. Phys. 83, 524–530.

Rooney, W.C., Biegler, L.T., 1999. Incorporating joint confidence regions into design under uncertainty. Comput. Chem. Eng. 23, 1563–1575.

Rusli, E., Drews, T.O., Braatz, R.D., 2004. Systems analysis and design of dynamically coupled multiscale reactor simulation codes. Chem. Eng. Sci. 59, 5607–5613.

Rusli, E., Drews, T.O., Ma, D.L., Alkire, R.C., Braatz, R.D., 2006. Robust nonlinear feedback–feedforward control of a coupled kinetic Monte Carlo–finite difference simulation. J. Process Control 16, 409–417.

Rusli, E., Xue, F., Drews, T.O., Vereecken, P.M., Andricacos, P., Deligianni, H., Braatz, R.D., Alkire, R.C., 2007. Effect of additives on shape evolution during electrodeposition II. Parameter estimation from roughness evolution experiments. J. Electrochem. Soc. 154, D584–D597.

Saltelli, A., Ratto, M., Tarantola, S., Campolongo, F., 2005. Sensitivity analysis for chemical models. Chem. Rev. 105, 2811–2828.

Schulze, T.P., 2008. Efficient kinetic Monte Carlo simulation. J. Comput. Phys. 227, 2455–2462.

Schwarm, A.T., Nikolaou, M., 1999. Chance-constrained model predictive control. AIChE J. 45, 1743–1752.

Sharma, O.P., Sirignano, W.A., 1969. Ignition of stagnation point flow by a hot body. Combust. Sci. Technol. 1, 95–104.

Siettos, C.I., Armaou, A., Makeev, A.G., Kevrekidis, I.G., 2003. Microscopic/stochastic timesteppers and "coarse" control: A KMC example. AIChE J. 49, 1922–1926.

Song, X., Williams, W.R., Schmidt, L.D., Aris, R., 1991. Bifurcation behavior in homogeneous-heterogeneous combustion: II. Computations for stagnation-point flow. Combust. Flame 84, 292–311.

Su, A.-J., Yu, C.-C., Ogunnaike, B.A., 2008. On the interaction between measurement strategy and control performance in semiconductor manufacturing. J. Process Control 18, 266–276.

Subramanian, K., Kumar, S., Patwardhan, S.C., Prasad, V., 2011. Extensions to experiment design and identification algorithms for large-scale and stochastic processes. Int. J. Adv. Mechatron. Syst. 3, 3–13.

Ulissi, Z., Prasad, V., Vlachos, D.G., 2011. Effect of multiscale model uncertainty on identification of optimal catalyst properties. J. Catal. 281, 339–344.

Ulissi, Z.W., Strano, M.S., Braatz, R.D., 2013. Control of nano and microchemical systems. Comput. Chem. Eng. 51, 149–156.

Varshney, A., Armaou, A., 2008a. Reduced order modeling and dynamic optimization of multiscale PDE/kMC process systems. Comput. Chem. Eng. 32, 2136–2143.

Varshney, A., Armaou, A., 2008b. Low-order ODE approximations and receding horizon control of surface roughness during thin-film growth. Chem. Eng. Sci. 63, 1246–1260.

Varshney, A., Armaou, A., 2006a. Identification of macroscopic variables for low-order modeling of thin-film growth. Ind. Eng. Chem. Res. 45, 8290–8298.

Varshney, A., Armaou, A., 2006b. Optimal operation of GaN thin film epitaxy employing control vector parametrization. AIChE J. 52, 1378–1391.

Varshney, A., Armaou, A., 2005. Multiscale optimization using hybrid PDE/kMC process systems with application to thin film growth. Chem. Eng. Sci. 60, 6780–6794.

Vlachos, D.G., 2012. Multiscale modeling for emergent behavior, complexity, and combinatorial explosion. AIChE J. 58, 1314–1325.

Vlachos, D.G., 2008. Temporal coarse-graining of microscopic-lattice kinetic Monte Carlo simulations via τ-leaping. Phys. Rev. E 78, 046713.

Vlachos, D.G., 2005. A review of multiscale analysis: Examples from systems biology, materials engineering, and other fluid–surface interacting systems, in: Advances in Chemical Engineering. Academic Press, pp. 1–61.

Vlachos, D.G., 1999. The role of macroscopic transport phenomena in film microstructure during epitaxial growth. Appl. Phys. Lett. 74, 2797–2799.

Vlachos, D.G., 1997. Multiscale integration hybrid algorithms for homogeneous–heterogeneous reactors. AIChE J. 43, 3031–3041.

Voter, A.F., 2007. Introduction to the kinetic Monte Carlo method. Springer Netherlands, pp. 1–23.

Wiener, N., 1938. The homogeneous chaos. Am. J. Math. 60, 897–936.

Xiong, R., Grover, M.A., 2012. In situ optical sensing and state estimation for control of surface processing, in: Feedback Control of MEMS to Atoms. Springer US, pp. 45–67.

Xiong, R., Wissmann, P.J., Gallivan, M.A., 2006. An extended Kalman filter for in situ sensing of yttria-stabilized zirconia in chemical vapor deposition. Comput. Chem. Eng. 30, 1657–1669.

Xiu, D., 2010. Numerical methods for stochastic computations: A spectral method approach. Princeton University Press.

Zhang, X., Hu, G., Orkoulas, G., Christofides, P.D., 2010. Controller and estimator design for regulation of film thickness, surface roughness, and porosity in a multiscale thin film growth process. Ind. Eng. Chem. Res. 49, 7795–7806.

Appendix A
Supplementary information for Chapter 5

For the multiple linear regressions required in Eq.(5-8), the operational substrate temperature region is divided into three regions and the parameters are estimated assuming that they are functions of substrate temperature and bulk mole fraction as follows:

$$\bar{\beta}_l = b_{0,l} + b_{1,l}T + b_{2,l}T^2 + b_{3,l}T\mathcal{X} + b_{4,l}T^2\mathcal{X} + b_{5,l}T^2\mathcal{X}^2,$$

where the parameters obtained from regression for upper and lower bounds on roughness for different regions in temperature are provided in Table A.1 and Table A.3 below. For each regression, the corresponding confidence bounds are also presented in Table A.2 and Table A.4, respectively.

Table A.1. Parameters of Eq.(5-10) to estimate upper bound on surface roughness.

Temperature	$\mathbf{600 \le T < 800}$			$\mathbf{800 \le T < 1000}$			$\mathbf{1000 \le T < 1400}$		
Parameter	$\bar{\beta}_1$	$\bar{\beta}_2$	$\bar{\beta}_3$	$\bar{\beta}_1$	$\bar{\beta}_2$	$\bar{\beta}_3$	$\bar{\beta}_1$	$\bar{\beta}_2$	$\bar{\beta}_3$
$b_{0,l}$	-8.5e-3	3.4e-1	5.3e-4	5.9e-2	-1.0	1.6e-2	3.4e-2	-6.7e-1	8.0e-3
$b_{1,l}$	7.2e-5	-1.7e-3	9.4e-6	-1.0e-4	1.9e-3	-2.8e-5	-4.7e-5	1.1e-3	-1.1e-5
$b_{2,l}$	-6.6e-8	1.6e-6	-9.9e-9	4.7e-8	-8.6e-7	1.2e-8	1.7e-8	-4.1e-7	3.9e-9
$b_{3,l}$	1.6	-3.5e1	6.6e-1	2.8	-5.8e1	3.6e-1	8.1e-1	-1. 8e1	2.8e-1
$b_{4,l}$	2.6e-4	-3.6e-3	-1.2e-4	-2.1e-3	4.2e-2	-1.2e-4	-5.2e-4	1.1e-2	-1.7e-4
$b_{5,l}$	-1.6e2	3.3e3	-6.0e1	-5.1e1	1.2e3	-1.6e1	-6.1	1.6e2	-2.8

Table A.2. Confidence bounds of the parameters listed in Table A.1.

Temperature		$600 \leq T < 800$			$800 \leq T < 1000$			$1000 \leq T < 1400$		
Parameter		$\bar{\beta}_1$	$\bar{\beta}_2$	$\bar{\beta}_3$	$\bar{\beta}_1$	$\bar{\beta}_2$	$\bar{\beta}_3$	$\bar{\beta}_1$	$\bar{\beta}_2$	$\bar{\beta}_3$
$b_{0,l}$	**Lower Bound**	-1.6e-2	1.7e-1	-1.2e-5	4.5e-2	-1.2	6.7e-3	3.1e-2	-7.4e-1	5.6e-3
	Upper Bound	-1.0e-3	5.0e-1	1e-3	7.2e-2	-8.5e-1	2.5e-2	3.6e-2	-6.1e-1	1.1e-2
$b_{1,l}$	**Lower Bound**	4.9e-5	-2.1e-3	8.0e-6	-1.3e-4	1.4e-3	-4.9e-5	-5.1e-5	9.8e-4	-1.5e-5
	Upper Bound	9.3e-5	-1.2e-3	1.1e-5	-7.1e-5	2.3e-3	-6.2e-6	-4.1e-5	1.2e-3	-6.7e-6
$b_{2,l}$	**Lower Bound**	-8.1e-8	1.2e-6	-2.1e-8	2.9e-8	-1.1e-6	3.0e-10	1.5e-8	-4.5e-7	2.2e-9
	Upper Bound	-5.0e-8	1.9e-6	1.5e-9	6.4e-8	-6.1e-7	2.4e-8	1.9e-8	-3.6e-7	5.9e-9
$b_{3,l}$	**Lower Bound**	1.1	-4.5e1	3.1e-1	2.2	-6.5e1	2.0e-3	6.7e-1	-2.1e1	1.7e-1
	Upper Bound	2.0	-2.5e1	1.0	3.2	-5.0e1	7.1e-1	9.3e-1	-1.5e1	3.9e-1
$b_{4,l}$	**Lower Bound**	-4.5e-4	-1.9e-2	-1.7e-4	-2.6e-3	3.3e-2	-5.3e-4	-6.4e-4	8.8e-3	-2.7e-4
	Upper Bound	9.9e-4	1.2e-2	-6.5e-5	-1.4e-3	5.0e-2	2.9e-4	-4.1e-4	1.4e-2	-7.1e-5
$b_{5,l}$	**Lower Bound**	-2.0e2	2.4e3	-9.0e1	-7.9e1	8.2e2	-3.5e1	-1.2e1	1.9e1	-9.8
	Upper Bound	-1.1e2	4.2e3	-2.9e1	-2.3e1	1.6e3	3.2	6.1e-1	3.1e2	1.9

Table A.3. Parameters of Eq.(5-10) to estimate lower bound on surface roughness.

Temperature	$600 \leq T < 800$			$800 \leq T < 1000$			$1000 \leq T < 1400$		
Parameter	$\bar{\beta}_1$	$\bar{\beta}_2$	$\bar{\beta}_3$	$\bar{\beta}_1$	$\bar{\beta}_2$	$\bar{\beta}_3$	$\bar{\beta}_1$	$\bar{\beta}_2$	$\bar{\beta}_3$
$b_{0,l}$	-3.3e-4	-8.0e-2	2.8e-3	3.9e-3	-2.2e-1	3.0e-3	3.5e-3	-4.7e-1	2.9e-3
$b_{1,l}$	1.2e-5	-9.5e-4	-1.6e-6	-3.1e-6	1.1e-4	-2.6e-6	-2.7e-6	6.9e-4	-2.4e-6
$b_{2,l}$	-1.1e-8	1.3e-6	-3e-11	7.2e-10	1.1e-7	8.7e-10	8.7e-10	-2.3e-7	8.4e-10
$b_{3,l}$	6.2e-1	-1.2e2	4.8e-1	2.9e-2	2.5	-2.6e-3	7.1e-2	-1.6e1	5.5e-2
$b_{4,l}$	-5.4e-4	1.1e-1	-5.4e-4	5.1e-5	-1.5e-2	3.6e-5	-4.0e-5	9.8e-3	-3.6e-5
$b_{5,l}$	-2.2e1	3.9e3	-6.1	-5.6	8.0e2	-1.9	-8.8e-1	1.2e2	-4.3e-1

Table A.4. Confidence bounds of the parameters listed in Table A.3.

Temperature		$600 \leq T < 800$			$800 \leq T < 1000$			$1000 \leq T < 1400$		
Parameter		$\bar{\beta}_1$	$\bar{\beta}_2$	$\bar{\beta}_3$	$\bar{\beta}_1$	$\bar{\beta}_2$	$\bar{\beta}_3$	$\bar{\beta}_1$	$\bar{\beta}_2$	$\bar{\beta}_3$
$b_{0,l}$	**Lower Bound**	-7.1e-4	-1.4e-1	1.1e-3	3.5e-3	-5e-1	8.3e-4	2.8e-3	-5.3e-1	2.4e-3
	Upper Bound	5.0e-5	-2.4e-2	4.4e-3	4.3e-3	5e-2	5.2e-3	4.2e-3	-3.9e-1	3.3e-3
$b_{1,l}$	**Lower Bound**	4.2e-7	-1.1e-3	-2.3e-6	-4.0e-6	-4.9e-4	-3.5e-6	-3.8e-6	5.7e-4	-3.1e-6
	Upper Bound	2.2e-5	-7.8e-4	1.0e-6	-2.1e-6	7.1e-4	-2.3e-6	-1.6e-6	8.0e4	-1.6e-6
$b_{2,l}$	**Lower Bound**	-1.9e-8	7.9e-8	-3e-11	2.3-10	-2.3e-7	5.9e-10	3.8e-10	-2.8e-7	5.2e-10
	Upper Bound	-3.2e-9	2.4e-6	3.0e-11	1.2e-9	4.5e-7	1.1e-9	1.3e-9	-1.8e7	1.1e-9
$b_{3,l}$	**Lower Bound**	3.7e-1	-1.5e2	3.8e-1	1.5e-2	-7.4	-1.1e-2	4.1e-2	-1.8e1	3.6e-2
	Upper Bound	8.6e-1	-8.5e1	5.8e-1	4.3e-2	1.2e1	5.6e-2	9.9e-2	-1.2e1	7.4e-2
$b_{4,l}$	**Lower Bound**	-9.1e-4	5.6e-2	-7.0e-4	3.4e-5	-2.7e-2	2.5e-5	-6.7e-5	7.0e-3	-5.2e-5
	Upper Bound	-1.6e-4	1.6e-1	-3.8e-4	6.8e-5	-3.3e-3	4.5e-5	-1.3e-5	1.2e-2	-1.8e-5
$b_{5,l}$	**Lower Bound**	-4.3e1	7.6e2	-6.9	-6.4	2.5e2	-4.4	-2.4	-3.2e1	-1.4
	Upper Bound	-1.0	6.9e3	-5.2	-4.8	1.3e3	6.3e-1	6.4e-1	2.7e2	5.4e-1

The parameters obtained for nonlinear regressions shown in Eq.(5-5) to estimate the upper bound on the surface roughness while the substrate temperature is 600 K and 700 K and the corresponding confidence bounds are listed in Table A.5 and Table A.6, respectively. The rest of the temperature regions were evaluated in the same fashion.

Table A.5. Parameters of Eq.(5-10) to estimate upper bound on surface roughness.

Temperature	$T = 600$ **K**			$T = 700$ **K**		
Bulk precursor mole fraction	β_1	β_2	β_3	β_1	β_2	β_3
$\mathcal{X} = 1 \times 10^{-6}$	3.13e-02	-9.97e-02	3.54e+02	1.92e-02	-7.85e-02	1.85e+02
$\mathcal{X} = 2 \times 10^{-6}$	3.05e-02	-1.34e-01	3.66e+02	3.19e-02	-8.06e-02	2.23e+02
$\mathcal{X} = 3 \times 10^{-6}$	3.09e-02	-1.51e-01	3.45e+02	2.89e-02	-1.11e-01	2.30e+02
$\mathcal{X} = 4 \times 10^{-6}$	2.88e-02	-1.75e-01	3.81e+02	3.03e-02	-1.25e-01	2.42e+02
$\mathcal{X} = 5 \times 10^{-6}$	3.56e-02	-1.66e-01	3.51e+02	3.22e-02	-1.32e-01	2.40e+02
$\mathcal{X} = 6 \times 10^{-6}$	3.74e-02	-1.74e-01	3.62e+02	3.00e-02	-1.51e-01	2.53e+02
$\mathcal{X} = 7 \times 10^{-6}$	3.77e-02	-1.82e-01	3.63e+02	2.71e-02	-1.68e-01	2.53e+02

Table A.6. Confidence bounds of the parameters listed in Table A.5.

Temperature		$T = 600$ K			$T = 700$ K		
Bulk precursor mole fraction		β_1	β_2	β_3	β_1	β_2	β_3
$\mathcal{X} = 1 \times 10^{-6}$	**Lower Bound**	3.09e-02	-1.01e-01	3.41e+02	1.89e-02	-7.97e-02	1.73e+02
	Upper Bound	3.18e-02	-9.86e-02	3.66e+02	1.96e-02	-7.73e-02	1.97e+02
$\mathcal{X} = 2 \times 10^{-6}$	**Lower Bound**	3.01e-02	-1.36e-01	3.53e+02	3.13e-02	-8.18e-02	2.11e+02
	Upper Bound	3.10e-02	-1.33e-01	3.78e+02	3.24e-02	-7.94e-02	2.35e+02
$\mathcal{X} = 3 \times 10^{-6}$	**Lower Bound**	3.05e-02	-1.52e-01	3.33e+02	2.84e-02	-1.12e-01	2.18e+02
	Upper Bound	3.14e-02	-1.50e-01	3.57e+02	2.93e-02	-1.10e-01	2.42e+02
$\mathcal{X} = 4 \times 10^{-6}$	**Lower Bound**	2.84e-02	-1.76e-01	3.68e+02	2.98e-02	-1.26e-01	2.29e+02
	Upper Bound	2.92e-02	-1.74e-01	3.93e+02	3.08e-02	-1.23e-01	2.54e+02
$\mathcal{X} = 5 \times 10^{-6}$	**Lower Bound**	3.51e-02	-1.67e-01	3.39e+02	3.17e-02	-1.33e-01	2.27e+02
	Upper Bound	3.61e-02	-1.65e-01	3.63e+02	3.27e-02	-1.30e-01	2.53e+02
$\mathcal{X} = 6 \times 10^{-6}$	**Lower Bound**	3.69e-02	-1.75e-01	3.50e+02	2.95e-02	-1.52e-01	2.41e+02
	Upper Bound	3.79e-02	-1.73e-01	3.75e+02	3.04e-02	-1.50e-01	2.66e+02
$\mathcal{X} = 7 \times 10^{-6}$	**Lower Bound**	3.72e-02	-1.83e-01	3.50e+02	2.67e-02	-1.70e-01	2.41e+02
	Upper Bound	3.83e-02	-1.80e-01	3.75e+02	2.75e-02	-1.67e-01	2.65e+02

Copyright Agreements

ELSEVIER LICENSE
TERMS AND CONDITIONS

Aug 12, 2015

This is an Agreement between Shabnam Rasoulian ("You") and Elsevier ("Elsevier"). It consists of your order details, the terms and conditions provided by Elsevier, and the payment terms and conditions.

All payments must be made in full to CCC. For payment instructions, please see information listed at the bottom of this form.

Supplier	Elsevier Limited The Boulevard,Langford Lane Kidlington,Oxford,OX5 1GB,UK
Registered Company Number	1982084
Customer name	Shabnam Rasoulian
Customer address	200 University Avenue West Waterloo, ON N2L 3G1
License number	3652551090566
License date	Jun 19, 2015
Licensed content publisher	Elsevier
Licensed content publication	Chemical Engineering Science
Licensed content title	Uncertainty analysis and robust optimization of multiscale process systems with application to epitaxial thin film growth
Licensed content author	Shabnam Rasoulian,Luis Alberto Ricardez-Sandoval
Licensed content date	6 September 2014
Licensed content volume number	116
Licensed content issue number	n/a
Number of pages	11
Start Page	590
End Page	600
Type of Use	reuse in a thesis/dissertation
Portion	full article
Format	both print and electronic
Are you the author of this Elsevier article?	Yes
Will you be translating?	No
Title of your thesis/dissertation	Uncertainty analysis and control of multiscale process systems
Expected completion date	Aug 2015
Estimated size (number of pages)	130
Elsevier VAT number	GB 494 6272 12
Price	0.00 CAD
VAT/Local Sales Tax	0.00 CAD / 0.00 GBP
Total	**0.00 CAD**

ELSEVIER LICENSE
TERMS AND CONDITIONS

Aug 12, 2015

This is an Agreement between Shabnam Rasoulian ("You") and Elsevier ("Elsevier"). It consists of your order details, the terms and conditions provided by Elsevier, and the payment terms and conditions.

All payments must be made in full to CCC. For payment instructions, please see information listed at the bottom of this form.

Supplier	Elsevier Limited The Boulevard,Langford Lane Kidlington,Oxford,OX5 1GB,UK
Registered Company Number	1982084
Customer name	Shabnam Rasoulian
Customer address	200 University Avenue West Waterloo, ON N2L 3G1
License number	3686650433684
License date	Jun 19, 2015
Licensed content publisher	Elsevier
Licensed content publication	Chemical Engineering Science
Licensed content title	A robust nonlinear model predictive controller for a multiscale thin film deposition process
Licensed content author	Shabnam Rasoulian,Luis A. Ricardez-Sandoval
Licensed content date	Available online 9 February 2015
Licensed content volume number	n/a
Licensed content issue number	n/a
Number of pages	1
Start Page	None
End Page	None
Type of Use	reuse in a thesis/dissertation
Intended publisher of new work	other
Portion	full article
Format	both print and electronic
Are you the author of this Elsevier article?	Yes
Will you be translating?	No
Title of your thesis/dissertation	Uncertainty analysis and control of multiscale process systems
Expected completion date	Aug 2015
Estimated size (number of pages)	
Elsevier VAT number	GB 494 6272 12
Price	0.00 CAD
VAT/Local Sales Tax	0.00 CAD / 0.00 GBP
Total	**0.00 CAD**